# Instabilities of Spatial Solitons in Saturable Nonlinear Media

Vom Fachbereich Physik
der Technischen Universität Darmstadt
zur Erlangung des Grades
eines Doktors der Naturwissenschaften
(Dr. rer. nat.)

genehmigte

**DISSERTATION**

von

**Dipl.-Phys. Christian Motzek**
aus Idar-Oberstein

Darmstadt 2005
D17

| | |
|---|---|
| Referent: | Prof. Dr. Friedemann Kaiser |
| Korreferentin: | Prof. Dr. Barbara Drossel |
| Tag der Einreichung: | 25.10.2005 |
| Tag der Prüfung: | 18.1.2006 |

# Contents

# Chapter 1

# Introduction

The scientific investigation of solitons began in 1834 when J. Scott Russell observed a wave that changed neither shape nor speed as it travelled along a shallow water canal [1]. The fascination of this observation came from the fact that the wave was localised, although it was subject to dispersion. Another example of such localised waves, equally fascinating though far more dangerous, are Tsunamis, giant waves generated by earthquakes travelling the oceans at high speed.

These two examples belong to the class of *temporal* solitons. This expression is generally used to describe pulses conserving their profile as they propagate through a medium. The location of the pulse changes, but not its shape. Therefore, there must be a physical mechanism that counterbalances dispersion. The physical mechanism is connected to nonlinear properties of the medium. Solitons are therefore an example of how nonlinear aspects of nature can explain otherwise inexplicable phenomena.

Temporal solitons have already gained some importance in the world of technology as well. Digital data transmission relies on the transmission of electrical or optical pulses over long distances. In that context, dispersion poses a major problem. In optical data transmission nonlinear media are being used to compensate the dispersion. This technique allows for faster data transmission and longer fibre lengths.

In the present work we will be concerned with the spatial counterpart of temporal solitons. *Spatial* solitons arise from the interplay of diffraction and the nonlinearities of the medium. It is well known that a light beam diffracts as it propagates. The smaller the diameter of the light beam, the stronger the diffraction, i.e. the faster its diameter will be growing under

propagation. In conventional optical setups this diffraction is compensated for by a system of lenses and/or curved mirrors. Media with strong optical nonlinearities offer a different approach: if the refractive index of the medium increases when light is incident upon it, then the increased refractive index in the illuminated area of the medium will act as a lens, leading to a focusing of the light. This phenomenon is called self-focusing. If the self-focusing exactly counterbalances the diffraction, the light beam propagates through the medium without changing its diameter or profile. In this case we speak of a spatial soliton [2].

The use of spatial solitons in optoelectronics has a great potential, because, contrary to lenses and mirrors, nonlinear media interact with the light. It is thus possible to create self-adaptive optical systems. However, there are still many obstacles to overcome before optical spatial solitons can be used in technological applications. An ongoing research on the topic is necessary, focusing on two major problems: (a) the stability of spatial solitons is still little understood and (b) media have to be developed that show large nonlinearities at moderate light intensities, while being inexpensive and of good quality (i.e. having a low number of impurities, being thermally stable, show no ageing effects etc.).

It has to be pointed out that the term 'soliton' was initially only used for integrable systems [3], whereas in all other systems one spoke of 'solitary solutions'. Nowadays, however, the word soliton is used in a broader sense, including non-integrable systems.

## 1.1 Diffraction and self-focusing

Let us quickly reconsider the phenomena that play the key roles in the formation of optical spatial solitons. The first phenomenon to consider is diffraction (figure 1.1):

It is well known that Maxwell's equations have solutions in the form of plane light waves that propagate in one direction, say $z$. Real light fields, however, do not extend to infinity along the axes perpendicular to the direction of propagation ($x$ and $y$). However, any light field can be described as a superposition of plane waves, because the plane wave solutions form a complete set of orthogonal functions. To arrive at a localised light field, one has to combine plane waves that propagate in different directions, i.e. the direction of propagation of each of these plane waves is inclined under

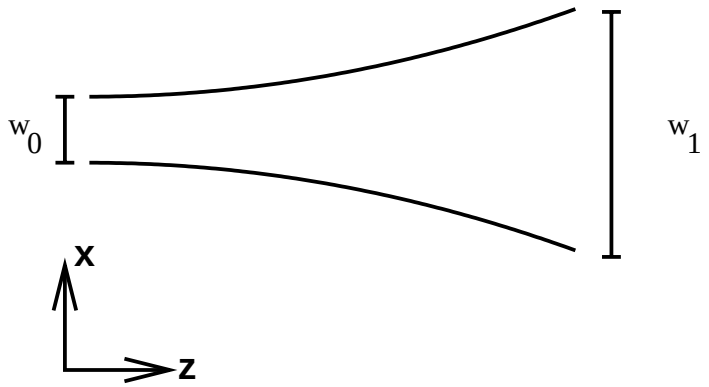


Figure 1.1: The linear diffraction of a light beam, increasing its diameter from initially $w_0$ to $w_1$.

a different angle with respect to the $z$-direction. For light beams with large diameters, the plane waves with big inclination angles only play a negligible role, whereas even large inclination angles become important for beams with small diameter.

The situation sketched in figure 1.1 changes when the light propagates through a nonlinear self-focusing medium. As mentioned above, these media change their refractive index as a function of the light intensity. The refractive index increases in places with high intensity and remains unchanged in regions with zero light intensity. The medium thus behaves like a focusing lens. There is a competition between the diffraction trying to widen up the beam and the focusing by the medium. If the focusing counterbalances the diffraction, the beam conserves its diameter. Spatial solitons are thus defined as light beams that do not change their transverse intensity profile as they propagate.

There is another equivalent definition of spatial solitons. As described above, the light beam induces a region with higher refractive index in the medium. This region can be considered as a waveguide. This waveguide has eigenmodes, i.e. light beams with a specific profile can propagate through this waveguide without changing their profile. If the eigenmode is identical with the profile of the light beam that induces the waveguide, then the light beam is a soliton [2].

## 1.2 Nonlinear optical media

A large number of nonlinear media has been used to generate optical spatial solitons. These nonlinear media are (ideally) absorptionless and thus fully characterised by the change in refractive index as a function of the light intensity $I$. Mathematically, the simplest case is a so-called Kerr medium, where $n^2(I) - n_0^2 = \alpha I$. Here, $n(I)$ is the refractive index, $n_0$ is the refractive index of the unperturbed medium, and $\alpha$ is a real constant. Examples for Kerr media are many glasses and liquid $CS_2$.

The major drawback of Kerr media for the experimental investigation of solitons is the fact that 2D solitons are always unstable in these media [4, 5], thus only (quasi-)1D solitons can be observed. 2D solitons are spatially extended in the two directions perpendicular to the direction of propagation,whereas 1D solitons are only extended along one of these directions. The latter is usually achieved by creating a slab waveguide (putting a thin slice of the nonlinear material between two layers of material with lower refractive index), creating an effectively (1+1)D System (i.e. a system with one transverse dimension and the propagation direction, i.e. one longitudinal dimension).

The instability of 2D solitons in Kerr media is the main reason for the popularity of saturable nonlinear media for the investigation of solitons. The prototype of a saturable nonlinearity looks like $n^2(I) - n_0^2 = \Gamma I/(1+I)$. The most widely used materials in soliton research are photorefractive crystals. Other experiments are carried out in metal vapours or liquid crystal cells. The main advantage of photorefractive crystals is that only low laser powers are needed to generate solitons (a few mW). It has to be mentioned however that photorefractive crystals have a very slow response time to changes in the light field (in the order of seconds) which means that they would not be suitable for optoelectronic applications.

Other nonlinear materials used in soliton research include the so-called quadratic media, where second harmonic generation is at the origin of the nonlinearity. Quadratic media also allow for the generation of stable 2D solitons. However, because of the interplay between the fundamental beam and the harmonic one the physical nature of solitons in these media is somewhat different from solitons in Kerr or saturable media and they will not play a major role in this work.

Throughout this work we will consider the prototype form of saturable nonlinearities ($I/(1+I)$) to gain a general insight into the physics of solitons.

In order to make these results accessible to an experimental verification we will use a more complex model [6], that is known to describe the nonlinearity of a photorefractive crystal very accurately.

## 1.3 Outline of the work

A mathematical description of light propagation in nonlinear media in general, and of the nonlinear response of photorefractive crystals in particular is given in chapter 2. This chapter also includes the differential equations that need to be solved to arrive at solitary solutions. After having introduced the basic mathematical tools, chapter 3 sheds some light on the nature of the instabilities that solitons can be subject to. The analytical approaches that have been introduced so far to explain soliton instabilities is discussed and complemented by numerical results that show that the analytical approach fails in the case of symmetry-breaking instabilities.

Chapter 4 investigates the relation between the existence of solitons and the instability of the plane wave solution. This instability also serves as the most basic example of the effects that the degree of coherence of the light can have on instabilities. The numerical results obtained are compared to experimental data.

The relation between the degree of coherence and the stability is being treated in chapter 5 in the special case of bright vortex rings. Here, the problem is twofold: (a) can bright vortex solitons be stabilised by using incoherent light and (b) how can the beam's vorticity be detected. The latter question is nontrivial because even in linear optics incoherent vortices are a topic of ongoing research and all methods to characterise them must be based on correlation functions.

Chapter 6 shows that it is sufficient to change the boundary conditions to completely change the spectrum of possible instabilities. Instead of considering the interaction between light beams propagating in the same direction, we investigate solitons formed from counterpropagating beams. The most fundamental new feature that arises is the existence of temporal dynamics of the system. We explain a novel kind of instability that was discovered and discuss the counterpropagation of light beams in photorefractive media in more detail, showing the importance of the non-local nature of the photorefractive effect.

Chapter 7 gives a very short introduction into the stability analysis of

gap solitons in photonic crystals, showing which direction the endeavour to understand the stability of solitons is likely to take.

Finally, chapter 8 summarises the basic results presented in this work and gives an outlook on possible future directions in the field of soliton research.

# Chapter 2

# Modelling of light propagation in nonlinear media

The starting point for any theoretical treatment of light propagation are Maxwell's equations:

$$\begin{aligned} \nabla \times \mathbf{E} + \frac{1}{c}\frac{\partial \mathbf{B}}{\partial t} &= 0 && (2.1)\\ \nabla \times \mathbf{H} &= \frac{4\pi}{c}\mathbf{j} + \frac{1}{c}\frac{\partial \mathbf{D}}{\partial t} && (2.2)\\ \nabla \cdot \mathbf{D} &= 4\pi\rho && (2.3)\\ \nabla \cdot \mathbf{B} &= 0\,, && (2.4) \end{aligned}$$

where $\mathbf{D} = \mathbf{E} + 4\pi\mathbf{P}$ bund $\mathbf{H} = \mathbf{B} - 4\pi\mathbf{M}$. In the following we will only consider non-magnetic media, i.e. we can set $\mathbf{M} = 0$. Furthermore, we assume that there are no free charges or electric currents in the medium. Using these assumptions, one easily combines Maxwell's equations to the wave equation for the electric field $\mathbf{E}$:

$$\nabla \times \nabla \times \mathbf{E} + \frac{1}{c^2}\frac{\partial^2 \mathbf{E}}{\partial t^2} + \frac{4\pi}{c^2}\frac{\partial^2 \mathbf{P}}{\partial t^2} = 0\,. \qquad (2.5)$$

This equation is nonlinear if the polarisation $\mathbf{P}$ of the medium depends on the electric field $\mathbf{E}$ in a nonlinear way. In the linear case equation (2.5) has solutions in the form of plane waves. The effect of the electric field on the polarisation depends on the frequency of these waves. Hence, one can write $\mathbf{D} = \mathbf{E} + 4\pi\mathbf{P} = \hat{\epsilon}(\omega)\mathbf{E}$, where we assume that $\mathbf{E}$ evolves in time like

$e^{i\omega t}$. Here, $\hat{\epsilon}(\omega)$ is a tensor of second degree, the so-called dielectric tensor. Equation (2.5) thus transforms into

$$\nabla \times \nabla \times \mathbf{E} + \frac{\hat{\epsilon}(\omega)}{c^2}\frac{\partial^2 \mathbf{E}}{\partial t^2} = 0 \tag{2.6}$$

Looking for plane wave solutions $\mathbf{E}(\mathbf{r}) = \mathbf{E}(z) = \mathbf{B}e^{i(\omega t - k_3 z)}$ and assuming that the second element of the $\mathbf{E}$ vector is zero, $E_2 = 0$, i.e. choosing a polarisation of the light in the $\mathbf{e}_x$-$\mathbf{e}_z$-plane, one finds that:

$$k_3^2 = \frac{\omega^2}{c^2}\left(\epsilon_{11} - \frac{\epsilon_{13}^2}{\epsilon_{33}}\right) \tag{2.7}$$

$$B_3 = -\frac{\epsilon_{13}}{\epsilon_{33}}B_1\,, \tag{2.8}$$

where $\mathbf{B}$ is a unit vector that defines the orientation of the electric field. One can hence define the effective refractive index to be:

$$n_{\text{eff}}^2 = \left(\epsilon_{11} - \frac{\epsilon_{13}^2}{\epsilon_{33}}\right)\,. \tag{2.9}$$

To obtain localised light fields we superimpose many plane wave solutions that are tilted at different *small* angles with respect to the $z$-axis:

$$\mathbf{E}(\mathbf{r}) = \int C(k_1, k_2)\mathbf{B}(k_1, k_2)\exp(i(\omega t - (k_1 x + k_2 y + k_3 z)))\mathrm{d}k_1\mathrm{d}k_2\,. \tag{2.10}$$

Knowing that each plane wave evolves in $z$ like $e^{-ik_3 z}$ and that $k_1^2 + k_2^2 + k_3^2 = \omega^2(\epsilon_{11} - \epsilon_{13}^2/\epsilon_{33})/c^2$ (compare with equation (2.7)), one easily shows that

$$-\partial_z^2\mathbf{E}(\mathbf{r}) = (\nabla_\perp^2 + \frac{\omega^2}{c^2}n_{\text{eff}}^2)\mathbf{E}(\mathbf{r})\,, \tag{2.11}$$

where $\nabla_\perp = \partial_x\mathbf{e}_x + \partial_y\mathbf{e}_y$, $\mathbf{e}_i$ being the unit vectors in space. It is essential to note that in nonlinear media $n_{\text{eff}}^2$ depends on the light intensity and can thus be split into the refractive index in the absence of light $n_0^2$ and the light induced refractive index shift $\delta n^2(I)$, where $I = |\mathbf{E}|^2$ is the light intensity. The effective refractive index is then given by $n_{\text{eff}}^2 = n_0^2 + \delta n^2(i)$.

To simplify calculations we do not consider the evolution of the electric field $\mathbf{E}$, but the evolution of its envelope $A$, where $\mathbf{E}(\mathbf{r}) = A(\mathbf{r})e^{i(\omega t - k_3 z)}\mathbf{S}$, $\mathbf{S}$

being the unit vector $(\epsilon_{33}\mathbf{e}_x - \epsilon_{13}\mathbf{e}_z)/\sqrt{\epsilon_{33}^2 + \epsilon_{13}^2}$, which, according to equation (2.8), is parallel to the electric field vector of a plane wave travelling in $z$-direction. From equation (2.11) one obtains the paraxial wave equation:

$$-ik\partial_z A(\mathbf{r}) = \frac{1}{2}(\nabla_\perp^2 + k_0^2 \delta n^2(I))A(\mathbf{r})\,, \tag{2.12}$$

where $k = \omega n_0/c$ is the wave-number of the light in the medium and $k_0 = \omega/c$ is its vacuum wave-number. The $\partial_z^2 A(\mathbf{r})$ term has been neglected, because we can assume that the envelope varies only slowly.

This equation can be derived in an easier way when a non-birefringent medium can be assumed. However, many optically nonlinear media are strongly birefringent, hence the necessity to show that the paraxial wave equation (2.12) is valid in birefringent media as well.

The special features of light propagation in nonlinear media comes from the $\delta n^2$ term in equation (2.12). Hence, it is necessary to consider the nonlinear response in more detail.

## 2.1 Photorefractive nonlinearities

A large number of experiments is being carried out in photorefractive crystals. Photorefractive crystals provide a strong nonlinear response to an incident light intensity. The response time, however, is quite slow – typically seconds. Although the nonlinearity of photorefractive crystals is very specific, we will consider it in more detail here, as an experimental verification of any theoretical or numerical result is most easily performed in photorefractive crystals.

The nonlinear refractive index change in photorefractive crystals is based upon the so-called Pockels-effect. The Pockels-effect exists in non-centrosymmetric crystals and consists of a refractive index change dependent on the electric field inside the crystal. In linear approximation, the refractive index change is characterised by the electro-optic tensor $r_{ijk}$. The electro-optic tensor $r_{ijk}$ is a third degree tensor. The refractive index can be calculated using equation (2.9) and

$$\epsilon_{ij} = \epsilon_{ij}^{(0)} + \left(\epsilon_{ij}^{(0)}\right)^2 r_{ijk} E_k\,, \tag{2.13}$$

where $\hat{\epsilon}$ is the dielectric tensor, $\hat{\epsilon}^{(0)}$ is the unperturbed dielectric tensor and $E_k$ are the components of the electric field. Photorefractive crystals are usually

most susceptible to electric fields applied parallel to their crystallographic ĉ-axis. Therefore, in most experiments on spatial solitons in photorefractive crystals the crystal is biased in that direction. Throughout the rest of this work we will choose the $x$-axis to be parallel to the ĉ-axis. Note that the Pockels-effect has its origin in the electronic configuration of the crystal lattice. It is hence a very fast effect.

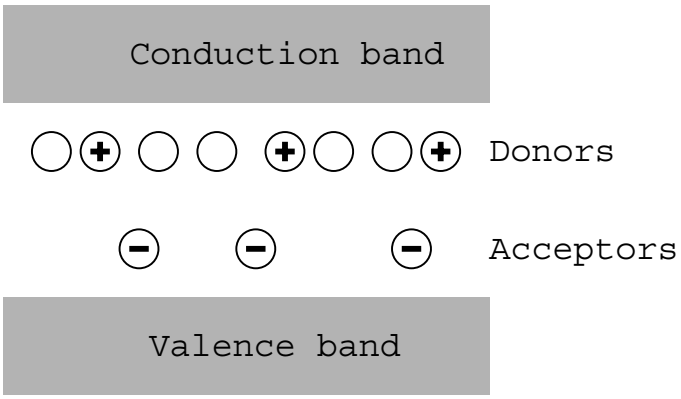


Figure 2.1: A sketch of the charge distribution inside a photorefractive crystal in the absence of light.

It is the electric field inside the crystal that evolves very slowly. Figure 2.1 shows a schematic picture of a photorefractive crystal in the absence of light. The main feature is that the crystal is doped with acceptors as well as donors, where the number of donors is typically much larger than the number of acceptors. When light of appropriate wavelength is incident upon the photorefractive crystal, some of the donors' electrons are being lifted into the conduction band, where they are free to move under the influence of drift and diffusion. When an external field is applied to the crystal, the electrons in the conduction band will move along the field out of the illuminated area and recombine with ionised donors. This process creates a space charge field inside the crystal that is oriented anti-parallel to the externally applied field. Hence, one speaks of a screening field. Due to this screening field, the electric field in the illuminated area is weaker than in the dark areas of the crystal. If the externally applied field is oriented parallel to the crystallographic ĉ-axis, this leads to an increase in the refractive index.

To know how incident light changes the refractive index, one has to know what the space charge field generated by the incident light looks like. This problem has been solved in 1979 by Kukhtarev *et. al.* [7]. They developed a

set of equations that describes the dynamics of the charge carriers inside the crystal. First, the rate $G_N$ at which electrons are lifted into the conduction band is given by

$$G_N = (\beta_e + sI)(N_D - N_D^+) - \gamma_e N N_D^+ \,, \tag{2.14}$$

where $N$ is the density of electrons in the conduction band, $N_D$ and $N_D^+$ are the densities of the non-ionised and ionised donors respectively and $\beta_e$ stands for excitation of electrons into the conduction band in the absence of light (mainly thermal). Finally, $s$ is proportional to the probability that an incoming photon lifts an electron into the conduction band and $\gamma_e$ is the probability for an electron from the conduction band to recombine with an ionised donor.

Once in the conduction band, the electrons will move according to the following equation:

$$\mathbf{j} = -e\mu N\mathbf{E} + \mu k_B T \nabla N + \hat{p}_n \mathbf{e}_x (N_D - N_D^+) I \,. \tag{2.15}$$

The first and second term on the right hand side stand for the drift and diffusion respectively. The electric field $\mathbf{E}$ is the sum of the external field applied to the crystal and the space charge field generated inside the crystal. The third term stands for the photovoltaic effect. Its strength is given by the photovoltaic tensor $\hat{p}_n$, multiplied by the direction of polarisation of the light used. In equation (2.15), like in the rest of the present work, the light is chosen to be polarised parallel to the $x$-direction.

The rate at which electrons are lifted into the conduction band and their equation of motion allows us to calculate the temporal dynamics of the electron concentration in the conduction band:

$$\frac{\partial N}{\partial t} = G_N - \frac{1}{e}\nabla \mathbf{j} \,. \tag{2.16}$$

The temporal dynamics of the concentration of ionised donors is given by:

$$\frac{\partial N_D^+}{\partial t} = G_N \,. \tag{2.17}$$

Finally, assuming that all acceptors are ionised and that the relative dielectrical constant of the crystal is $\epsilon_r$, the electric field $\mathbf{E}$ inside the crystal has to solve the following equation:

$$\nabla \mathbf{E} = -\frac{4\pi e}{\epsilon_r}(N + N_A - N_D^+) \,, \tag{2.18}$$

where $N_A$ is the concentration of acceptors. Solving this equation, one has to make sure that the externally applied electric field $\mathbf{E}_0$ is taken into account.

In 1995 Zozulya and Anderson were able to show that the system of equations (2.14-2.18) can be solved quite easily, using a few extremely well justified approximations. Instead of trying to obtain a differential equation for the electric field, they found a differential equation for the electric potential inside the crystal, where, for the sake of simplicity, the externally applied field is being eliminated. The electric field is thus given by: $\mathbf{E} = \nabla\tilde{\Phi} - \mathbf{E}_0$, where $\tilde{\Phi}$ is the electric potential. They found, that $\tilde{\Phi}$ solves the following equation [6]:

$$\begin{aligned} \nabla^2\tilde{\Phi} + \nabla \ln(1+I)\,\nabla\tilde{\Phi} &= E_0\,\partial_x \ln(1+I) \\ &\quad +(k_BT/e)\left[\nabla^2 \ln(1+I) + (\nabla \ln(1+I))^2\right] \\ &\quad -\eta\nabla \ln(1+I)\ , \end{aligned} \tag{2.19}$$

where the light intensity $I$ is scaled to $I_D$, the so-called dark intensity. $I_D$ is a material constant, which reflects the fact that even in the absence of light, some electrons are present in the conduction band.

The last term on the right hand side of equation (2.19) stands for the photovoltaic effect. The vector $\eta$ is given by $\eta = N_A\hat{p}_n\mathbf{e}_x/(e\mu)$. Although the photovoltaic term can not generally be neglected, its $y$- and $z$- components are negligibly small in the most commonly used photorefractive crystals – such as SBN – so that the term takes the simpler form $\eta_x\frac{\partial}{\partial_x}\ln(1+\tilde{I})$. Hence, the photovoltaic term has a form identical to the first term on the right hand side of equation (2.19). It is hence only a correction to the externally applied bias field $\mathbf{E}_0 = E_0\mathbf{e}_x$. In other words, the photorefractive crystal acts as a solar cell and generates an electric field that adds to the externally applied field. Thus, shifting $E_0$, we can simplify equation (2.19) and obtain

$$\begin{aligned} \nabla^2\tilde{\Phi} + \nabla \ln(1+I)\,\nabla\tilde{\Phi} &= E_0\,\partial_x \ln(1+I) \\ &\quad +(k_BT/e)\left[\nabla^2 \ln(1+I) + (\nabla \ln(1+I))^2\right]\ . \end{aligned} \tag{2.20}$$

This equation can be solved numerically quite easily and has been shown to be in excellent agreement with experimental results [8, 9].

In the following, equation (2.20) will be solved numerically in two- and three-dimensional space. In 1D equation (2.20) can even be solved analytically [10]. In that case we obtain

$$\mathbf{E} = \left(E_0\frac{I}{1+I} + \frac{k_BT}{e}\frac{\partial_x I}{1+I} - E_0\right)\mathbf{e}_x\,. \tag{2.21}$$

This one-dimensional solution is only a very rough approximation in the two-dimensional case. Neglecting the diffusion term as well, the electric field takes the form

$$\mathbf{E} = (E_0 I/(1+I) - E_0)\mathbf{e}_x \,, \tag{2.22}$$

which is known as the isotropic model. The name is chosen in contrast to the full model equation (2.20), which yields an anisotropic electric field in the two-dimensional case, even if the light intensity $I$ is circularly symmetric. Note that the electric field obtained from equation (2.22) is not only isotropic, but also local. This means that the electric field in one point only depends on the light intensity $I$ in that one point, whereas in the full anisotropic model equation (2.20) the electric field in one point also depends on the light intensity in the region around that point.

Now that we have full knowledge of the electric field inside the crystal, we can calculate the refractive index distribution inside the crystal. Let us assume the most important configuration for soliton experiments, where the light propagates in $z$-direction and is polarised in $x$-direction. (Remember that we chose the $x$-direction to be parallel to the crystal's ĉ-axis and that the externally applied electric field is also applied along that direction.) We then obtain from equations (2.9) and (2.13) the refractive index:

$$n_{\text{eff}}^2 = n_e^2 + n_e^4 r_{111} E_x \,, \tag{2.23}$$

where $n_e^2 = \epsilon_{11}^{(0)} = n_0^2$ is the unperturbed refractive index in the absence of any electric field for extraordinary polarised light. Here, we have used the fact that most of the elements of the electro-optic tensor are negligibly small. Hence, the term proportional to $\epsilon_{13}^2$ in equation (2.9) can be neglected. The value of the $x$-component of the electric field can be obtained by solving equation (2.20), or, if the isotropic model is being used, by using equation (2.22). Splitting the refractive index into a part $n_0^2$ that is equal to the refractive index in the absence of light and a light induced refractive index change $\delta n^2(I)$, we find that

$$\delta n^2(I) = n_e^4 r_{111} \partial_x \tilde{\Phi} \tag{2.24}$$

for the anisotropic model and

$$\delta n^2(I) = n_e^4 r_{111} \left( E_0 \frac{I}{1+I} + \frac{k_B T}{e} \frac{\partial_x I}{1+I} \right) \tag{2.25}$$

for the isotropic model. Together with equation (2.12) this fully describes the propagation of light through the crystal.

Due to its simplicity the isotropic model often is a good starting point when trying to understand the behaviour of light in photorefractive crystals or other saturable nonlinear media. Furthermore, it can be shown that the isotropic model describes the nonlinear optical properties of metal vapour cells in good approximation. In this work we will use the isotropic model to gain qualitative insight into the behaviour of solitons in saturable media, whereas we will use the full anisotropic model whenever we link our theoretical and numerical results to experimental results.

## 2.2 Solitary solutions

It is often convenient to use scaled units when looking for solitary solutions to the system of equations (2.12) and (2.24) or (2.25). Throughout the rest of this work we will use the scaled units $x' = x/x_0$, $y' = y/x_0$ and $z' = z/z_0$, where $x_0 = 1/(k_0 n_e^2 \sqrt{r_{111} E_0})$ and $z_0 = 2kx_0^2$, unless otherwise noted. In the following we will drop the primes on the dimensionless units for brevity.

To give an impression of the orders of magnitude that play a role in the investigation of solitons, we note that a typical soliton has a diameter of around $5x_0$, provided that the values of the relevant parameters are somewhere near those in table 2.1, which are typically encountered in experiments on spatial solitons in Strontium Barium Niobate (SBN) crystals.

| | |
|---|---|
| $E_0$ | 2 kV/cm |
| $r_{111}$ | 180 pm/V |
| $n_e$ | 2.3 |
| $k_0$ | 11.8 $10^9$ 1/m |

Table 2.1: Values typically encountered in experiments on spatial solitons in SBN crystals.

To obtain a characteristic order of magnitude for lengths in the propagation direction, we note that in a linear medium a gaussian beam with an initial diameter of $5x_0$ would spread during propagation such that after a propagation distance of $L_D = 25z_0$ its maximum intensity would reduce to a fraction of $1/e$ of its initial value, with $e$ being the natural logarithmic base. $L_D$ is called diffraction length and is used to estimate whether a given propagation distance is long enough to allow for an interplay between diffraction

and nonlinearity. This is the case when the propagation distance is longer than 1 or $2L_D$.

Using these dimensionless units, we obtain the propagation equation

$$-i\partial_z A(\mathbf{r}) = (\nabla_\perp^2 + \delta n^2(I))A(\mathbf{r}) \tag{2.26}$$

from equation (2.12) and $\delta n^2$ is given by $\partial_x \Phi$, where $\Phi$ solves

$$\begin{aligned} \nabla^2\Phi + \nabla \ln(1+I)\,\nabla\Phi &= \partial_x \ln(1+I) \\ &\quad +(k_B T/(eE_0))\left[\nabla^2 \ln(1+I) + (\nabla \ln(1+I))^2\right] \end{aligned} \tag{2.27}$$

for the anisotropic and

$$\delta n^2 = \frac{I}{1+I} \tag{2.28}$$

for the isotropic case. As already done in equation (2.22), we have neglected the temperature-dependent diffusion term in equation (2.28) for the sake of simplicity. In the following, we will also set $T = 0$ when using equation (2.27), unless noted otherwise.

Solitary solutions are, by definition, solutions of equation (2.26) that do not change their intensity profile as they propagate. When there is only one single beam present, the intensity is given by $I = |A|^2$. Hence, for the beam to be a soliton, $A$ must not depend on $z$, except for a phase factor, i.e. $A(x, y, z) = \varphi_\beta(x, y)\exp(i\beta z)$. Inserting this ansatz into equation (2.26), we obtain the soliton equation

$$\beta\varphi_\beta(x, y) = (\nabla_\perp^2 + \delta n^2(I))\varphi_\beta(x, y)\,. \tag{2.29}$$

This means that the light beam $\varphi_\beta$ is a guided mode of the waveguide $\delta n^2$ that it induces itself. Solutions to this equation are also called scalar solitons.

The so-called propagation constant $\beta$ reflects the fact that the light experiences a phase shift caused by the nonlinearity $\delta n^2$. Therefore $\beta$ is always positive in the case of homogeneous self-focusing media.

The situation changes slightly when the light used to generate the soliton is partially incoherent. As mentioned above, photorefractive crystals have a rather long response time to changes in the light intensity. Hence, the crystal ignores any fast intensity fluctuations and just reacts to the time-averaged light intensity. According to the modal theory of solitons [11] a soliton formed from partially incoherent light can be decomposed into (infinitely) many

coherent, yet mutually incoherent components:

$$\varphi_{\{\beta\}}(x,y) = \sum_{j=1}^{N} \varphi_{j,\{\beta\}}(x,y) \exp(i\beta_j z) \exp(i\gamma_j(t)) \,, \tag{2.30}$$

where $N$ is the number of components, $\{\beta\}$ is the ensemble of the propagation constants $\beta_j$ and $\gamma_j(t)$ is a random phase factor making the single components mutually incoherent. The time averaged intensity is then given by $I = \sum_{j=1}^{N} |\varphi_{j,\{\beta\}}|^2$. (Note that for the interference effects between the single components to cancel out, the random phase fluctuations $\gamma_j(t)$ have to be much faster than the response time of the medium.)

Inserting the ansatz (2.30) into the propagation equation (2.26), we obtain a system of $N$ equations

$$\beta_j \varphi_{j,\{\beta\}}(x,y) = (\nabla_\perp^2 + \delta n^2(I)) \varphi_{j,\{\beta\}}(x,y) \,, \tag{2.31}$$

that the profiles of the single components $\varphi_{j,\{\beta\}}$ have to solve to form a solitary solution. In other words: each of the components $\varphi_{j,\{\beta\}}$ has to be a guided mode of the waveguide $\delta n^2$ that is induced into the crystal by the superposition of all the components.

The number $N$ of components does not need to be very large. For small $N$ solutions to equation (2.31) are called vector solitons [12]. They can be realized experimentally quite easily. For $N = 2$, for instance, one can take the light from two lasers (such that the beams are mutually incoherent) imprint a gaussian-like profile on one of the beams, a dipole profile on the other beam and then combine the two beams on the input face of the crystal. If the profiles and intensities of the beams are chosen adequately, the result will be a dipole-mode vector soliton [12, 13, 14, 15].

## 2.3 Finding solitary solutions numerically

For several decades now, numerical methods have played an important role in research on solitons [3]. This is due to the fact that even for relatively simple cases, the soliton profiles $\varphi_{j,\{\beta\}}$ cannot be calculated analytically. In these cases one has to rely on numerical methods. Although it might seem trivial, it is essential to keep in mind that any numerical solution to a problem in a continuous space is only an approximation. Computers can only solve

discretised problems. This can lead to numerical calculations that reflect artifacts of the algorithm rather than physically meaningful results [16].

The numerical algorithm used in this work to obtain solitary solution goes back to Petviashvili [17]. The algorithm is well described in references [15, 18]. Therefore, we will only briefly sketch the algorithm.

The basic idea is to represent the $\nabla_\perp^2$ operator in equations (2.31) by a multiplication with the square of the transverse wave vector $\mathbf{k}_\perp^2$ in Fourier space. This transforms equations (2.31) into the following form:

$$\varphi_{j,\{\beta\}}(\mathbf{k}_\perp) = \frac{\hat{F}[\delta n^2(I)\varphi_{j,\{\beta\}}(x,y)](\mathbf{k}_\perp)}{\beta_j + \mathbf{k}_\perp^2}\,, \tag{2.32}$$

where $\varphi_{j,\{\beta\}}(\mathbf{k}_\perp)$ are the Fourier coefficients of $\varphi_{j,\{\beta\}}(x,y)$ and $\hat{F}$ is the operator of the Fourier transform.

The system of equations (2.32) is fixed point equation. In many cases it is enough to iterate fixed point equations to arrive at the solution. However, Petviashvili found that for the iterations to converge, the right hand side of equations (2.32) has to be multiplied with functionals $|M_j[\varphi_{j,\{\beta\}}(x,y)]|^{-1}$, given by

$$M_j[A_j(x,y)] = \frac{\int \mathrm{d}\mathbf{k}_\perp \hat{F}[\delta n^2(I)A_j(x,y)]A_j^*(\mathbf{k}_\perp)}{\int \mathrm{d}\mathbf{k}_\perp(\beta_j + \mathbf{k}_\perp^2)|A_j(\mathbf{k}_\perp)|^2}\,. \tag{2.33}$$

As this functional takes the value $M_j = 1$ if $A_j = \varphi_{j,\{\beta\}}$ multiplying $|M_j|^{-1}$ to the right hand sides of equations (2.32) does obviously not change the fixed point. As was shown by Petviashvili, iterating the equations

$$A_j^{\{n+1\}}(\mathbf{k}_\perp) = |M_j|^{-1}\frac{\hat{F}[\delta n^2(I)A_j^{\{n\}}(x,y)](\mathbf{k}_\perp)}{\beta_j + \mathbf{k}_\perp^2} \tag{2.34}$$

converges very rapidly into the solitary ground state solution. (Note that the light intensity $I = \sum_j |A_j|$ has to be recalculated in each iteration step.) A more advanced analysis of the algorithm can be found in reference [19].

To give a first impression of spatial solitons in nonlinear media, we will have a short look at a so-called dipole-mode vector soliton. We use equations (2.31), assuming that we have $N$ =2 components. In that case, we have two equations coupled over the nonlinear $\delta n^2$ term. In the most simple non-trivial case of a two-component soliton, one of the components is the fundamental, the other component is the dipole mode of the waveguide that

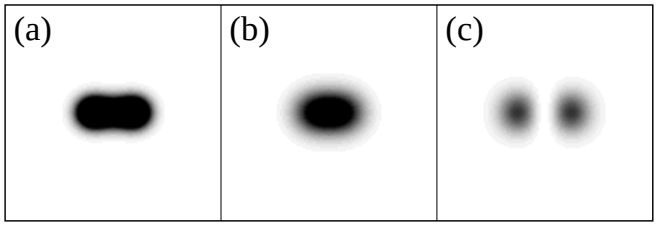


Figure 2.2: A two-component soliton consisting of a fundamental mode in the first and a dipole mode in the second component. The propagation constants are $\beta_1 = 0.5$ and $\beta_2 = 0.3$. (a) shows the total intensity $I = |\varphi_1|^2 + |\varphi_2|^2$, (b) the intensity of the fundamental mode $|\varphi_1|^2$ and (c) the intensity of the dipole mode $|\varphi_2|^2$. The axes are chosen such that the $x$-axis is horizontal and the $y$-axis vertical.

they jointly induce into the medium. Figure 2.2 shows an example of such a soliton with propagation constants $\beta_1 = 0.5$ for the fundamental and $\beta_2 = 0.3$ for the dipole mode. Figure 2.2(a) shows the total intensity $I = |\varphi_1|^2 + |\varphi_2|^2$, that induces a waveguide in the medium, (b) shows the intensity of the first component $|\varphi_1|^2$. That component has a profile identical to the profile of the fundamental mode of the induced waveguide. Figure 2.2(c) shows the intensity of the second component $|\varphi_2|^2$. Its profile is identical to the profile of the dipole mode of the induced waveguide. Note that the two beamlets of the dipole are $\pi$ out of phase. We therefore have a $\pi$ phase-jump at the symmetry line $x = 0$. Note that in figure 2.2, like in all other figures showing a soliton in the $x$-$y$ plane in this work, the $x$-axis is chosen to be horizontal.

We thus have two light beams that jointly induce a waveguide in a medium, while being at the same time guided modes of that waveguide. Hence, when these two beams jointly propagate through the medium, they form a soliton. Neither of the beams would be a soliton in the absence of the other. Calculating such a soliton on a 128×128 grid on a 2.5GHz PC using the Petviashvili algorithm takes only a few seconds.

# Chapter 3

# Stability analysis of solitons

One of the most important problems in the theoretical investigation of optical spatial solitons is the question of the solitons' stability. One of the first phenomena observed in experiments with two-dimensional solitons in media with Kerr-nonlinearity ($\delta n^2 = I$) was the so-called 'catastrophic self-focusing' which is the collapse of the soliton and its focusing into a very small peak, producing light intensities that can even damage the material used [20]. This is a consequence of the instability of two-dimensional solitons in Kerr-media. This instability could be explained by Vakhitov and Kolokolov [4, 5]. Their work lead to the widely used Vakhitov-Kolokolov-criterion for soliton stability. However, the validity of this criterion is restricted to solitons without any nodes or topological charge (vorticity), as the intensity of the soliton must not equal zero anywhere. Nodes are typically encountered at the $\pi$ phase jumps in multipole beams (such as dipoles). Furthermore, the Vakhitov-Kolokolov-criterion cannot account for symmetry-breaking instabilities.

We will quickly reconsider the Vakhitov-Kolokolov-criterion, following the argumentation of Pelinovsky *et al.* [21]. First, we make the ansatz that the soliton solution is slightly perturbed in the following form:

$$A(x,y,z) = \sum_{j=1}^{N} \left( \varphi_{j,\{\beta(Z)\}}(x,y) \exp(i \int_0^z \beta(Z')\mathrm{d}z' + \sum_{n=1}^{\infty} \epsilon^n c_j^{(n)}(x,y,z) \right) \exp(i\gamma_j(t)) \,, \quad (3.1)$$

where $\epsilon$ is a small real number, $Z = \epsilon z$ and the functions $c_j^{(n)}(x,y,z)$ represent the perturbation of the soliton. Note that the propagation constants $\beta_j$ are allowed to vary in $Z$, i.e. to vary slowly in $z$.

Again, we have $N$ components made mutually incoherent by the $\exp(i\gamma_j(t))$ random phase shift. We can thus split $A(x,y,z)$ into $N$ components of the form

$$A_j(x,y,z) = \varphi_{j,\{\beta(Z)\}}(x,y)\exp(i\int_0^z \beta(Z')\mathrm{d}z') + \sum_{n=1}^{\infty}\epsilon^n c_j^{(n)}(x,y,z) \qquad (3.2)$$

Using equation (2.26) to propagate these components,we obtain in first order in $\epsilon$ the set of equations

$$\hat{L}_i c_i^{(1)} = -i\sum_{j=1}^{N}\frac{\partial\beta_j}{\partial Z}\frac{\partial\varphi_{j,\{\beta\}}}{\partial\beta_j}\,, \qquad (3.3)$$

where $\hat{L}_i = -\beta_i + \nabla_\perp^2 + \delta n^2(I)$. Because the solution of the equation $\hat{L}_i c_i^{(1)} = 0$ is known to be $\varphi_{j,\{\beta\}}$, equation (3.3) can be integrated. In the 1D case this can be done straightaway:

$$c_i^{(1)} = -i\varphi_{i,\{\beta\}}(x)\int_0^x\left\{\frac{1}{\varphi_{i,\{\beta\}}^2(x')}\int_0^{x'}\varphi_{i,\{\beta\}}(x'')\sum_{j=1}^{N}\frac{\partial\beta_j}{\partial Z}\frac{\partial\varphi_{j,\{\beta\}}}{\partial\beta_j}\mathrm{d}x''\right\}\mathrm{d}x'\,.$$

Here, we can see why the Vakhitov-Kolokolov-criterion is restricted to nodeless solitons and symmetry-conserving instabilities: the first restriction is due to the factor $1/\varphi_{i,\{\beta\}}^2(x')$ in the first integral. The singularity that appears if the intensity of one of the components equals zero somewhere can make the Vakhitov-Kolokolov-criterion fail, although in some cases it still works despite this singularity, as we will show below. The latter restriction is due to the fact that the above formula can only have solutions with the same symmetries as the solitary solution itself.

In the 2D case a more sophisticated calculation is needed. Details can be found in reference [22]. It can be shown that equation (3.3) has a localised solution only if

$$\sum_{j=1}^{N}\frac{\partial\beta_j}{\partial Z}\frac{\partial P_i}{\partial\beta_j} = 0\,. \qquad (3.4)$$

Here, $P_j = \int|\varphi_j|^2\mathrm{d}x\,\mathrm{d}y$. The set of equations (3.4) has a nontrivial solution only if the determinant

$$D \equiv \det\{\partial P_i/\beta_j\} = 0\,. \qquad (3.5)$$

Equation (3.5) is the Vakhitov-Kolokolov-criterion, generalised to the case of partially incoherent solitons. If $D < 0$ the solitons are stable, according to this criterion. For $D > 0$ they are unstable. (Strictly speaking, we have only shown that the solitons are marginally stable for $D = 0$. Showing that they are stable for $D < 0$ requires a more sophisticated calculation.)

The advantage of the Vakhitov-Kolokolov-criterion (3.5) is its simplicity. Once the solitary solutions are found, one only has to calculate the power $P_j$ of the single components and examine their dependence on the propagation constants $\beta_j$.

The fact that the set of equations (3.3) has a solution only if $D = 0$ shows that the ansatz (3.1) of slowly varying propagation constants $\beta_j$ is valid only if $D = 0$. To make a complete linear stability analysis, one has to perturb the solitary solution by the more general ansatz

$$A_j(x,y,z) = \exp(i\beta_j z)\left\{\varphi_{j,\{\beta\}}(x,y) + \left[(v_j(x,y) + iw_j(x,y))\exp(\gamma z) + (v_j^*(x,y) + iw_j^*(x,y))\exp(\gamma^* z)\right]\right\}, \quad (3.6)$$

where $v_j(x,y)$ and $w_j(x,y)$ represent small perturbations. Inserting the ansatz (3.6) into equation (2.26), we obtain in linear order in $v_i$ and $w_i$

$$\gamma v_j = -\hat{L}_j w_j \quad (3.7)$$

$$\gamma w_j = \hat{L}_j v_j + 2\frac{d(\delta n^2(I))}{dI}\varphi_j \sum_{i=1}^{N} \varphi_i v_i \,. \quad (3.8)$$

Keep in mind that the intensity $I = \sum_{j=0}^{N} |A_j|^2$. As mentioned above, the operator $\hat{L}_j$ is given by

$$\hat{L}_j = -\beta_j + \nabla_\perp^2 + \delta n^2(I) \,. \quad (3.9)$$

In many cases, it is most convenient to combine equations (3.7) and (3.8) into one set of equations:

$$\gamma^2 v_j = -\hat{L}_j \left(\hat{L}_j v_j + 2\frac{d(\delta n^2(I))}{dI}\varphi_j \sum_{i=1}^{N} \varphi_i v_i\right) . \quad (3.10)$$

One has to consider three different scenarios: if the eigenvalue $\gamma$ of the system of equations (3.7) and (3.8) is purely imaginary, one is dealing with an oscillatory mode of the soliton. If $\gamma$ is purely real, one has discovered an

unstable eigenmode of the soliton. This is true even if $\gamma < 0$, because with the simple transformation $w_j \to -w_j$ one gets $\gamma \to -\gamma$. In that case one can choose $v_j$ and $w_j$ to be real functions of $x$ and $y$. Finally, when $\gamma$ has a real and an imaginary component, one has an oscillatory instability. However, as the numerical simulations of soliton propagation show no signs of oscillatory instabilities for the solitons considered in this work, they shall be discarded in the following.

Restricting to unstable eigenmodes with real eigenvalues, the occurrence of unstable eigenmodes can be explained by the collision of a pair of conjugated oscillatory modes of the soliton at $\gamma = 0$. This is shown schematically in figure 3.1. The conjugated pair of oscillatory modes evolves into a pair consisting of an exponentially growing and an exponentially suppressed eigenmode.

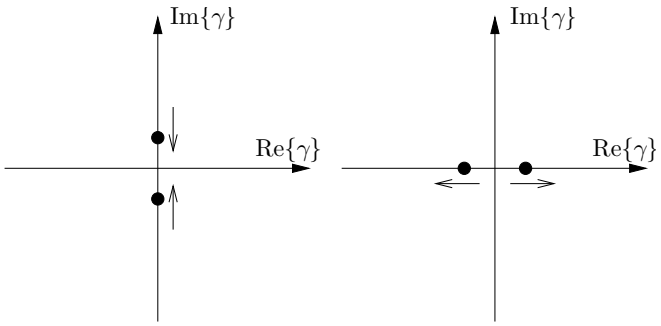


Figure 3.1: At the stability threshold of a soliton, a pair of conjugated oscillatory eigenmodes collides at $\gamma = 0$ and evolves into one exponentially growing and one exponentially suppressed eigenmode.

According to standard linear stability analysis, the soliton is unstable if the system of equations (3.7) and (3.8) has eigenmodes $v_j$ and $w_j$ with $\mathrm{Re}\{\gamma\} > 0$. At the stability threshold $\mathrm{Re}\{\gamma\} = 0$ one has either the case that $\hat{L}_j w_j = 0$ or that $\hat{L}_j v_j + 2(d(\delta n^2(I))/dI)\varphi_j \sum_{i=1}^{N} \varphi_i v_i = 0$. The first case leads directly to the Vakhitov-Kolokolov-criterion. However, it is the second case that leads to symmetry-breaking instabilities not accounted for by the Vakhitov-Kolokolov-criterion.

In reference [23] the stability of $N = 2$ component vector solitons was studied numerically. In the case of solitons consisting of a fundamental mode in the first and a dipole (double-humped) mode in the second component, good agreement was found between the numerical solutions of equations (3.7) and (3.8) on the one hand and the Vakhitov-Kolokolov-criterion on the other

hand. However, the results for the solitons consisting of a fundamental mode in the first and a triple-humped component in the second component do not seem to agree with the Vakhitov-Kolokolov-criterion. Furthermore, the results presented in [23] are obtained for one-dimensional solitons only. Hence, repeating the calculations for two-dimensional solitons yielded new results.

## 3.1 Examples of instabilities

Figure 3.2 shows the unstable eigenvalues obtained by solving equations (3.7) and (3.8) numerically for two-dimensional solitons with a fundamental mode in the first and a dipole mode in the second component (so-called dipole-mode vector solitons). Note that the imaginary part of the unstable eigenvalues is zero.

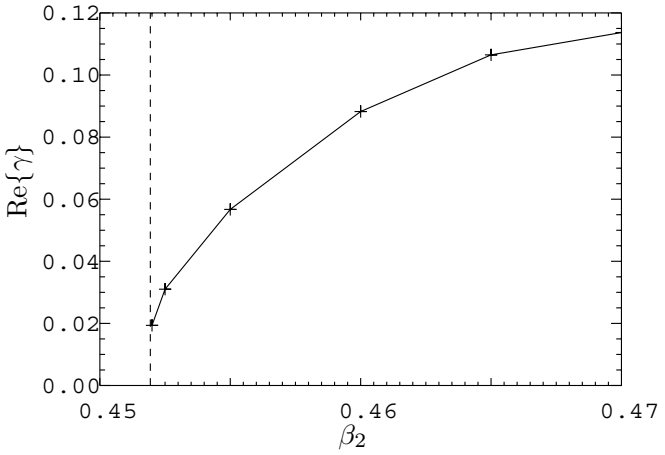


Figure 3.2: The unstable eigenvalues of a $N = 2$ component vector soliton with a fundamental mode in the first and a dipole mode in the second component. The propagation constant of the fundamental mode is $\beta_1 = 0.5$. The vertical dashed line shows the stability threshold predicted by the Vakhitov-Kolokolov-criterion.

The propagation constant of the fundamental mode is kept fixed $\beta_1 = 0.5$ and the propagation constant of the dipole mode $\beta_2$ is varied. As can be seen, the solitons get unstable if $\beta_2$ exceeds a certain threshold. The dashed vertical line in figure 3.2 shows the stability threshold predicted by the Vakhitov-Kolokolov-criterion. It can be seen that the numerical results agree very well with the Vakhitov-Kolokolov-criterion. (Note that solving

the equations (3.7) and (3.8) numerically becomes increasingly difficult near the stability threshold. Hence the threshold cannot be determined to a high precision with this method.)

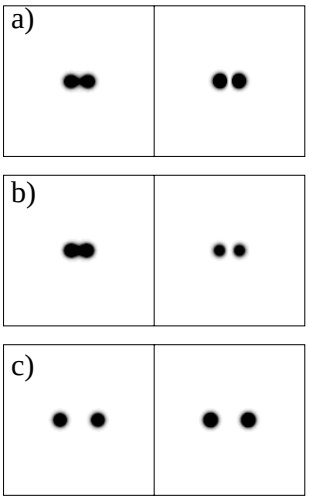


Figure 3.3: (a) shows an unstable dipole-mode vector soliton with propagation constants $\beta_1 = 0.5$ for the fundamental and $\beta_2 = 0.465$ for the dipole component. The left picture shows the fundamental, the right picture the dipole component. (b) shows the square modulus of its unstable eigenmode (the perturbation of the fundamental mode is shown on the left, the perturbation of the dipole mode is shown on the right). (c) shows a snapshot after a propagation of $2L_D$ as the soliton decays. Again, the light beam that initially was the fundamental mode is shown on the left and the dipole beam on the right.

Figure 3.3 shows an example of an unstable dipole-mode vector soliton. (a) shows the intensity profile of both components. The fundamental mode is shown on the left and the dipole mode on the right side. Because the dipole mode is much stronger than the fundamental (its more is more than twice the power of the fundamental) the fundamental beam adjusts its shape to the shape of the dipole and is thus barely recognisable as a fundamental mode. (b) shows the square modulus $v_j^2 + w_j^2$ of the unstable eigenmode (the left picture shows the perturbation in the fundamental, the right one the perturbation in the dipole component). Finally, (c) shows a snapshot of the soliton after a propagation of two diffraction lengths as it decays. Note that the unstable eigenmode does not break the symmetry of the soliton. Figures 3.2 and 3.3 were calculated using the isotropic nonlinearity described

by equation (2.28).

In many publications showing numerical simulations of soliton propagation, the solitons are only subject to computational noise, i.e. the round-off errors of the computer. This is insufficient, as computational noise may have certain symmetries, which can hide the symmetry-breaking unstable eigenmodes of a soliton. In order to excite all instabilities of the solitons, we added random noise to the initial light field put into the medium at $z = 0$. This was done for every simulation of soliton propagation presented in this work. The noise was uncorrelated in $x$ and $y$. For simplicity, we chose uniformly distributed noise. The maximum amplitude of the noise varies in the different simulations presented in this work, but is was typically around 1% of the maximum intensity of the soliton.

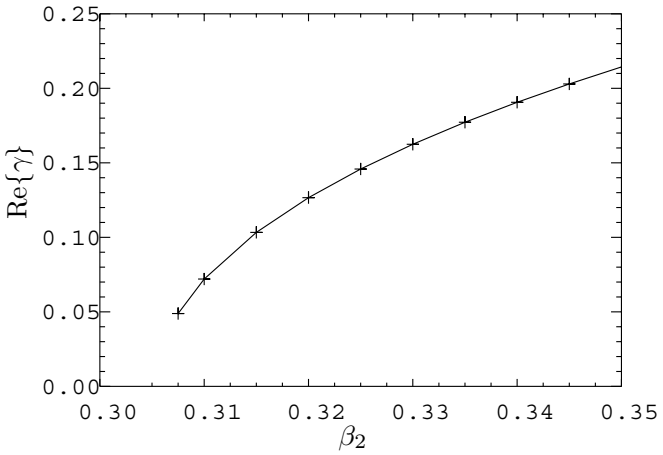


Figure 3.4: The unstable eigenvalues of a $N = 3$ component vector soliton with a fundamental mode in the first and two crossed dipole components in the second and third component. The propagation constant of the fundamental mode is $\beta_1 = 0.5$. Both dipoles have the same propagation constant $\beta_3 = \beta_2$.

To study an example of a symmetry-breaking instability, we take a look at an $N = 3$ component soliton with a fundamental mode in the first and two crossed dipoles in the second and third component. Figure 3.4 shows the unstable eigenvalues obtained by solving equations (3.7) and (3.8) numerically. The propagation constant of the fundamental mode is $\beta_1 = 0.5$ and for the sake of simplicity, we only consider the case where both dipoles have the same propagation constant $\beta_3 = \beta_2$. From the figure, one can see that the solitons get unstable for $\beta_2 \geq 0.305$. The Vakhitov-Kolokolov-criterion,

however, does not predict any stability threshold in that region of parameter space. The reason for that can be seen in figure 3.5. (a) shows a soliton with $\beta_1 = 0.5$ for the fundamental mode (left column) and $\beta_3 = \beta_2 = 0.32$ for the two dipoles (middle and right column). (b) shows the square modulus of the unstable eigenmode and (c) shows a snapshot of the soliton as it decays. The soliton splits up into three beamlets that move away from each other. It can be clearly seen that the instability breaks the soliton's symmetry. Hence, this instability cannot be detected by the Vakhitov-Kolokolov-criterion.

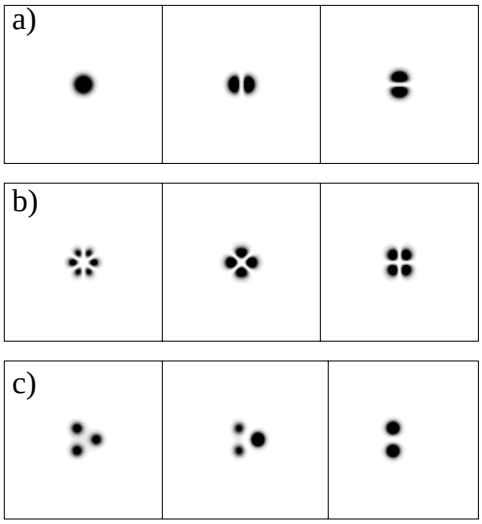


Figure 3.5: (a) shows an unstable vector soliton with propagation constants $\beta_1 = 0.5$ for the fundamental and $\beta_2 = \beta_3 = 0.32$ for the two crossed dipole components. (b) shows the components of the unstable eigenmode and (c) a snapshot of the soliton after three diffraction lengths of propagation as it decays.

Because only the square moduli of the unstable eigenmodes were plotted in figures 3.3 and 3.5, the pictures contain no information about the phase of the eigenmode relative to the soliton. However, the phase of the eigenmode is far from being irrelevant. A look at the equations (3.7) and (3.8) shows that close to the stability threshold $\gamma = 0$ the symmetry-conserving eigenmodes are $\pi/2$ phase-shifted with respect to the soliton (i.e. $|w_j| \gg |v_j|$), whereas in the symmetry-breaking case the eigenmode is in phase with the soliton, i.e. $|w_j| \ll |v_j|$. This is due to the fact that at $\gamma = 0$ one has $\hat{L}_j w_j = 0$ in the symmetry-conserving and $\hat{L}_j v_j + 2(d(\delta n^2(I))/dI)\varphi_j \sum_{i=1}^{N} \varphi_i v_i = 0$ in the symmetry-breaking case.

The unstable eigenmodes that were unveiled solving equations (3.7) and (3.8) numerically prove that the solitons are unstable. In the case when the numerical method does not detect any unstable eigenmode, one cannot be sure that the soliton is indeed stable. Unstable eigenmodes might exist that the numerical method does simply not discover. However, Yang and Pelinovsky showed in 2003 that for the limiting case when the dipole modes are much weaker than the fundamental mode, the stability of the solitons can be proven categorically [24].

To see whether these symmetry-breaking instabilities are also of practical interest, numerical simulations were performed using the anisotropic model for the photorefractive nonlinearity. The results are compared to experimental results obtained at the 'Laser Physics Centre' of the 'Australian National University' (ANU) in figure 3.6. Note that in these pictures the two dipoles are fundamentally different although they have the same propagation constant. This is a consequence of the anisotropy of the photorefractive nonlinearity.

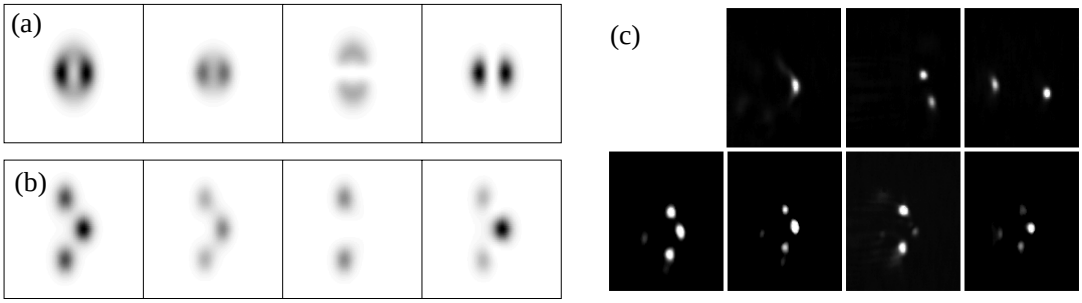


Figure 3.6: (a) shows a soliton calculated in the anisotropic model with $\beta_1 = 0.25$ for the fundamental mode and $\beta_2 = \beta_3 = 0.16$ for the two crossed dipole modes. The soliton is unstable and (b) shows its decay as it is propagated numerically. (c) shows corresponding experimental results, displaying the same kind of decay. In (a) (b) and (c), the leftmost picture shows the total intensity, the other pictures show the single components.

Figure 3.6(a) shows the numerically calculated soliton solution with propagation constants $\beta_1 = 0.25$ for the fundamental mode and $\beta_2 = \beta_3 = 0.16$ for the dipole modes. (b) shows the result of propagating this soliton until the instability breaks it up. The columns show the total intensity of all three components combined, the fundamental mode and the two dipole mode from left to right. It can be seen that the decay is very similar to the one shown

in figure 3.5, hence we can assume that it is caused by the same symmetry-breaking instability.

An experimental observation of this instability is shown in figure 3.6(c). The top row shows the result of propagating each of the components without the others and the bottom row shows the result of a joint propagation of the three components. It can be seen that the numerically obtained results agree very well with the experimental results.

Giving up the constraint $\beta_2 = \beta_3$ one can obtain more complicated kinds of decay, as shown in figure 3.7. Here, the isotropic model was used again. The decay differs from the one shown in figure 3.5 as the soliton does not decay into three beamlets that move away from each other, i.e. into three fundamental solitons, but into one fundamental soliton and one rotating dipole soliton (marked by the dashed circle in the figure). A rotating dipole is a dipole-mode vector soliton that is rotating around its axis as it propagates [25]. The rotating dipole-mode vector soliton remains stable in the subsequent propagation.

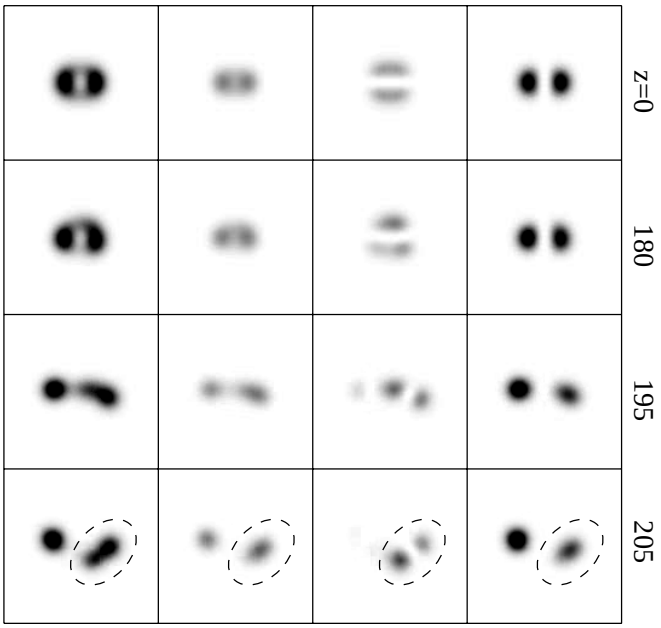


Figure 3.7: Decay of a soliton with propagation constants $\beta_1 = 0.5$ for the fundamental mode, $\beta_2 = 0.25$ for the dipole oriented vertically and $\beta_3 = 0.4$ for the dipole oriented horizontally. It decays into a fundamental soliton and a rotating dipole-mode vector soliton.

More on the symmetry-breaking instabilities of three-component vector solitons can be found in references [26] and [27].

Note that in all the examples presented so far the instability can be eliminated by increasing the intensity of the fundamental mode. The reason for this is that for a sufficiently strong fundamental, the influence of the higher modes on the waveguide induced into the medium can be neglected, hence they can be regarded as guided modes of the waveguide induced by the fundamental mode. Analysing the stability of the vector soliton then comes down to analysing the stability of the fundamental mode, hence the stability analysis of a scalar soliton. And in saturable media, scalar solitons are known to be stable.

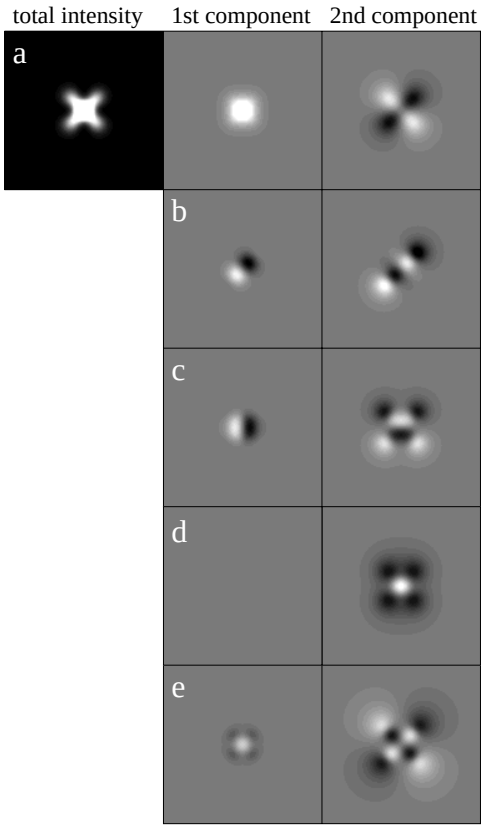


Figure 3.8: A quadrupole-mode vector soliton and its eigenmodes. (a) shows the soliton, (b)-(d) show the symmetry-breaking eigenmodes and (e) shows the symmetry-conserving eigenmode. Shown are the real parts of the modes.

Finally, it has to be stated, that even for relatively simple vector solitons, such as a quadrupole-mode vector solitons, several unstable eigenmodes can play a role in the decay of the soliton. Furthermore, stable eigenmodes,

representing oscillations of the soliton, can also come into play. To give an impression of the complexity of these modes, figure 3.8 show the eigenmodes of a quadrupole-mode vector soliton (i.e. a soliton with a fundamental mode in one and a quadrupole mode in the other component). The propagation constants are $\beta_1 = 0.5$ for the fundamental mode and $\beta_2 = 0.1$ for the quadrupole mode.

Figure 3.8(a) shows the soliton, (b)-(d) show the symmetry-breaking eigenmodes and (e) shows the symmetry-conserving eigenmode. Here we show the real part of the components instead of their intensity to allow for a better understanding of how the eigenmodes deform the soliton. For the propagation constants chosen, the only unstable eigenmode is shown in (d). As can be seen, it leaves the fundamental mode almost unaffected, but it deforms the quadrupole. The other eigenmodes represent oscillating modes of the soliton. However, decreasing the intensity of the fundamental mode (e.g. decreasing $\beta_1$) these eigenmodes get unstable as well. In that case, the decay can be quite complicated and yield very irregular structures. Note that there are probably more eigenmodes that can become unstable than the five shown here. However, these five seem to be the dominating ones.

# Chapter 4

# Modulational and transverse instabilities

## 4.1 Modulational instability

From a practical point of view, the instability of solitons can be seen as a hindrance for their practical use in technological applications. However, it is only due to the instability of plane wave solutions in self-focusing media that bright solitons exist at all. This kind of instability is called modulational instability. Obviously, it is symmetry-breaking. In this case the stability analysis becomes particularly simple. Combining equations (3.7) and (3.8) one obtains for the real part of the eigenmodes the equation

$$\gamma^2 v(x,y) = -\nabla_\perp^2(\nabla_\perp^2 v + 2Iv)\,, \tag{4.1}$$

where we have assumed a medium with Kerr-nonlinearity $\delta n^2(I) = I$. Furthermore, we have used that for plane waves in a Kerr medium we get from equation (2.29) $\beta\varphi = (\nabla_\perp^2 + I)\varphi = I\varphi \Rightarrow \beta = I$. Using the ansatz $v(x,y) = v(\mathbf{r}_\perp) = v_0 \exp(i\mathbf{k}_\perp\mathbf{r}_\perp) + cc$ we get

$$\gamma^2 = 2I|\mathbf{k}_\perp|^2 - |\mathbf{k}_\perp|^4\,. \tag{4.2}$$

The situation is sketched in figure 4.1. Because $I > 0$, the plane wave solution is linearly unstable. This is also the case for saturable self-focusing nonlinearities such as the isotropic and the anisotropic model for the photorefractive nonlinearity.

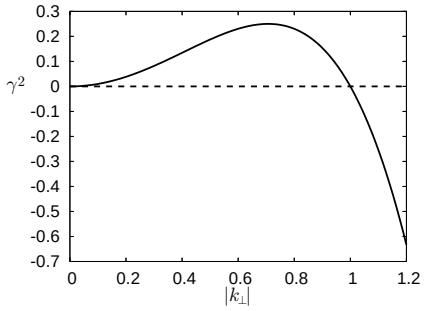


Figure 4.1: Graphical illustration of equation (4.2). In the vicinity of $|k_\perp| = 0$, $\gamma^2$ is always $> 0$.

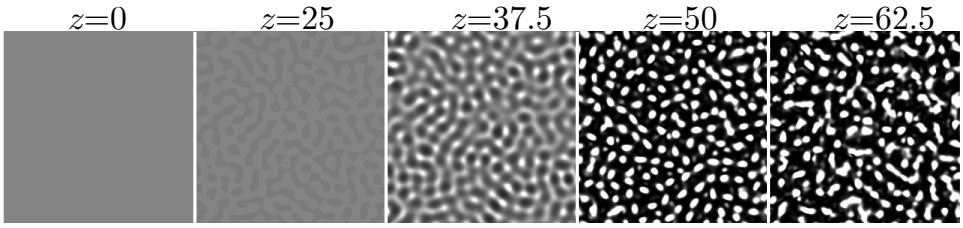


Figure 4.2: Modulational instability in the isotropic model. An initial plane wave is shown after different lengths of propagation.

We start by reviewing modulational instability in the isotropic model. (For more information about this phenomenon see e.g. [28] and references therein.) Figure 4.2 shows how the modulational instability develops. The light intensity is shown after different propagation distances $z$. When the instability sets in, one can clearly see that only perturbations on a certain length scale are growing exponentially. Looking at the picture for $z = 37.5$ one can see that the pattern is still fairly regular, almost hexagonal in some regions. At $z = 50$ solitons form and start to interact. This interaction leads to the completely irregular pattern seen at $z = 62.5$.

So far, we have silently assumed that the light used is fully coherent. However, it has been shown that using partially incoherent light can suppress the modulational instability [29, 30]. Hence, we come back to equation (2.30) and try to represent a spatially homogeneous partially incoherent light beam as a superposition of (infinitely) many coherent, yet mutually incoherent components. The easiest way to do this is to assume that each of the components is a plane wave. However, for the beam to be partially incoherent, these plane waves have to be slightly tilted all at slightly different angles with respect to

the $z$-axis. We hence write

$$A(x,y,0) = \sum_{k_x,k_y} \exp(i(k_x x + k_y y)) \times \frac{L_c}{\sqrt{\pi}} \sqrt{\exp(-(k_x^2+k_y^2)L_c^2/2)}\exp(i\gamma_{k_x,k_y}(t))\,, \qquad (4.3)$$

where $k_x$ and $k_y$ stand for the slight tilting of the different components and $\gamma_{k_x,k_y}(t)$ are random phase factors that are uncorrelated to each other,thus making the single components mutually incoherent. $L_c$ is the coherence length of the light. When two points in the $x$-$y$-plane are further than $L_c$ apart from each other, then the phases of the light in those two points are essentially uncorrelated. $L_c$ is a parameter that can be chosen freely in the numerical simulations. The approach of using a superposition of many components tilted at slightly different angles is also the basis of the so-called coherent density model [31].

It may look surprising that the ansatz (4.3) is able to fully describe an incoherent light field. Shkunov and Anderson proposed in 1998 [32] an equation to describe the propagation of incoherent light through non-instantaneous nonlinear media that seems far more complex than the ansatz (4.3). By using the propagation equation (2.26) to propagate the spatial coherence function $\Gamma(\mathbf{r}_1,\mathbf{r}_2;z) = \langle E^*(\mathbf{r}_2,z,t)E(\mathbf{r}_1,z,t)\rangle$, where the brackets $\langle\ldots\rangle$ denote the average in time, they could show that the spatial coherence function, evolves like

$$\partial\Gamma/\partial z - i\nabla_\rho\nabla_{\mathbf{R}}\Gamma = i\{\delta n^2(\mathbf{r}_1,z) - \delta n^2(\mathbf{r}_1,z)\}\Gamma\,, \qquad (4.4)$$

where $\mathbf{R} = (\mathbf{r}_1+\mathbf{r}_2)/2$ and $\rho = \mathbf{r}_1 - \mathbf{r}_2$. This equation fully describes the evolution of the beam. However, in reference [33] Christodoulides *et al.* could show that equation (4.4) and the ansatz (4.3) are equivalent. Because the latter is numerically more efficient, the following calculations were carried out using the ansatz (4.3).

Obviously, $A(x,y,0)$ from equation (4.3) is a solitary solution, though a trivial one. The stability of this solitary solution depends crucially on the coherence length $L_c$. Reference [29] contains a detailed study of the stability for the one-dimensional case. The two-dimensional case is more difficult and is still not completely understood [34]. Figure 4.3 confirms that in analogy to the one-dimensional case, the instability can be suppressed. The pictures show the propagation of a light beam identical to the one shown in figure 4.2.

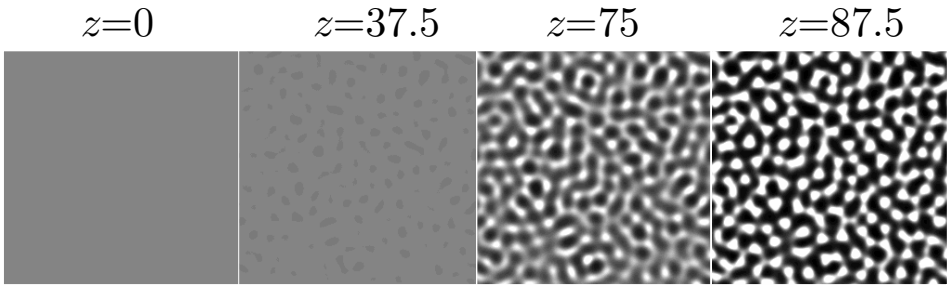


Figure 4.3: Modulational instability in the isotropic model. Here, the light is incoherent. All other parameters are identical to figure 4.2. $L_c = 14$.

The only difference is that it is partially incoherent. One can see that the instability sets in much later. Furthermore, the filaments have a bigger size. Hence, using partially incoherent light does suppress modulational instability. In fact, using light with a smaller coherence length than the light used in figure 4.3 leads to a complete suppression of the instability.

### 4.1.1 Theory and experiment

As experiments on modulational instability are most conveniently carried out in photorefractive crystals, one has to simulate the propagation of initially plane waves through a medium with a nonlinear response given by equation (2.20) (the anisotropic model) to compare theoretical and experimental results. The photorefractive medium used in the experiments was an SBN crystal with an estimated value of $r_{111}$ =180pm/V for the relevant element of the electro-optic tensor. The light used came from a frequency-doubled Nd:YAG laser (532nm).

Figure 4.4 shows the propagation of initially plane waves with different coherence lengths $L_c$. One can immediately see that the anisotropy of the photorefractive nonlinearity leads to important differences to the case of an isotropic saturable nonlinearity. For all coherence lengths $L_c$ the plane wave first breaks up into stripes parallel to the $y$-axis (perpendicular to the crystal's $\hat{c}$-axis). Hence, it seems that the unstable eigenmode with the highest growth rate is a stripe solution. However, for longer coherence lengths $L_c$ these stripes are again unstable and break up into filaments, thus yielding a final state similar to the one already encountered in the isotropic saturable model. Here as well, the filaments start to interact and hence form a completely irregular pattern.

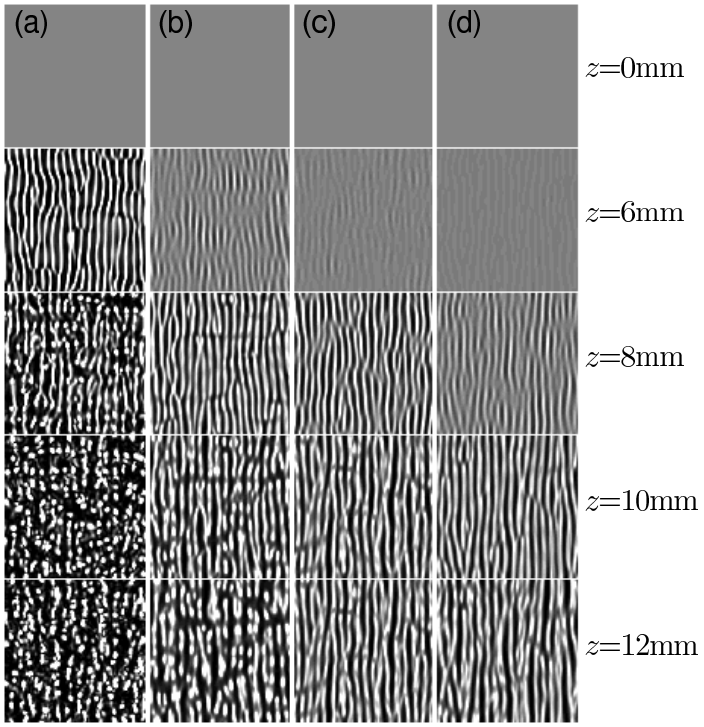


Figure 4.4: The propagation of initially plane waves with different coherence lengths $L_c$, calculated numerically. $L_c = \infty$ for (a), 16$\mu$m for (b), 13$\mu$m for (c) and 11$\mu$m for (d). For these simulation the anisotropic model equation (2.20) was used.

However, for shorter coherence lengths the instability of the stripes can be suppressed as figure 4.4(d) shows. The stripes persist for arbitrarily long propagation distances without breaking up into filaments. Partially incoherent light can therefore be used to generate stable stripe solutions in photorefractive nonlinearities, which is a point that we will investigate in more detail later on in this chapter.

Decreasing $L_c$ further leads to a complete suppression of the modulational instability, i.e. the plane wave can propagate through the medium without experiencing any changes to its phase front. We therefore have a more complicated scenario than in the case of the isotropic nonlinearity. With the isotropic nonlinearity we only had one threshold for $L_c$, where modulational instability sets in. Now, we have to consider two thresholds: the first threshold, where the stripe solutions become stable, and a second threshold, where modulational instability is suppressed altogether.

At the Westfälische Wilhelms-Universität Münster, Björn Gütlich carried

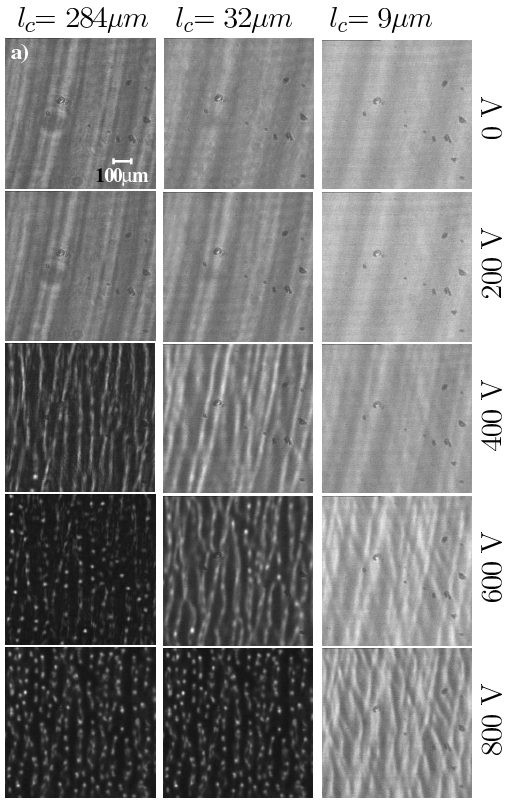


Figure 4.5: The propagation of initially plane waves with different coherence lengths $L_c$, as observed in experiment. Each column shows beams with equal coherence length, each row the output after propagating through an equally strong biased photorefractive crystal (picture by Björn Gütlich) [35].

out experiments that show good qualitative agreement with the numerical results. The results are shown in figure 4.5. Note that in experiment the beam can only be observed after a fixed propagation length (the length of the crystal used). Hence all pictures in figure 4.5 show the output after 23mm of propagation. However, the electric bias field applied to the crystal was varied, thus varying the strength of the nonlinearity. It can be shown from equations (2.12) and (2.20) that this is theoretically equivalent to varying the propagation length, provided that the transverse lengths (along the $x$- and $y$-axis) are scaled accordingly. Hence, it is legitimate to compare figures 4.4 and 4.5 and to state that there is a good qualitative agreement. The experimental pictures also show that the plane wave first breaks up into stripes (as is most clearly seen in the row for $E_0$ =400V). For large coherence

lengths ($L_c$ =284$\mu$m and 32$\mu$m) these stripes are unstable and break up into filaments. However, for $L_c$ =9$\mu$m this is no longer the case. Note also, that the stripes survive a much stronger nonlinearity for $L_c$ =32$\mu$m (up to 600V) compared to the (almost) coherent case $L_c$ =284$\mu$m.

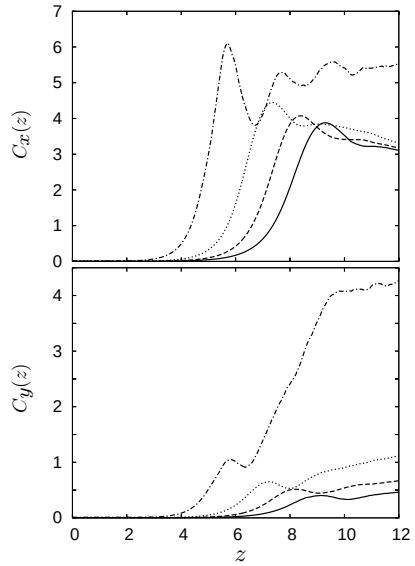


Figure 4.6: The 'weighted contrast' along the $x$- and $y$-axis as obtained from the simulations shown in figure 4.4. The dash-dotted line corresponds to column (a) in figure 4.4, the dotted line to (b), the dashed line to (c) and the solid line to (d). The propagation distance $z$ is given in mm.

To quantify the difference between the $x$- and the $y$-axis, one can use a measure, which might be called 'weighted contrast' which is defined as follows:

$$C_x(z) = \langle\{N_{Max}(y)(\langle I_{max}\rangle(y) - \langle I_{min}\rangle(y))/(\langle I_{max}\rangle(y) + \langle I_{min}\rangle(y))\}\rangle_y\,,$$
$$C_y(z) = \langle\{N_{Max}(x)(\langle I_{max}\rangle(x) - \langle I_{min}\rangle(x))/(\langle I_{max}\rangle(x) + \langle I_{min}\rangle(x))\}\rangle_x\,. \quad (4.5)$$

Here, $N_{Max}(y)$ and $N_{Max}(x)$ are the number of intensity maxima along the $y$ and $x$ axis respectively. $\langle I_{max}\rangle(y)$ is the average value of an intensity maximum along the $y$ axis. $\langle I_{min}\rangle(y)$, $\langle I_{max}\rangle(x)$ and $\langle I_{min}\rangle(x)$ are defined analogously. To calculate $C_x(z)$ and $C_y(z)$, we performed the average over the entire area visible in figure 4.4. The result is shown in figure 4.6.

One can see from figure 4.6 that the intensity modulation is much weaker along the $y$ than along the $x$-axis for all coherence lengths $L_c$. Furthermore,

the intensity modulation along the $y$-axis is suppressed much stronger by decreasing $L_c$. This confirms that we have to deal with two different thresholds: one at which stripes along the $y$-axis become stable, and one where modulational instability is suppressed altogether.

The above results motivate a more careful investigation of solitary stripe solutions in photorefractive media. Prior to the investigation of partially incoherent light it was believed that such solutions are always unstable because of a phenomenon known as transverse instability, which is the topic of the next section.

## 4.2 Transverse instability

Looking at equations (2.29) and (2.28), one quickly sees that there is a set of solitary solutions which is infinitely extended in one direction and localised in the other direction. This means that there are solitary solutions having the form of infinitely long stripes. The profile of these stripes corresponds to a solitary solution in a system with only one transverse dimension and is hence easy to calculate. However, using fully coherent light, they are unstable. The stripe breaks up into filaments that start to interact with each other. This effect is called transverse instability.

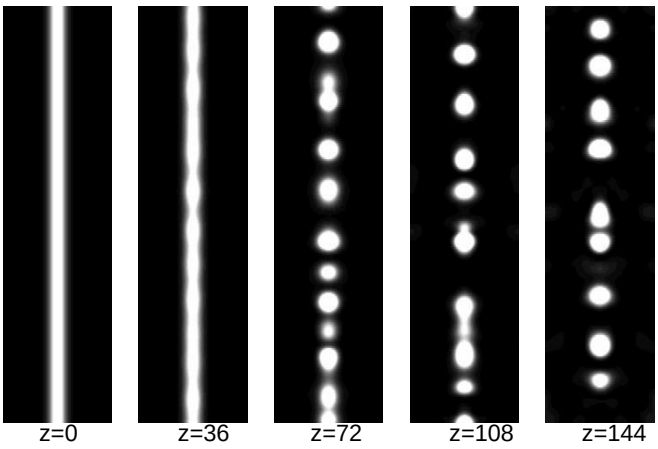


Figure 4.7: A solitary stripe solution of equation (2.29) and the isotropic model equation (2.28) as it decays under the influence of the transverse instability.

An example is shown in figure 4.7. The effect of transverse instability is closely related to modulational instability. And indeed, figure 4.7 resembles

the decay of the stripes in figure 4.4. Remember, however, that figure 4.7 was calculated using the *isotropic* model.

In analogy to modulational instability, transverse instability can be eliminated by using partially incoherent light. However, there is one important difference: to eliminate the transverse instability of a solitary stripe solution, one does not have to reduce the coherence along both spatial transverse dimensions, but only along one. It is sufficient to reduce the coherence along the stripe. Hence, at the input of the medium we use:

$$\begin{aligned} A(x,y,0) &= \varphi_{1\mathrm{D}}(x)\sum_{k_y}\exp(ik_y y)\times \\ &\quad \frac{L_c}{\sqrt{\pi}}\sqrt{\exp(-k_y^2L_c^2/2)}\exp(i\gamma_{k_y}(t))\,, \end{aligned} \tag{4.6}$$

where $\varphi_{1\mathrm{D}}(x)$ is the profile of the 1D solitary solution. For the other terms, see equation (4.3).

In reference [36] Anastassiou *et al.* present theoretical and numerical results showing the suppression of the transverse instability by reducing the degree of coherence of the light used. These results are complemented by experimental results presented in the same paper. However, as the theoretical and numerical results are obtained for a medium with Kerr-nonlinearity, whereas the experiments were carried out in a photorefractive crystal, it seems necessary to reproduce these results (i) using a saturable nonlinearity and (ii) using the full anisotropic model for the photorefractive nonlinearity.

Figure 4.8 shows the same scenario as figure 4.7, only that now the input beam is made spatially incoherent along the $y$-axis, using equation (4.6) with $L_c = 3$. One can see from figure 4.8 that the incoherence clearly suppresses the transverse instability, even if it is still present in that example. However, further decreasing the degree of coherence does lead to a complete elimination of the transverse instability. Hence, partial incoherence along one spatial direction offers a possibility to study 1D solitary solutions in bulk media by eliminating the undesired effect of transverse instability.

However, the absence of transverse stability does not necessarily mean that the solitary solution is now stable. Figure 4.9 shows again the propagation of the light stripe from figure 4.8, but this time with $L_c = 1.5$. There is indeed no sign of the transverse instability. Instead, we observe a snake instability. Snake instabilities are well known from experiments on dark soliton stripes in self-defocusing media [37, 38], and also play a role in Bose-Einstein condensates with positive scattering length [39]. Here, however, the medium

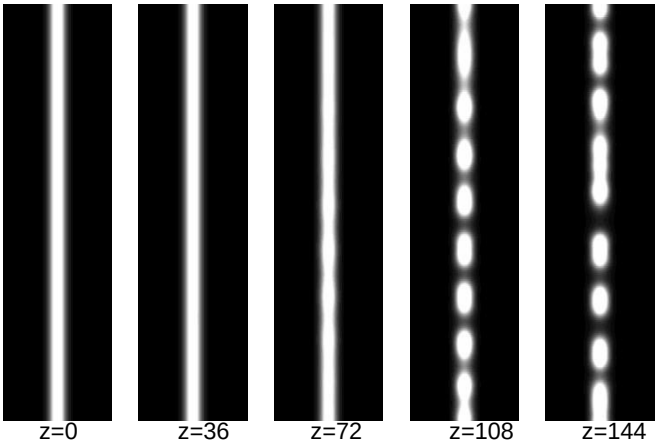


Figure 4.8: A solitary stripe solution of equations (2.29) and (2.28), that is made partially incoherent along the $y$-axis with a coherence length of $L_c = 3$. All other parameters are identical to the ones used in figure 4.7. One can see that the transverse instability is suppressed, but still present.

is self-focusing and the existence of the instability is rather surprising. This is, to my best knowledge, the first example of a snake instability in self-focusing media. Future investigations will show whether this phenomenon is limited to a few special cases or whether it is something to be taken into account when dealing with partially incoherent light.

The snake instability only appears for large propagation distances, which means that it is weak and hard to excite. Therefore, it is questionable whether there is a realistic chance of observing this instability in experiment. Most probably, photorefractive crystals available to researchers will not be sufficiently long to observe this effect.

### 4.2.1 Theory and experiment

As in the case of modulational instability, the relevance of the theoretical results can only be judged by comparison with experimental data. And again, one has to take care of the anisotropic nature of photorefractive crystals to bring theory and experiment into agreement. One consequence of the anisotropy is that solitary stripe solutions that are oriented along the crystal's $\hat{c}$-axis (the $x$-axis throughout this thesis) cannot exist. The reason for that is that for a light stripe oriented along that axis no screening field can build up. The electrons that are lifted into the conduction band drift under the influence of the external field, which is also parallel to the $\hat{c}$-axis and therefore

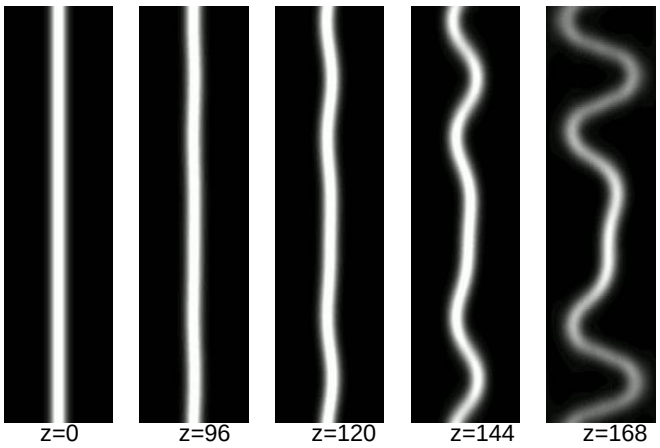


Figure 4.9: A solitary stripe solution of equations (2.29) and (2.28), that is made partially incoherent along the $y$-axis with a coherence length of $L_c = 1.5$. All other parameters are identical to the ones used in figure 4.7. The transverse instability is completely suppressed. Instead, for long propagation distances one observes a snake instability.

will not leave the illuminated area to recombine with ionised donors to build up a space charge field.

Therefore it is necessary to consider the behaviour of coherent light stripes in photorefractive media, depending on their orientation.

Figure 4.10 depicts typical results of such an investigation. When the light stripe is perpendicular to the crystal's ĉ-axis, it behaves much like it would in an isotropic medium (see figure 4.7). The reason for this is obvious, since the isotropic model is just the 1D solution of the anisotropic potential equation (2.27).

When the stripe is oriented parallel to the crystal's ĉ-axis, the stripe also breaks up into filaments. However, this effect cannot be called transverse instability, because it is not a solitary solution that is breaking up. As mentioned above, due to the infinite (very large) extent of the beam parallel to the externally applied field, a screening field cannot develop. Consequently, a homogeneous light stripe oriented parallel to the crystal's ĉ-axis will always diffract.

Finally, considering the case where the light stripe is oriented under an angle of 45° with respect to the crystal's ĉ-axis, one can see that the transverse instability appears just like in the isotropic case. However, the subsequent dynamics are more complex due to the anisotropy of the medium.

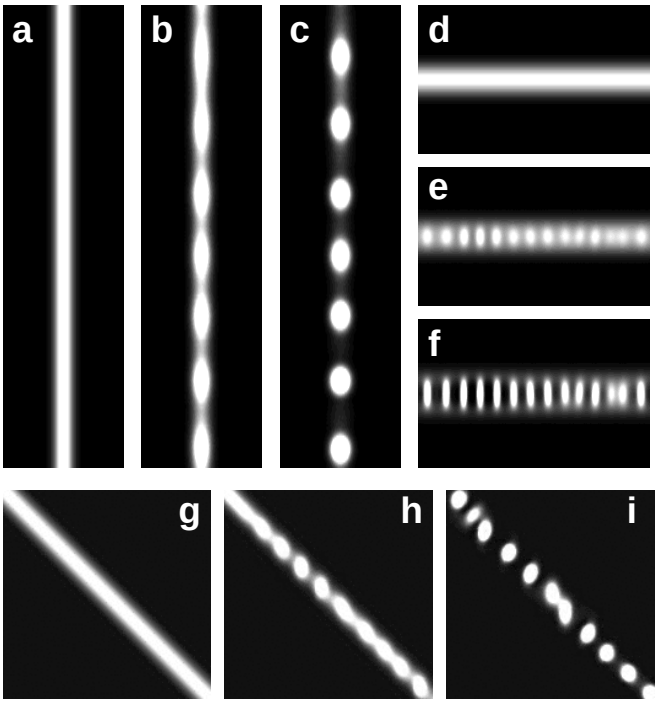


Figure 4.10: Numerical results for the propagation of coherent light stripes through a photorefractive medium: (a-c) the soliton stripe is perpendicular to the external electric field, (d-f) the soliton stripe is parallel to the field, and (g-i) the stripe is tilted at 45° with respect to the field.

These numerical results are in good agreement with experimental data provided by Wen-Hen Chu and Ming-Feng Shih shown in figure 4.11.

We proceed to investigate the behaviour of partially incoherent light stripes in photorefractive media. Again, we use a partially incoherent light beam described by equation (4.6) at the input of the medium. Equation (4.6) can also be written in a different form:

$$\begin{aligned} A(x,y,0) &= \varphi(x)\sum_{\theta}\exp(i2\pi\sin(\theta)y/\lambda)\times \\ &\quad (\pi^{1/2}\theta_0)^{-1}\sqrt{\exp(-\theta^2/\theta_0^2)}\exp(i\gamma_\theta(t)) \approx \\ \varphi(x)\sum_{\theta}\exp(i2\pi\theta y/\lambda)&(\pi^{1/2}\theta_0)^{-1}\sqrt{\exp(-\theta^2/\theta_0^2)}\exp(i\gamma_\theta(t))\,, \end{aligned} \tag{4.7}$$

where $\theta$ is the angle at which the single components are tilted with respect to the $z$-axis and $\theta_0$ determines the coherence length. The last expression in equation (4.7) is obtained by replacing $\sin(\theta)$ by $\theta$, which is perfectly valid for

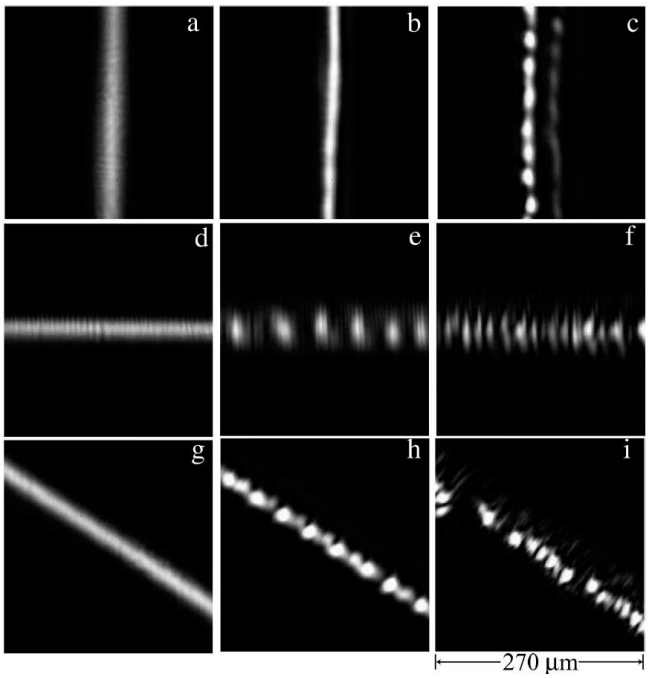


Figure 4.11: Experimentally observed instability of light stripes in a photorefractive SBN crystal. The pictures (a), (d) and (g) show the input face of the crystal, all others the output face. The crystal used was a cube with 7mm long edges. The applied voltage was 1kV in (b) and (h), 2kV in (c) and (i), 0.5kV in (e) and 1KV in (f). Note the good agreement with figure 4.10. (Pictures by Wen-Hen Chu and Ming-Feng Shih of the Taiwan National University.) [40]

the degrees of coherence used in the following. The relation $L_c = \lambda/(\sqrt{2}\pi\theta_0)$ follows immediately from the comparison between equations (4.6) and (4.7).

The results of the numerical simulations are shown in figure 4.12. (a) and (b) show the suppression of the transverse instability for the case of a light stripe perpendicular to the crystal's $\hat{c}$-axis. Again, the results of the simulation are rather similar to the results obtained for the isotropic model. For a moderate degree of incoherence, the instability is suppressed, increasing the incoherence further leads to the elimination of the instability. This is shown more clearly in figure 4.12(e), which shows a numerical estimate of the growth rate of the transverse instability as a function of $\theta_0$. (Remember that increasing $\theta_0$ decreases the coherence length $L_c$.) The growth rate of the instability clearly goes to zero for $\theta_0 \approx 0.375°$. The corresponding coherence length is $L_c = \lambda/(\sqrt{2}\pi\theta_0) \approx 18.3\mu$m. This is roughly the spatial extent

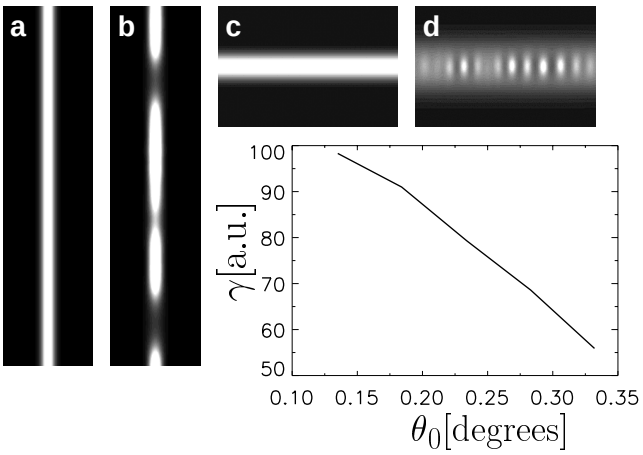


Figure 4.12: Numerical results for the propagation of partially incoherent light stripes through a photorefractive medium: (a-b) the soliton stripe is perpendicular to the external electric field, (c-d) the soliton stripe is parallel to the field, and (e) shows a numerical estimate of the growth rate of the transverse instability stripes perpendicular to the crystal's ĉ-axis as a function of $\theta_0$.

that a soliton formed from fully coherent light would have in the $y$-direction (around $10\mu$m). Comparing this to the stabilisation of the stripes developing from modulational instability in figure 4.4 we notice that there the stripes could only be stabilised for smaller coherence lengths of around $11\mu$m. This is probably due to the additional perturbation of the single stripes by interaction with its neighbours.

Figures 4.12(c) and (d) show the case of a stripe parallel to the crystal's ĉ-axis. Here as well, the filamentation is not as pronounced as in the coherent case, which leads to a diffraction of the stripe, as no screening field, and hence no nonlinear index shift can develop.

The case of an intermediate orientation of the partially incoherent beam is left for future research, as it requires more computational resources than the orientation parallel and perpendicular to the $\hat{c}$-axis.

Again, the agreement with the experimental results provided by Wen-Hen Chu and Ming-Feng Shih and shown in figure 4.13 is quite satisfactory. Note that the experimental realization of light stripes that are incoherent along only one spatial direction, while being completely coherent along the other, is quite difficult, so that the light stripes shown in figure 4.13 are not fully coherent along their profile, which leads to a broadening of the stripes.

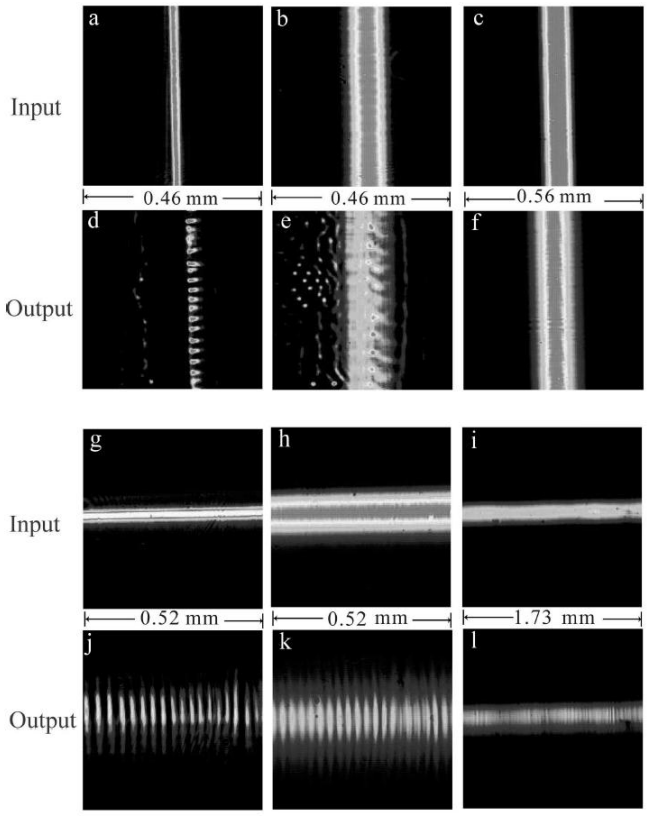


Figure 4.13: Experimentally observed instability of partially incoherent light stripes in a photorefractive SBN crystal. (Pictures by Wen-Hen Chu and Ming-Feng Shih of the Taiwan National University.)

Despite these difficulties in comparing numerical and experimental results, one can state that the use of partially incoherent light can suppress the transverse instability of light stripes. Furthermore, the differences observed using different orientation of the stripes emphasises the need to properly consider the anisotropy of photorefractive crystals when carrying out experiments.

# Chapter 5

# Stabilisation of bright vortices

In many areas of physics vortices play an important role. They can be found in the theory of super-conduction as well as in Bose-Einstein-condensates and in liquid crystals. In nonlinear optics vortices have attracted much attention for more than two decades now. Vortices made their first appearance in nonlinear optics as phase defects in otherwise homogeneous light beams. In self-defocusing media these phase defects can self-trap and thus form 'dark solitons' [41].

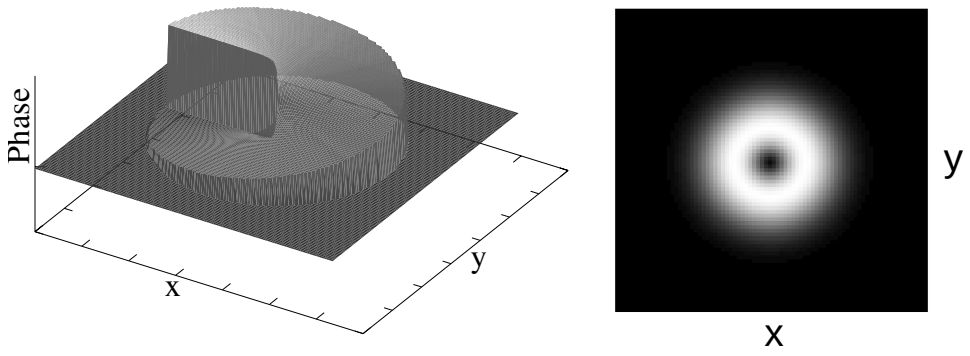


Figure 5.1: A schematic representation of a bright vortex ring. The left picture shows the phase structure, the right one the intensity profile.

However, since this work focuses on self-focusing media, we will only consider so-called bright vortex rings, i.e. light beams with an annular intensity profile and a helical phase structure. (See figure 5.1.) Such rings can be solitary solutions of the nonlinear propagation equation (2.26) [42], provided that the nonlinearity is isotropic. (In anisotropic media solitary solutions

with a topological charge cannot exist, because such solutions need to be radially symmetric.) However, vortex ring solitons are well known to be unstable when they are fully coherent [43]. The ring breaks up into filaments that fly off the ring. This effect seems to be connected to the phenomenon of transverse instability discussed in the previous chapter. The vortex ring can be thought of as a stripe that is bent so that it closes to a ring. The vorticity prevents the beam from merging into a conventional gaussian shaped ground-state soliton. This is due to the fact that – as can be seen in figure 5.1 – there is a $\pi$ phase shift going from point $(x, y)$ to point $(-x, -y)$ (with $(x = 0, y = 0)$ being the centre of the vortex).

In the last chapter we have demonstrated that the transverse instability can be eliminated by making the light stripes partially incoherent along their direction of infinite spatial extent. Something similar should be possible for vortex solitons. However, the situation here is more complicated. It is not possible to make the beam partially incoherent only along its azimuthal direction and to preserve the topological charge at the same time. The reason for this will be discussed below.

Before going into a detailed discussion about the interaction of partially incoherent bright vortex rings with self-focusing media, it has to be pointed out that even in linear optics the properties of partially incoherent vortices are nontrivial and subject of ongoing investigations [44].

## 5.1 Numerical evidence of vortex stabilisation

As mentioned above, the generation of partially incoherent vortices is not an entirely trivial task. There are several possible ways of doing this, but the most straightforward approach is probably to take a partially incoherent plane wave and imprint the vortex intensity profile and phase structure on it. The results thus obtained will most likely not be optimal, but they allow for a first evaluation of the basic effects that partial incoherence has on the vortex propagation. We thus choose as initial profile

$$\begin{aligned} A(r, \varphi, z = 0) &= r \exp(-r^2/b^2) \exp(im\varphi) \sum_{\theta_x, \theta_y} \exp(i2\pi(\theta_x x + \theta_y y)/\lambda) \times \\ &\quad (\pi\theta_0)^{-1/2} \sqrt{\exp(-(\theta_x^2 + \theta_y^2)/\theta_0^2)} \exp(i\gamma_{\theta_x, \theta_y}(t)) \,, \end{aligned} \tag{5.1}$$

where $b$ determines the diameter of the vortex and $m$ is the topological charge of the vortex ($m = 1$ unless otherwise noted). The degree of coherence is

controlled like in equation (4.7).

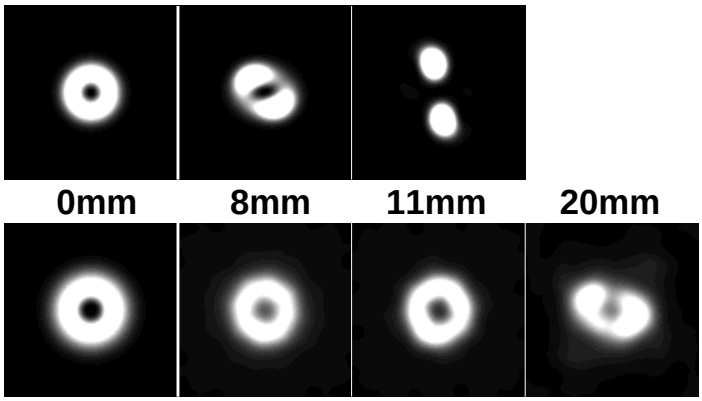


Figure 5.2: Comparison between the evolution of a vortex created by coherent (top row) and partially incoherent (lower row) light ($\theta_0 = 0.38°$).

Figure 5.2 shows the comparison between the evolution of a vortex created by coherent and partially incoherent light. A stabilising effect can indeed be observed. The incoherent vortex survives almost twice the propagation distance of the coherent one. However, using the input described by equation (5.1) a complete elimination of the instability was not possible, because for larger values of $\theta_0$ the incoherence induced diffraction becomes so strong that most of the vortex' intensity is radiated off before the instability can set in.

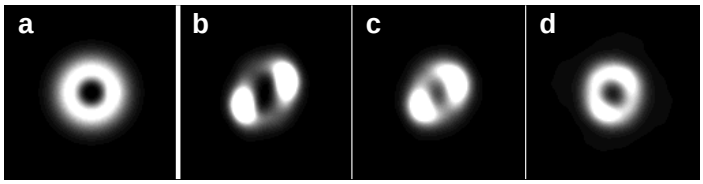


Figure 5.3: Numerical results showing the stabilisation of the vortex with growing incoherence: (a) input intensity, (b) vortex after 9mm of propagation for the coherent case, (c) vortex after 9mm for the partially incoherent case, $\theta_0 = 0.14°$, and (d) vortex after 9mm for the partially incoherent case, $\theta_0 = 0.29°$.

Figures 5.3(a-d) show the numerical results for the propagation of an input beam carrying a phase singularity (a) after the total propagation (9 mm) in a nonlinear medium for the coherent case (b) and two different partially incoherent beams (c,d), corresponding to the values $\theta_0 = 0.14°$ and

$\theta_0 = 0.29°$, respectively. To allow for an easy comparison with results from the last chapter, we note that $\theta_0 = 0.29°$ corresponds to a coherence length $L_c \approx 10$. The most obvious difference to the scenario of the propagation of a coherent vortex is that the vortex decay undergoes a visible delay when the degree of incoherence grows. Furthermore, in the incoherent case the vortex changes its profile only very slowly as it propagates and thus can be considered as being in a transition stage between the decay and stabilisation.

The stabilisation of bright vortices by incoherent light has also been confirmed by experiments performed by Chien-Chung Jeng and Ming-Feng Shih of the National Taiwan University [45]. Although they used a photorefractive crystal (i.e. an anisotropic nonlinearity) for their experiments, in which vortices do not exist as a solitary solution at all, the use of partially incoherent light led to a strong stabilising effect on the propagation of the vortices. We have to note though that for experiments on incoherent vortices in photorefractive crystals another effect might be important for the stabilisation of the vortex. In reference [46] it could be shown that nonlocal effects can have a strong stabilising effect on vortices. Since photorefractive crystals are strongly nonlocal, the interplay between the reduced degree of coherence of the light and the nonlocality calls for further investigations into the subject. However, these are left for the future.

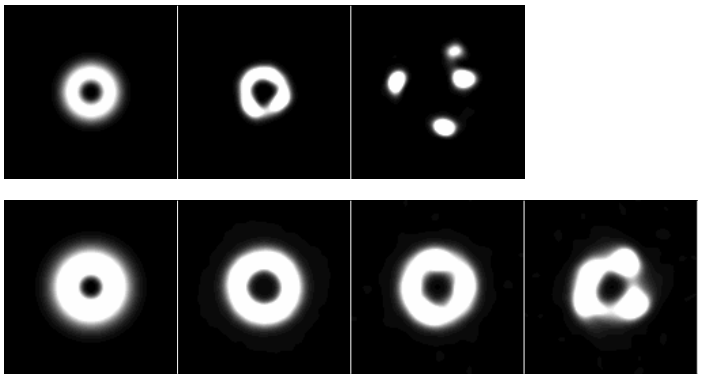

Figure 5.4: Propagation of a double-charge vortex ($m = 2$) in (top row) the coherent case at $z$ =0, 8.6, and 14.5 mm, and (bottom row) in the partially incoherent case with $\theta_0 = 0.35°$ at $z$ =0, 8.6, 14.7, and 18.8 mm.

We have also studied the propagation of a double-charge vortex beam (i.e. $m = 2$) in both the coherent and the partially incoherent case, as shown in Fig. 5.4. The initial perturbation in both cases has been chosen to be very small in order to obtain a clearer picture of the instability, therefore

the propagation distances are quite long. In numerics, since we have the possibility to observe long propagation distances, we did not find that the vortices can be completely stabilised by decreasing the degree of coherence. When using values of $\theta$ far above the value $\theta = 0.35°$ used in Fig. 5.4, we observe that the vortex just radiates off a lot of its intensity and then decays. The problem is obviously that the vortices are not only incoherent along the azimuthal, but also the radial direction.

Hence, it could be shown that reducing the degree of spatial coherence can suppress the azimuthal instability of bright vortex solitons. However, when the solitons are generated by imprinting the intensity and phase structure of a vortex on an incoherent plane wave, the vortices are incoherent not only along the azimuthal, but also the radial directions, which leads to strong intensity losses to radiation. To circumvent this problem, it would be necessary to generate incoherent vortex solitons in a different way. One way might be to combine many coherent vortices with different topological charges into one incoherent vortex soliton. This idea will be elaborated in section 5.3. Before that, however, it is useful to consider the problems one faces when trying to unveil the topological charge of an incoherent light beam.

## 5.2 Spatial coherence singularities

The observation of the stabilising effect of partially incoherent light on self-trapped vortex beams calls for additional studies of the specific properties of partially coherent light carrying phase singularities and propagating in a nonlinear medium. Indeed, if a vortex-carrying beam is partially incoherent, the phase front topology is not well defined, and statistics are required to quantify the vortex phase. In the case of strong incoherence neither the helical phase nor the characteristic zero intensity at the vortex centre can be observed directly.

The problem has been pointed out and – partly – solved by Palacios *et al.* [47]. Under linear propagation an incoherent vortex loses its most obvious characteristic: the vanishing light intensity in the centre. The reason for this becomes immediately clear when reconsidering equation (5.1). The incoherent vortex can be thought of as a superposition of many components that propagate all in slightly different directions. In the absence of a nonlinearity each of these components will continue to propagate in that direction without interacting with the others. Each of the components does have a dark centre.

But as they propagate in different directions, the centres of the components move away from each other, such that after a certain propagation distance there is not only light in the centre of the incoherent vortex, but indeed there won't even be an intensity minimum in the centre anymore.

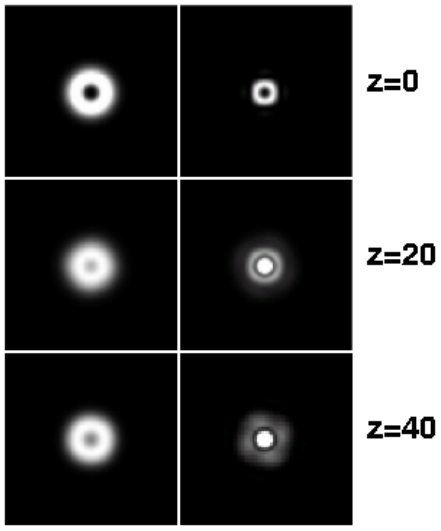


Figure 5.5: Images of the intensity (left column) and the modulus of the cross-correlation (right column) of an incoherent vortex with $\theta_0 = 0.64°$.

How can the topological charge of the beam be unveiled in that case? Obviously, one will have to use the spatial coherence function

$$\Gamma(\mathbf{r}_1, \mathbf{r}_2; z) = \langle E^*(\mathbf{r}_2, z, t) E(\mathbf{r}_1, z, t) \rangle \ , \tag{5.2}$$

where the brackets $\langle \ldots \rangle$ denote the average in time. The problem is to find the fingerprint of vorticity in this function. Palacios *et al.* [47] suggested to consider the cross-correlation $\Gamma(-\mathbf{r}, \mathbf{r})$. They could show that for the case of linear propagation of the incoherent vortex the phase singularities manifest themselves in a dark ring in the cross-correlation $\Gamma(-\mathbf{r}, \mathbf{r})$.

The cross-correlation also seems to be well-suited for a more in-depth investigation of the nonlinear propagation of incoherent vortices. Hence, the numerical simulations from the previous section were repeated with two differences: First, we used a modified form of the nonlinearity

$$\delta n^2 = \frac{I}{1 + sI} \tag{5.3}$$

instead of equation (2.28). Here, $s$ is a saturation parameter chosen to be $s = 0.5$. The reason to introduce this saturation parameter is that it has an

additional stabilising effect on the vortices, thus making it possible to study *stable* incoherent vortex solitons. The second difference to the simulations from the previous section is that now, the cross-correlation is calculated in each propagation step.

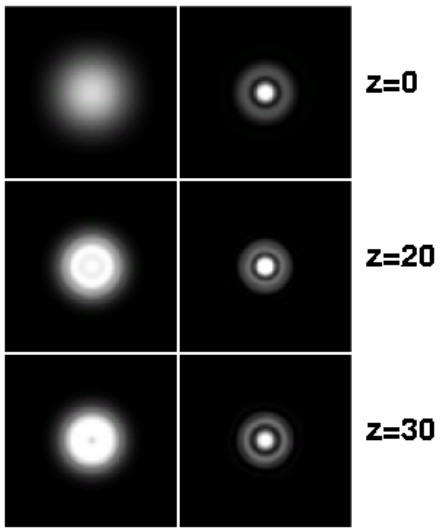


Figure 5.6: Images of the intensity (left column) and the modulus of the cross-correlation (right column) of an incoherent vortex with $\theta_0 = 0.64°$ in the far field.

Figure 5.5 shows the results for an incoherent vortex with $\theta_0 = 0.64°$. The effects of the nonlinearity are clearly visible: the vortex does not diffract and it preserves a minimum in its centre, which would not be the case in the absence of the nonlinearity. Nonetheless the cross-correlation shows the same dark ring of phase singularities one would see under linear propagation. The important point about this observation is that this is the first direct evidence that the topological charge is still present in the stabilised incoherent vortex. Hence, the stabilisation of vortices by using partially incoherent light is *not* due to any reduction of the topological charge (which e.g. might be radiated off).

The ring of phase singularities is even more clearly visible in the far-field. Figure 5.6 shows results from the same simulation as used for figure 5.5. The left column shows the intensity distribution in the far-field (i.e. the Fourier-transform of the near-field shown in figure 5.5) and the cross-correlation in the far-field $\Gamma(-\mathbf{f}, \mathbf{f})$, where $\mathbf{f}$ stands for the spatial coordinates in the far field. The intensity distribution in the far field can also show a local minimum in the centre of the beam, contrary to what one would obtain if the

vortex was propagating through a linear medium [47], and also in contrast to the result we would obtain if we were propagating a light beam without topological charge. This emphasises the importance of the interaction between the beam's coherence function and the nonlinearity.

The cross-correlation $\Gamma(-\mathbf{r}, \mathbf{r})$ thus offers a way to track the vorticity of an incoherent vortex under nonlinear propagation. However, one has to note that it is not possible to fully characterise an incoherent vortex using just the cross-correlation. The cross-correlation is, for instance, insufficient to tell if the vortex is positively or negatively charged. Simple though they seem, incoherent vortices will be nontrivial to deal with also in the future – in linear as well as in nonlinear media.

## 5.3 Modal theory of incoherent vortex solitons

Although the coherence density approach [31] (used in equations (4.3) and (5.1)) can be used to simulate the propagation of partially incoherent light with an arbitrary accuracy, it is of a little use when it comes to finding an explanation for the results obtained from the numerical simulations such as those presented above. A deeper physical insight can be obtained by using the modal theory of incoherent solitons [11]. According to the modal theory, the incoherent solitons can be regarded as an incoherent superposition of guided modes of the waveguide induced by the total light intensity. Since the incoherent vortices that we are dealing with induce circularly symmetric waveguides, the guided modes we have to consider are also circularly symmetric. To explain our numerical findings, we construct numerically, using a standard relaxation technique [15], *a partially incoherent vortex soliton* that consists of the circularly symmetric modes with the topological charges $m = 0$, 1 and 2:

$$E(\mathbf{r}) = \sum_{m=0}^{2} E_m(\mathbf{r}) \exp(im\varphi) \exp(i\gamma_m(t)) \,. \tag{5.4}$$

A more precise modelling of incoherent vortices would require more modes. Here, we restrict ourselves to *three modes* only, assuming that for a partially incoherent vortex the $m = 1$ component should be dominant and that the next strongest components should be those with topological charge $m' = m \pm 1$, i.e. $m' = 0$, 2. Indeed, we find that the main features of incoherent vortex solitons can be explained qualitatively using only these three modes.

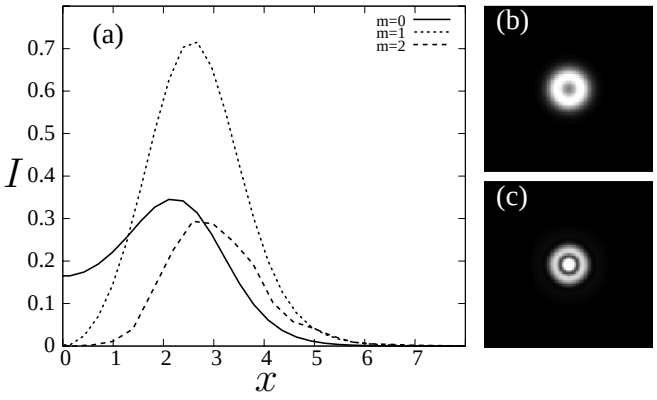


Figure 5.7: A composite soliton calculated by using the three modes with the topological charges $m = 0$, 1 and 2: (a) profiles of the three components, (b) total intensity of the vortex soliton, and (c) vortex cross-correlation $\Gamma(-\mathbf{r}, \mathbf{r})$.

For this three-mode composite vortex soliton, the relative power of the $m = 0$ and $m = 2$ modes, as compared to the $m = 1$ main vortex mode, determines the soliton's coherence. However, in order to assure that the total topological charge of the beam

$$m_{\mathrm{tot}} = \mathrm{Im}\{\left\langle \int E^*(\mathbf{r} \times \nabla E)\mathrm{d}\mathbf{r} \right\rangle\}\mathbf{e}_z / \int I \mathrm{d}\mathbf{r}, \tag{5.5}$$

is equal to one, we have to chose the $m = 0$ and $m = 2$ components of equal power. It has to be noted that apparently incoherent vortex solitons do not need to have integer topological charges, but that the charge can take any value. For our purposes of comparing the predictions of the modal theory with the results of the numerical results presented above, we restrict ourselves to the case where the topological charge is equal to one.

In order to check whether this simple approach of representing an incoherent vortex soliton by only three modes yields results that agree, at least qualitatively, with the full numerical model of an incoherent vortex soliton, we calculate the resulting shape of the vortex components, the total intensity, and cross-correlation $\Gamma(-\mathbf{r}, \mathbf{r})$ shown in Fig. 5.7. Comparing Fig. 5.5 and Fig. 5.7, we notice the presence of two similar features: (i) the local minimum of the intensity in the centre of the beam, and (ii) the ring-like structure of the cross-correlation. Hence, these two phenomena can be explained by considering a simple modal representation of the incoherent vortex consisting of only three modes with the topological charges $m = 0$, $m = 1$, and $m = 2$.

First, the local minimum in the centre of the beam can be explained by the

fact that the waveguide induced by the $m = 1$ and $m = 2$ components affects the $m = 0$ mode in such a way, that it also develops a local intensity minimum in its centre, a fact well known from the vortex-mode vector solitons [48]. Second, the ring-like structure of the cross-correlation comes from the different radial extent of the single components. As is known from the physics of vortex-mode vector solitons [48], the $m = 0$ component has the smallest radial extent, whereas the $m = 1$ and $m = 2$ components have larger radii. Hence the cross-correlation given by $\Gamma(-\mathbf{r}, \mathbf{r}) = \sum_{m,m'=0}^{2} \langle E_{m'}^*(-\mathbf{r}) E_m(\mathbf{r}) \rangle = \sum_{m=0}^{2} E_m^*(-\mathbf{r}) E_m(\mathbf{r})$, is dominated for small $\mathbf{r}$ by the auto-correlated $m = 0$ component, whereas the $m = 1$ component dominates for larger $\mathbf{r}$. For even larger $\mathbf{r}$, the $m = 2$ component can also come into play which can eventually result in a second ring of auto-correlation.

One can conclude that for a qualitative prediction about the behaviour of incoherent vortex solitons the modal theory consisting of only very few modes seems to be sufficient. This allows for (i) an intuitive approach to understanding them and (ii) for a simple and quick way to test ideas using only very limited computing resources before moving to the computationally rather demanding coherence density approach

## 5.4 Destabilising effects of partially incoherent light

All the results presented so far in this work showed a stabilising effect of partially incoherent light on the propagation of solitary solutions. The plane wave solution from section 4.1, the light stripes from section 4.2 and the vortices in this chapter – all these solitary solutions could be stabilised using partially incoherent light. However, the impression that partially incoherent light always has stabilising effects is wrong. This section illustrates the destabilising effects partially incoherent lightcan have, using the example of vortex-mode vector solitons, i.e. a fundamental mode and a vortex mode ($m = 1$) propagating through a self-induced waveguide.

Before considering the case where partially incoherent light is being used, we first have to recall the results obtained in the fully coherent case. When the fundamental mode is weak, the dynamics of the vector soliton does not greatly differ from the case of a vortex propagating alone: the vortex breaks up due to an azimuthal instability and the two filaments move away from

each other. In that process, the fundamental mode is split and each of the filaments takes a part of its intensity. This scenario doesn't change until the power of the fundamental mode is increased to values, where the fundamental mode is clearly stronger than the vortex mode.

When the fundamental mode has sufficiently high power, a second scenario can be observed: initially, the vortex still breaks up into two filaments. But in the subsequent evolution, these filaments are trapped and kept together by the fundamental mode – the beams evolve into a dipole-mode vector soliton. Because the angular momentum of the vortex is conserved, the soliton is rotating.

Finally, when the power of the fundamental mode is much larger than the power of the vortex mode, the azimuthal instability in the vortex mode is suppressed and hence the vortex-mode vector soliton is stable. However, this is only the case when the ratio between the power of the vortex and the fundamental beam is very small indeed. In these cases, the vortex can be regarded as a small perturbation to the fundamental mode. The stability of the vortex-mode vector solitons in this case has been rigorously proven by Yang and Pelinovsky [24].

An example of such a stable vortex-mode vector soliton is shown in figure 5.8 (upper row). The question was whether decreasing the degree of coherence of the fundamental beam would stabilise of destabilise the system. Therefore, the lower row of figure 5.8 shows the joint propagation of a vortex- and an incoherent fundamental mode. Both modes have the exact same powers as in the fully coherent case shown in the upper row. Although the degree of coherence of the fundamental has been greatly reduced, no effect of the incoherence on the stability is visible. This result has also been confirmed by numerous other simulations.

The next question to investigate was whether an effect on the stability would occur when slightly reducing the power of the fundamental beam, thus going to the regime, where in the coherent case the vortex evolves into a rotating dipole that is trapped by the fundamental beam. The coherent case is shown in the top row of figure 5.9. In this case, a reduced degree of coherence of the fundamental beam has obvious effects on the stability, as the lower row of figure 5.9 shows. As in the coherent case, the vortex breaks due to the azimuthal instability. However, in the incoherent case the fundamental cannot trap the two filaments and thus lead to the formation of a rotating dipole. Hence, the copropagation of a vortex and a partially incoherent fundamental mode is the first example encountered that shows a

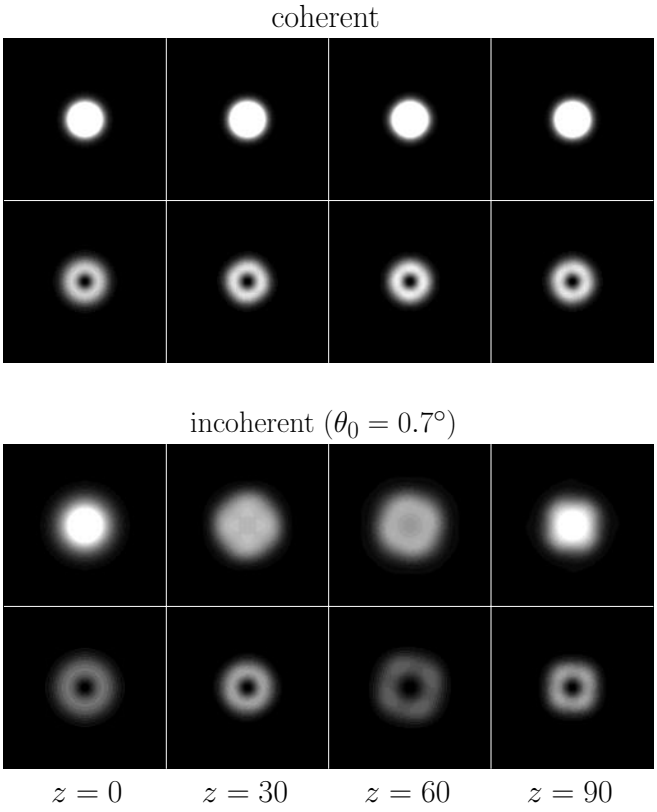


Figure 5.8: Stable propagation of the vortex-mode composite soliton with $\beta_1 = 1.0$. Upper rows: coherent fundamental mode with $\beta_2 = 1.5$. Lower rows: The same for the partially incoherent fundamental mode (at $\theta_0 = 0.7°$); both beams have the same power as in the coherent case. Pictures taken from reference [49].

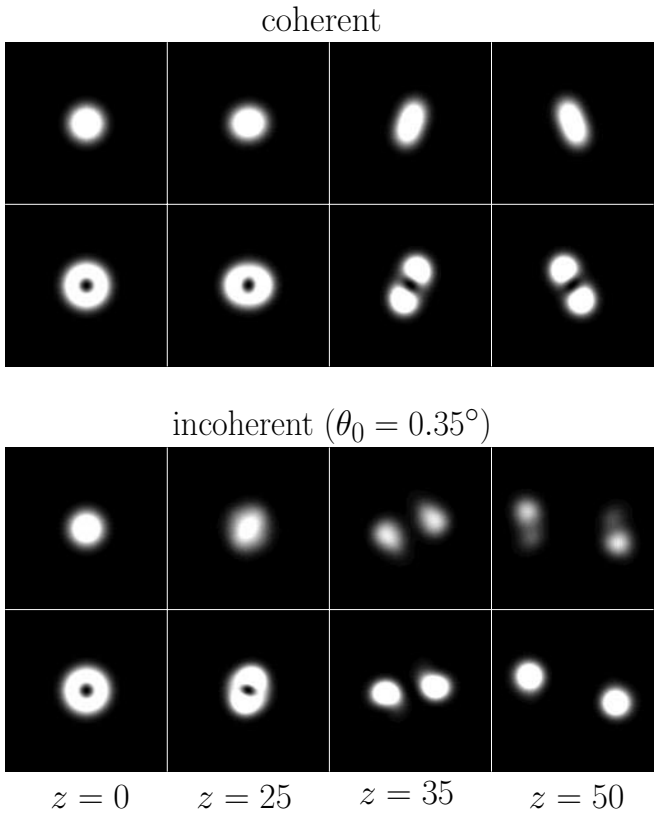


Figure 5.9: Comparison between the unstable propagation of coherent and partially incoherent vortex-mode solitons. Upper rows: coherent vortex at $\beta_1 = 1.0$ and the coherent fundamental mode at $\beta_2 = 1.45$. The vortex-mode soliton evolves into a rotating dipole-mode soliton. Lower rows: The same for the partially incoherent fundamental mode (at $\theta_0 = 0.35°$); the vortex breaks up into two separate beams that move away from each other. Pictures taken from reference [49].

destabilising effect of partially incoherent light.

We believe this type of dynamics can be understood with a simple physical argument. Indeed, the incoherent fundamental beam can be thought of as many beams that have different momenta in the transverse plane; these momenta, pointing away from the centre of the beam, add to the momentum of the vortex beam that therefore decays faster than for the coherent case.

# Chapter 6

# Temporal instabilities of counterpropagating solitons

Although some exceptions exist [50], most of the work published on vector solitons considered only the scenario where all the light beams forming the soliton are propagating in the same direction. It was only in 2002 that two papers drew attention to the case of *counter*propagating beams [51, 52]. Due to the symmetry of the propagation equation (2.26) and the isotropic nonlinear refractive index modulation equation (2.28), it is trivial to show that the solitary beam profiles are identical whether the beams are co- or counterpropagating. However, in the counterpropagating case, one has to take into account the temporal evolution of the system. We will show later on that counterpropagating solitons can be regarded as a system with delayed feedback.

Counterpropagating light fields are also used for investigating pattern formation in nonlinear optical systems in 2D [53]. In these experiments the interference of the counterpropagating fields and the resulting index grating in the medium play a key role. This is due to the geometry used in the experiments on pattern formation, where the $\hat{c}$-axis of the photorefractive crystals is oriented parallel to the direction of propagation of the beams. Later in this work, it will be shown that in the typical soliton configuration of photorefractive crystals ($\hat{c}$-axis perpendicular to the direction of propagation of the beams) interference effects have no noticeable influence on the nonlinear refractive index change. Hence, we will first focus on the case of two mutually incoherent counterpropagating beams, where interference effects do not occur at all. The focus will therefore be on the qualitative changes brought about

by the different boundary conditions as compared to the copropagating case.

## 6.1 Temporal dynamics of counterpropagating beams

We consider two mutually incoherent light fields in a saturable nonlinear medium. In paraxial approximation the propagation of the beams can be expressed by the set of wave equations:

$$i\partial_z F(x,y,z) = -\nabla_\perp^2 F(x,y,z) - \delta n^2(x,y,z,t)F(x,y,z)\ , \tag{6.1}$$

$$-i\partial_z B(x,y,z) = -\nabla_\perp^2 B(x,y,z) - \delta n^2(x,y,z,t)B(x,y,z)\ . \tag{6.2}$$

Here $F$ is the amplitude of the beam propagating in the positive $z$-direction, and $B$ is the amplitude of the beam propagating in the opposite direction. For the counterpropagating beams one has split boundary conditions, i.e. the beam amplitudes $F(x,y,z=0)$ and $B(x,y,z=L)$ are specified at the opposite crystal faces. This is in contrast to the copropagating case, where the amplitudes of both beams are specified at $z=0$.

We use the isotropic model for the nonlinearity, but also have to consider its temporal development, which we introduce by

$$\tau\partial_t \delta n^2 + \delta n^2 = \frac{I}{1+I}\,, \tag{6.3}$$

$\tau$ being the relaxation time of the crystal and $I$ the light intensity $|F|^2 + |B|^2$. Equation (6.3) is a strongly simplified version of the temporal evolution of the photorefractive nonlinearity described by Zozulya and Anderson in reference [6]. However, it is sufficient to fully describe all the phenomena that one observes using the full model equation.

First, we investigate the counterpropagation of two beams, each being the fundamental mode of the jointly induced waveguide, thus forming a soliton. As input we use two identical numerically calculated solitary beam profiles, with a maximum intensity of about $I_{max} = 3$ at the input faces of the crystal. Up to the length of the medium of $0.65L_D$ no sign of instability is observed, and both beams propagate through the jointly induced waveguide as solitons. However, at $L = 0.68L_D$ the solitary solution becomes unstable. The result is shown in figure 6.1. At $t = 25\tau$ the beams still propagate as solitons through their jointly induced waveguide. But the white noise included in the

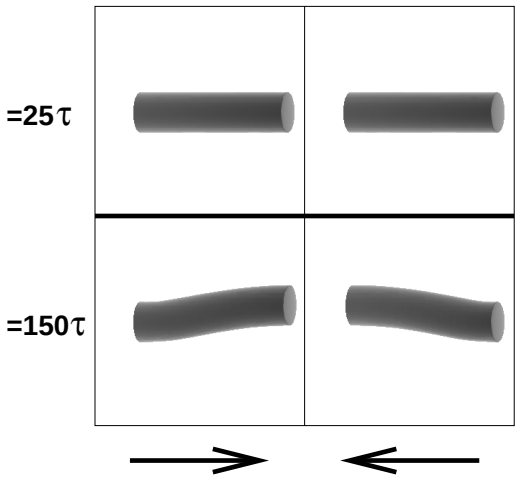


Figure 6.1: Counterpropagating fundamental beams for a medium of length $L = 0.68L_D$. The left column shows the forward, the right column the backward beam (the arrows indicate the direction of propagation). Both beams have a maximum intensity of around $I_{max} = 3$. The top row is a snapshot after $t = 25\tau$. Both beams propagate through the medium as solitons. At $t = 150\tau$ (bottom row) the beams no longer propagate as solitons, but instead deviate on their way through the crystal.

system excites an eigenmode that grows in time, and at $t = 100\tau$ the beams no longer propagate as solitons, i.e. their intensity profiles change along the propagation direction. Both beams deviate inside the medium from their straight initial trajectories. As a consequence the beams no longer coincide at $z = 0$ and $z = L$. Since the initial problem is rotationally symmetric, the direction into which the beams deviate is random. The intensity distribution at $t = 150\tau$, presented in the bottom row of figure 6.1, is stationary.

Thus, the numerical results show that the length of the medium plays a significant role in the stability of counterpropagating solitons. Another important factor is the power of the beams. Decreasing the power of the beams stabilises the counterpropagating solitons. However, if $L$ is increased, the solitons become unstable again in a way similar to figure 6.1. In addition, if $L$ is further increased, the beams do not reach a steady state, but keep changing in time. The dynamics observed in that case seem erratic and are possibly chaotic. An example from the 1D case is shown in figure 6.2. The pictures show the counterpropagation of two solitary profiles with a maximum intensity of around $I_{max} = 1$ in a medium of length $L = 4.0L_D$. After the instability sets in, the beams start oscillating around each other

in space, crossing each other at several points. The points where the beams cross each other are moving constantly in time, leading to erratic dynamics of the beams. A more in depth investigation can be found in reference [54].

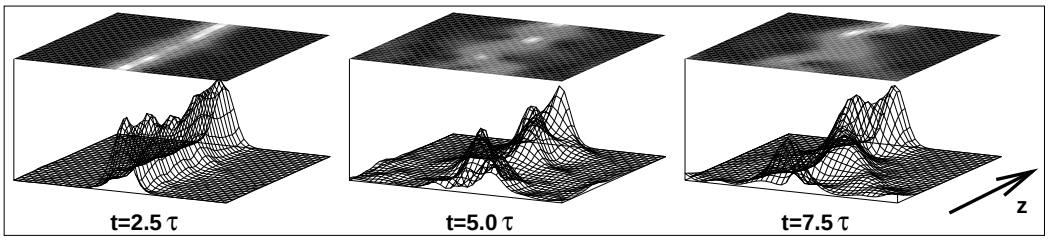


Figure 6.2: Erratic dynamics or two counterpropagating beams in the 1D case. The beams have a maximum intensity of $I_{max} = 1$ and propagate in a medium of length $L = 4.0L_D$. Only one of the beams is shown.

These results seem to contradict results obtained for the solitons in co-propagating geometry. Two mutually incoherent solitons always attract each other, therefore one would expect that the two counterpropagating beams always form a stable soliton. To find an explanation for this instability, we consider the counterpropagating beams as particles whose motion along the $z$ axis is subject to forces caused by the refractive index change in the medium [55]. Thus, we will only be concerned with the motion of the 'centre of mass' of the beams, $\mathbf{c}_1(z,t)$ and $\mathbf{c}_2(z,t)$. The centre of mass of each beam will be attracted by the waveguide induced in the medium by the beams. Because the medium is non-instantaneous, we assume that the motion of the $\mathbf{c}_i$ is determined by the light distribution a time $\tau$ ago. Furthermore, it is assumed that the force acting on $\mathbf{c}_i$ is proportional to the distance from the centre of the waveguide. We thus arrive at a simple linear set of equations:

$$\begin{aligned} \partial_{zz}\mathbf{c}_1(z,t) &= K(\mathbf{c}_1(z,t-\tau) - \mathbf{c}_1(z,t)) \\ &\quad + K(\mathbf{c}_2(z,t-\tau) - \mathbf{c}_1(z,t)) \ , \qquad (6.4) \\ \partial_{zz}\mathbf{c}_2(z,t) &= K(\mathbf{c}_1(z,t-\tau) - \mathbf{c}_2(z,t)) \\ &\quad + K(\mathbf{c}_2(z,t-\tau) - \mathbf{c}_2(z,t)) \ , \qquad (6.5) \end{aligned}$$

where the constant $K$ is determined by the strength of the nonlinearity, i.e. the power of the counterpropagating beams, and represents a measure for the mutual attraction of two beams. An approximate value of $K$ is calculated below. To further simplify the problem, the separation of the centres of mass of two beams $\mathbf{d}(z,t) = \mathbf{c}_1(z,t) - \mathbf{c}_2(z,t)$ is introduced as one dynamical

variable, and the centre of mass of the system $\mathbf{C}(z,t) = (\mathbf{c}_1(z,t) + \mathbf{c}_2(z,t))/2$ as the other. Furthermore, $\mathbf{c}_i(z, t-\tau)$ is replaced by $\mathbf{c}_i(z,t) - \partial_t \mathbf{c}_i(z,t)\tau$. Then the temporal evolution of the system can be described as:

$$0 = -\partial_{zz}\mathbf{d}(z,t) - 2K\mathbf{d}(z,t) \ , \tag{6.6}$$

$$2K\tau\partial_t\mathbf{C}(z,t) = -\partial_{zz}\mathbf{C}(z,t) \ . \tag{6.7}$$

(Note that there is no $\partial_t \mathbf{d}(z,t)$ term.)

We analyse the stability of the solution $\mathbf{d}(z,t) \equiv 0$ and $\mathbf{C}(z,t) \equiv 0$ using the tools of nonlinear dynamics. The following unstable eigenmode is identified:

$$\mathbf{d}(z,t) = \exp(\lambda t)\sin(\sqrt{2K}(z - L/2))\mathbf{e}_{x,y} \ , \tag{6.8}$$

$$\mathbf{C}(z,t) = A\exp(\lambda t)\cos(\sqrt{2K\tau\lambda}(z - L/2))\mathbf{e}_{x,y} \ , , \tag{6.9}$$

where $\mathbf{e}_{x,y}$ is a unit vector in the transverse plane. The constant $A$ and the growth rate of the instability $\lambda$ can be determined from the boundary conditions $\mathbf{c}_1(0,t) = \mathbf{c}_2(L,t) = 0$ and $\partial_z\mathbf{c}_1(0,t) = \partial_z\mathbf{c}_2(L,t) = 0$. Using equations (6.8) and (6.9) this translates into:

$$2A\cos(\sqrt{2K\tau\lambda}L/2) = \sin(\sqrt{2K}L/2) \ , \tag{6.10}$$

$$2A\sqrt{\tau\lambda}\sin(\sqrt{2K\tau\lambda}L/2) = -\cos(\sqrt{2K}L/2) \, . \tag{6.11}$$

Discarding the unphysical case $\tau\lambda > 1$ (in this case $\mathbf{c}_i(z, t-\tau)$ can no longer be replaced by $\mathbf{c}_i(z,t) - \partial_t\mathbf{c}_i(z,t)\tau$ as done in the above calculations) it can be shown that the solutions with positive $\lambda$ (unstable eigenmodes) can only exist if $L > L_c$, where

$$L_c = \pi/\sqrt{2K} \, . \tag{6.12}$$

To ascertain whether this simple criterion can serve as an estimate for predicting the onset of instability of counterpropagating solitons, one needs an estimate for $K$. To this end, we consider the case where the two beams that form the soliton are slightly shifted relative to each other, i.e. $F(x,y,z) = \psi(x + \epsilon(z), y)$ and $B(x,y,z) = \psi(x - \epsilon(z), y)$. Here $\psi(x,y)$ is the solitary beam profile and $\epsilon(z)$ measures the distance between the two beams. Because the problem is rotationally symmetric, we chose the beams only to be shifted relative to each other along the $x$-axis, not the $y$-axis. Inserting this into equations (6.1) and (6.2), and assuming a steady state, we find

$$i\partial_z F = \beta F + \epsilon(z)(\mathbf{e}_x\nabla_\perp)\delta n^2 F \tag{6.13}$$

and an analogous equation for $B$, where the real constant $\beta$ is the propagation constant of the soliton. Here, we have developed the steady state nonlinear answer of the medium into a Taylor series and neglected the quadratic and higher terms. (Keeping only the linear term is only rough approximation. However, we are only interested in a rough estimate here.) The last term on the right-hand side of equation (6.13) bends the beam towards the counterpropagating beam and also deforms it. Since we are only interested in the motion of the centre of mass, we ignore this deformation. Thus, the bending of the beam is averaged over the transverse plane. From the motion of the centre of mass we obtain the equation:

$$\partial_{zz}\epsilon = \frac{\int (\mathbf{e}_x \nabla_\perp)^2 \delta n^2 |\Psi|^2 dxdy}{\int |\Psi|^2 dxdy}\epsilon \ . \tag{6.14}$$

We thus have:

$$K = -\frac{1}{2}\frac{\int (\mathbf{e}_x \nabla_\perp)^2 \delta n^2 |\Psi|^2 dxdy}{\int |\Psi|^2 dxdy} \ . \tag{6.15}$$

Note that equation (6.14) is of the same form as equation (6.6).

Inserting the value of $K$ thus obtained into equation (6.12) we find that $L_c = 0.84 L_D$ for the soliton in figure 6.1, which is longer than the numerically determined stability threshold of about $0.68 L_D$. Nonetheless, this is still reasonably close, considering the crude approximations used. In addition, equations (6.12) and (6.15) can explain the fact that solitons with lower intensity can be stable in longer media, because they have a lower value of $K$. This is due to the fact that the refractive index change induced by weaker beams is smaller, and therefore the waveguides are not as attracting.

In the next step we investigate the stability of solitons consisting of a fundamental and a dipole mode. In the copropagating geometry dipole-mode vector solitons have already been investigated in chapter 3.1. In copropagating geometry they are known to be very robust [12, 13, 56]. As in the case of two counterpropagating fundamental modes, the simulations show that the beams no longer propagate as solitons through the medium if the medium length exceeds a certain value. In figure 6.3 we present a case where the medium length is slightly above that critical value. As already seen in figure 6.1, the beams deviate from their initial trajectories as they propagate. It is interesting to notice that the deviation occurs in a direction perpendicular to the plane of the dipole. This fact can be explained by reconsidering the arguments that lead to the set of equations (6.4) and (6.5). There, we considered the case of two counterpropagating rotationally symmetric solitons.

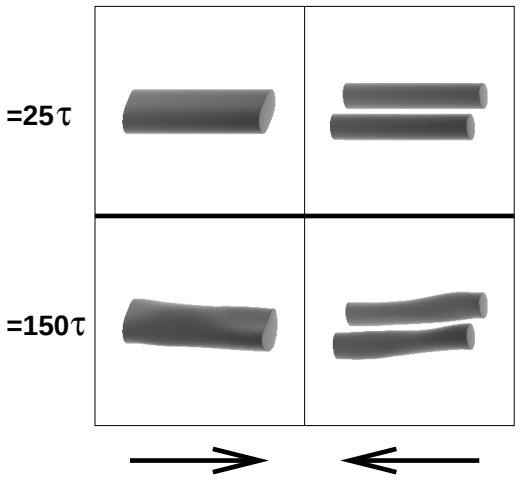


Figure 6.3: Counterpropagating fundamental and dipole beam for a medium length of $L = 0.82L_D$. As in figure 6.1, the beams initially propagate as solitons (upper row). When the instability sets in, the light distribution is no longer symmetric to the dipole axis. The state at $t = 150\tau$ (bottom row) is stationary.

Because of the rotational symmetry, the value of $K$ is independent of the direction into which the beams deviate. The problem of a counterpropagating fundamental and dipole beam, however, is not rotationally symmetric. Numerical calculations show that the two beams attract each other more strongly when they deviate perpendicular to the dipole plane than when they deviate parallel to the plane. This leads to a higher effective value of $K$ for deviations perpendicular to the dipole plane, and therefore to a shorter critical length $L_c$, according to the estimate equation (6.12).

To demonstrate the unique properties of the temporal dynamics of counterpropagating beams, figure 6.4 shows snapshots of the counterpropagation of a vortex and a fundamental mode. The images show the two beams at their respective exit face of the medium. The propagation distance used here is longer than in the previous figures, because we found that for short values of $L$, used so far, there is no deviation of the beams during their propagation through the medium. But, as could be expected from the analogy to the copropagating case, the vortex breaks up into a dipole beam during propagation, if the medium is long enough. Moreover, this system does not possess a steady state. An example of the temporal dynamics is shown in figure 6.4. Here $L = 1.1L_D$. At $t = 15\tau$ the vortex has not yet broken up into a dipole. At $t = 25\tau$ however, the vortex beam incident upon the crystal leaves the

crystal as a dipole. This also leads to a deformation of the fundamental beam. Note that the dipole and the fundamental beam are not aligned in the figure, because the two beams are shown at two different positions in the crystal, $z = 0$ and $z = L$. The dipole and the fundamental beam do rotate in time. In the simulations the rotation continues indefinitely (we stopped the simulations at $t = 200\tau$). This rotation, therefore, represents a periodic dynamic state of the system. More on the dynamics of counterpropagating light fields in nonlinear media can be found in references [57, 58, 59]. Recent results focusing on the steady state can be found in references [60, 61].

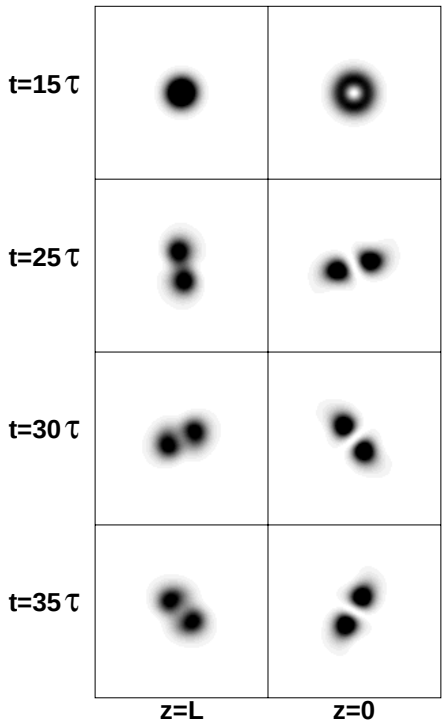


Figure 6.4: Temporal evolution of a fundamental beam and a counterpropagating vortex for $L = 1.1L_D$. After a certain time, the vortex breaks up into a dipole that rotates in time. The fundamental beam splits into two beamlets that co-rotate with the dipole. The left column shows the fundamental beam, the right column the vortex at their respective output face of the medium.

One can conclude that changing the boundary conditions from a co- to a counterpropagating geometry has remarkable consequences on the temporal evolutions of the beams. Whereas in the copropagating case the system alway settles into a steady state, the counterpropagating case is more difficult. Two

new phenomena can arise. On the one hand, stable solitary solutions from the copropagating case can be temporally unstable in the counterpropagating case and the system settles down in a different steady state, as shown in figure 6.1. On the other hand, one can observe dynamics where the system does not seem to have a stable steady state solution at all, as is shown in figure 6.4. Both effects can be explained by the fact that counterpropagating solitons in a non-instantaneous medium can be seen as a system with delayed feedback. With the medium being non-instantaneous, it is obvious that the propagation of the light fields is being influenced by the state of the light fields a time $\tau$ ago. Furthermore, there is also an effect that could be called 'spatial feedback'. In the absence of the counterpropagating beam, the state of the forward propagating beam in the $z = z_0 + \delta z$ plane has no influence on the propagation of the beam at $z = z_0$. If, however, a counterpropagating beam is present, then the forward beam at $z = z_0 + \delta z$ will have an influence on the backward propagating beam, which has, on his part, an influence on the forward beam at $z = z_0$. The temporal and spatial dynamics of counterpropagating beams in nonlinear media can therefore be very complex and leave lots of space for further investigations.

## 6.2 Counterpropagation in photorefractive media

Coherent interaction of counterpropagating light beams in Kerr-type and photorefractive media has been treated in a number of papers [50, 51, 52, 62, 63, 64, 65], using mainly an isotropic and local approximation to the nonlinear response of the medium. This means that the change in the refractive index, caused by light, is spatially isotropic and depends locally on the light intensity. As has been shown earlier in the work, however, the agreement between theoretical predictions and experimental results in photorefractive crystals can be improved by using the full anisotropic nonlocal model for the nonlinearity.

An anisotropic nonlocal theory of the space charge field induced by the coherent *counter*propagating beams in biased photorefractive crystals is not difficult to formulate, however [66]. The following will show that the anisotropic nonlocal theory yields significantly different results from the isotropic local model, especially when the crystal ĉ-axis is tilted with respect to the direc-

tion of propagation of the beams. It is demonstrated that a more complete description of counterpropagating beams requires inclusion of both the drift and diffusion terms.

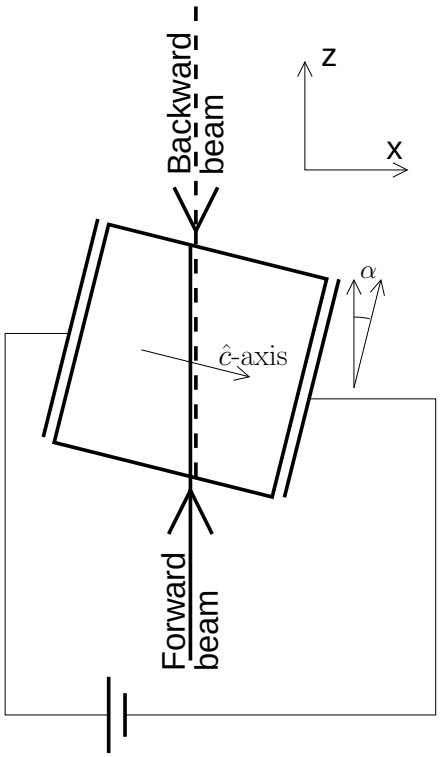


Figure 6.5: Geometry of beam propagation in a tilted biased photorefractive crystal.

We assume that the optical electric field is given as the sum of slowly varying amplitudes $F\exp(ikz) + B\exp(-ikz) + c.c.$, $k$ being the wave vector in the crystal, and $F$ and $B$ the envelopes of the beams counter-propagating along the $z$ axis. The light intensity, after averaging in time, builds an interference pattern of the form

$$I = I_0 + \nu[FB^* \exp(2ikz) + c.c.]\,, \tag{6.16}$$

where $I_0 = |F|^2 + |B|^2$ is the unmodulated light intensity and $\nu$ is the degree of beam coherence ($\varepsilon = 1$ for fully coherent and $\nu = 0$ for fully incoherent beams). This pattern modulates the space charge field in the crystal and generates a reflection-type grating in the index of refraction. Our aim is to evaluate the strength of this grating and its phase shift relative to the intensity interference pattern, and to investigate its influence on the propagation

of beams. We expect both the strength and the phase to depend on the angle $\alpha$ between the beams' direction of propagation and the crystal ĉ axis.

We assume that the beams in the transverse plane are localised in the $x$ direction and that the space charge field is confined to the $x$-$z$ plane (1D geometry). It presents no difficulty to extend our results to two transverse dimensions. figure 6.5 depicts the geometry of the problem.

For incoherent beams ($\nu = 0$) the space charge field consists only of an unmodulated component $\mathbf{E}_{sc}(\mathbf{r}) = \mathbf{E_0}(\mathbf{r})$, where $\mathbf{r} = x\mathbf{e}_x + z\mathbf{e}_z$, and $\mathbf{e}_x$ and $\mathbf{e}_z$ are the unit vectors. For coherent beams the interference pattern induces an additional modulation of the electric potential $\phi$ generated by the separated space charges in the medium, proportional to $\nu$:

$$\phi(\mathbf{r}) = \phi_0(\mathbf{r}) + (\nu/2)\left[\phi_+(\mathbf{r})\exp(i2kz) + c.c.\right] \ . \tag{6.17}$$

Here, the fast and slow oscillations in the $z$ direction are separated in the leading order, by introducing the slowly varying envelope $\phi_+$ of the potential, with $|\partial_z\phi_+(\mathbf{r})| \ll 2k|\phi_+(\mathbf{r})|$. The potential $\phi$ generates the space charge field, which also consists of a modulated and an unmodulated part: $\mathbf{E}_{sc} = \mathbf{E}_u + \mathbf{E}_+(\exp(i2kz) + c.c.)$. Thus we have $\mathbf{E}_u = \nabla\phi_0$ and $\mathbf{E}_+ = \mathbf{e}_x\mathcal{E}_x + \mathbf{e}_z\mathcal{E}_z = \mathbf{e}_x\partial_x\phi_+ + \mathbf{e}_z\nu ki\phi_+$, where $\nabla = \mathbf{e}_x\partial_x + \mathbf{e}_z\partial_z$.

The charge distribution inside a photorefractive crystal is modelled by the Kukhtarev equations [7]. These equations can be reduced to the following potential equation:

$$\begin{aligned}\frac{\tau}{1+I_0}\partial_t(\nabla^2\phi) + \nabla^2\phi + \nabla\ln(1+I)\nabla\phi = \\ \mathbf{E}_0\nabla\ln(1+I) + \frac{k_BT}{e}\{\nabla^2\ln(1+I) + \\ (\nabla\ln(1+I))^2\}\,,\end{aligned} \tag{6.18}$$

using a few well justified approximations [6]. Looking for steady-state solutions of this equation one obtains equation (2.27). Here, $\tau$ is the relaxation time of the crystal, $\mathbf{E}_0$ is the external biasing field, $k_B$ is the Boltzmann constant, $T$ is the temperature, and $q$ is the elementary charge.

In the case $\nu = 0$ the potential can be calculated just as in the well-known case of incoherent copropagating light beams. Substituting (6.17) into (6.18) and setting $\nu = 0$ yields

$$\begin{aligned}\tau\partial_t\partial_x^2\phi_0 + (1+I_0)\partial_x^2\phi_0 + \partial_x I_0\partial_x\phi_0 = \\ E_0^x\partial_x I_0 - \kappa\partial_x^2 I_0\,,\end{aligned} \tag{6.19}$$

where $E_0^x$ is the $x$-component of $\mathbf{E}_0$ and $\kappa = k_B T/q$ is the strength of the diffusion. Here we have neglected the derivatives of $\phi_0$ and $I_0$ with respect to $z$, because the beams typically used in experimental setups have a diameter of about $10\mu m$, i.e. $\phi_0$ and $I_0$ vary in the $x$-direction on a length scale of $10\mu m$, whereas in the $z$-direction they vary on the length scale of a diffraction length $L_D \approx 2mm$. Therefore, in steady state, i.e. when setting $\partial_t \phi_0 = 0$, one obtains the well-known result

$$\mathbf{E}_u = -\mathbf{e}_x [E_0^x I_0 + \kappa \partial_x I_0]/(1 + I_0) \tag{6.20}$$

already encountered in equation (2.21). Note that we have chosen the coordinate system such that the $z$-direction is always parallel to the direction of propagation of the beams. Hence $\mathbf{E}_u$ is parallel to the $x$-direction, because variations of the light intensity in $z$-direction are small and hence both drift- and diffusion-terms in $z$-direction can be neglected. Under normal experimental conditions $\kappa < 0.05 x_0 |\mathbf{E}_0|$, where $x_0 = 10\mu m$ is the beam size, which means that $\mathbf{E_0}$ is well approximated by $\mathbf{E}_u = -\mathbf{e}_x E_0^x I_0/(1+I_0)$, i.e. for room temperature and $\nu = 0$ diffusion of the charge carriers plays only a minor role. Hence, in that case the space charge field is obtained is local and isotropic. However, it has been shown that the term $\kappa \partial_x I_0/(1 + I_0)$, which causes self-bending of the beams, can be of crucial importance for counterpropagating beams [67], particularly for longer propagation lengths, if $\alpha \leq 5°$.

In the case of mutually coherent counterpropagating beams, i.e. $\nu > 0$, substituting expression (6.17) into equation (6.18), one can separate the slow and fast oscillating parts, because the terms proportional to $\exp(i2kz)$ and the unmodulated terms have to solve the equation separately. Keeping the terms up to the first order in $\nu$, one finds that $\mathbf{E}_u$ is again given by equation (6.20), and that $\phi_+$ solves

$$\begin{aligned} \tau \partial_t (\partial_x^2 \phi_+/2 - 2k^2 \phi_+) + (1 + I_0) m \partial_x^2 \phi_0/2 + \\ (1 + I_0)(\partial_x^2 \phi_+/2 - 2k^2 \phi_+) + \\ \partial_x [(1 + I_0) m/2] \partial_x \phi_0 + \partial_x I_0 \partial_x \phi_+ = \\ E_0^x \partial_x [(1 + I_0) m] + ikE_0^z (1 + I_0) m - \\ \kappa \{\partial_x^2 [(1 + I_0) m]/4 - 2k^2 (1 + I_0) m\}, \end{aligned} \tag{6.21}$$

where $m = 2FB^*/(1 + I_0)$ is the modulation depth. This fairly complicated equation can be simplified by noticing that it contains terms of different orders of magnitude. On the one hand there are the terms proportional to

$k^2 = 4\pi/\lambda^2$, where $\lambda$ is the wavelength in the medium, typically around $200nm$. On the other hand there are the terms containing $\partial_x$ derivatives. Since $\phi$, $I_0$ and $m$ vary in the $x$-direction on the length scale of the size of the beam, i.e. $10\mu m$, their partial derivatives can be neglected. Therefore, only the terms proportional to $k^2$ and the term $ikE_0^z(1+I_0)m$ need to be taken into account. Thus we get:

$$\begin{aligned} 2k^2\tau\partial_t\phi_+ + 2k^2(1+I_0)\phi_+ = \\ -2k^2\kappa(1+I_0)m - ikE_0^z(1+I_0)m\,. \end{aligned} \tag{6.22}$$

The steady state solution is $\phi_+ = -[\kappa + iE_0^z/(2k)]m$, hence

$$\mathcal{E}_x = -[\kappa + iE_0^z/(2k)]\partial_x m \tag{6.23}$$

and

$$\mathcal{E}_z = -\nu(ik\kappa - E_0^z/2)m\,. \tag{6.24}$$

Even for values of $E_0^z$ as high as several kV/cm, $k\kappa$ is bigger than $E_0^z$, which means that the modulated part of the field in the $z$ direction, $\mathcal{E}_z$, is diffusion dominated.

With equations (6.20), (6.23) and (6.24) we have a closed set of equations that gives us the space charge field inside the crystal to a good approximation. One still has to find out how the space charge field changes the refractive index and thus influences the propagation of beams. The fact that the (birefringent) crystal is tilted with respect to the direction of propagation of the beams has to be taken into account. Linear optics gives us the effective refractive index of the crystal:

$$n_{\text{eff}}^2 = \frac{n_{33}^2 n_{11}^2 - n_{13}^4}{n_{33}^2\sin^2\alpha + n_{11}^2\cos^2\alpha + 2n_{13}^2\sin\alpha\cos\alpha}\,, \tag{6.25}$$

where $\varepsilon_0\{n_{ij}^2\} = \hat{\varepsilon}$ is the dielectric tensor already encountered in chapter 2. $n_{33}$ is the index of refraction for the beams polarised parallel to the crystal $\hat{\text{c}}$ axis and $n_{11}$ is the index for the beams polarised perpendicular to $\hat{\text{c}}$. $\alpha$, as mentioned above, is the angle by which the crystal is tilted with respect to the direction of propagation of the beams (see figure 6.5). To show how the modulated and unmodulated parts of the space charge field influence $n_{\text{eff}}$ we take SBN:75 crystal as an example. The generalisation to other photorefractive crystals is straightforward.

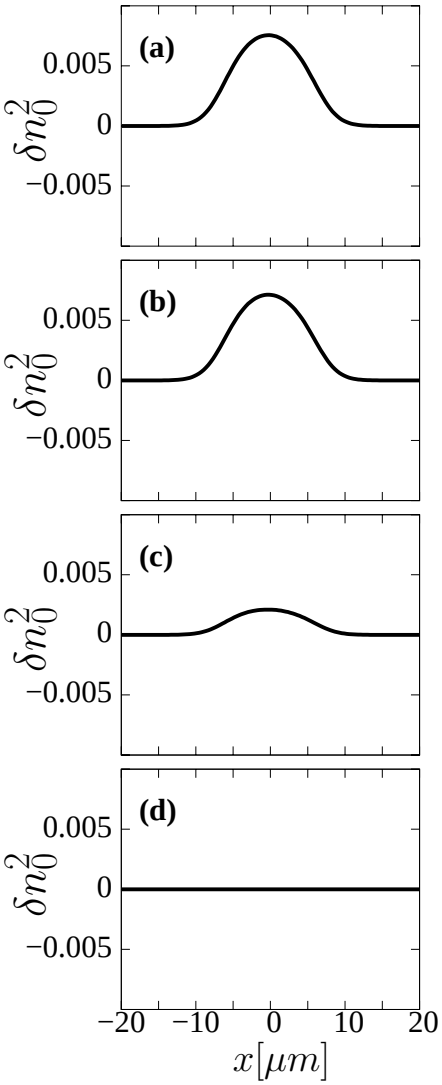


Figure 6.6: Unmodulated part $\delta n_0^2$ of the refractive index change. Gaussian beams $F = B = \exp[-x^2/(2\sigma^2)]$ with $\sigma = 5\mu m$ are chosen as the beam profiles. The crystal is tilted by $\alpha = 0°$ in (a), 10° in (b), 45° in (c) and 90° in (d). $E_0 = 3kV/cm$.

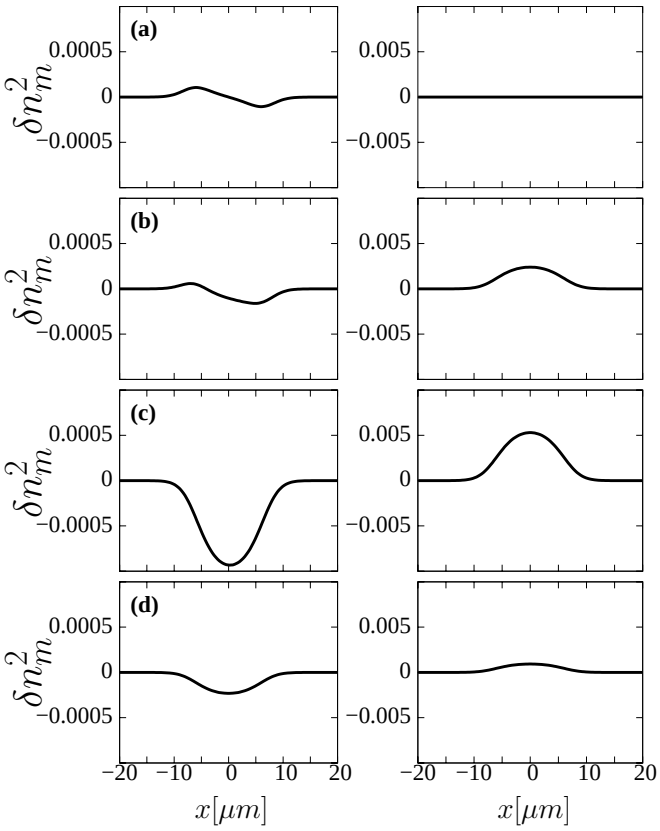


Figure 6.7: Modulated part $\delta n_m^2$ of the refractive index change. The left column shows the real part, the right column the imaginary part. All parameters are as in figure 6.6. Note that a different scale is used in the pictures for the real and the imaginary part.

In SBN:75 the refractive index can be influenced by three components of the electro-optic tensor: $r_{33} = 1340pm/V$, $r_{13} = 67pm/V$ and $r_{42} = 42pm/V$. The values are taken from Ref. [68] and are valid for light of a vacuum wavelength of $633nm$. Let us now decompose the nonlinear refractive index change $\delta n^2$ into a modulated and an unmodulated part: $\delta n^2 = \delta n_0^2 + \delta n_m^2[\exp(2ikz) + \exp(-2ikz)]/2$. The space charge field influences the refractive index as follows:

$$\begin{aligned} \delta n_0^2 &= \mathbf{E}_u \cdot \mathbf{e}_x[(r_{33}\tilde{n}_{33}^4 a_{33} + r_{13}\tilde{n}_{11}^4 a_{11})\cos\alpha - \\ &\qquad r_{42}\tilde{n}_{33}^2\tilde{n}_{11}^2 a_{13}\sin\alpha]\,, \\ \delta n_m^2 &= (\mathcal{E}_x\cos\alpha + \mathcal{E}_z\sin\alpha)(r_{33}\tilde{n}_{33}^4 a_{33} + r_{13}\tilde{n}_{11}^4 a_{11}) + \\ &\qquad (\mathcal{E}_x\sin\alpha + \mathcal{E}_z\cos\alpha) r_{42}\tilde{n}_{33}^2\tilde{n}_{11}^2 a_{13}\,, \end{aligned} \tag{6.26}$$

where $\varepsilon_0\{\tilde{n}_{ij}\}$ is the unperturbed dielectric tensor, $a_{ij} = \partial n_{\text{eff}}^2/\partial n_{ij}^2$, and $\mathbf{E}_u$ is given by equation (6.20).

The propagation equations of the beam envelopes in paraxial approximation are then given by:

$$i\partial_z F + \frac{1}{2}\partial_x^2 F = \delta n_0^2 F + \frac{1}{2}\delta n_m^2 B\,, \tag{6.27}$$

$$-i\partial_z B + \frac{1}{2}\partial_x^2 B = \delta n_0^2 B + \frac{1}{2}(\delta n_m^2)^* F\,, \tag{6.28}$$

where we have neglected the terms proportional to $\partial\delta n_0^2/\partial\alpha$ and $\partial\delta n_m^2/\partial\alpha$, as they only result in weak self-bending of the beams, which is an effect already taken into account by the second term in equation (6.20).

It is important to distinguish between the real and imaginary parts of $\delta n_m^2$, because of the fact that when the Bragg-grating inside the crystal is $\pi/2$ phase shifted with respect to the intensity grating, the backward beam gets stronger as it travels through the crystal, while the forward beam gets depleted. In other words, the imaginary part of $\delta n_m^2$ breaks the $z \to -z$ symmetry between the forward and the backward propagating beam and induces energy transfer between them.

In figure 6.6 we show the unmodulated part $\delta n_0^2$ of the refractive index change for crystals tilted at different angles $\alpha$, calculated using equations (6.20) and (6.26). It can be seen that it is strongest for $\alpha = 0°$, as should be expected. This configuration is typically employed in the investigations of spatial solitons. For $\alpha = 90°$, which is the standard configuration

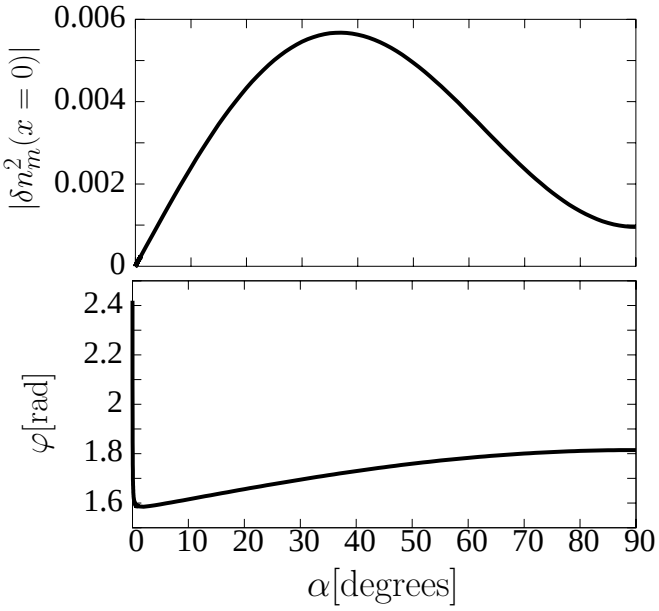


Figure 6.8: Amplitude and phase of $\delta n_m^2$ at $x = 0$. The upper plot shows the amplitude, the lower plot shows the phase $\varphi$, defined by $\varphi = \arctan(\mathrm{Im}\{\delta n_m^2(x=0)\}/\mathrm{Re}\{\delta n_m^2(x=0)\})$.

for experiments on pattern formation, it almost vanishes, owing to the small value of $r_{42}$.

Using equations (6.23), (6.24) and (6.26) leads to the modulated part $\delta n_m^2$ of the refractive index change shown in figure 6.7. It can be seen that the imaginary part is dominant for tilted crystals (by a factor of about 10), i.e. the symmetry between the forward and the backward beam is broken. Furthermore, $\delta n_m^2$ is strongest at some intermediate value of $\alpha$. Therefore, in experiments where a strong transfer of energy from one beam to the other is desired, it might be useful to tilt the crystal by $\alpha \approx 45°$.

To confirm observations concerning the dependence of $\delta n_m^2$ on $\alpha$, we plot in figure 6.8 the amplitude and the phase of $\delta n_m^2$ at $x = 0$, as functions of $\alpha$. It can be seen that the amplitude is biggest for a value of $\alpha \approx 35°$, and that even for small angles the phase is close to $\pi/2$. This means that the energy transfer from one beam to the other has to be taken into account.

Thus, we can state that the counterpropagation of coherent beams in biased photorefractive crystals combines the features of both soliton formation without energy exchange and two-wave mixing in photorefractive media, namely self-focusing by the unmodulated part $\delta n_0^2$ of the refractive index change and energy exchange by the modulated part, which is $\sim \pi/2$ phase

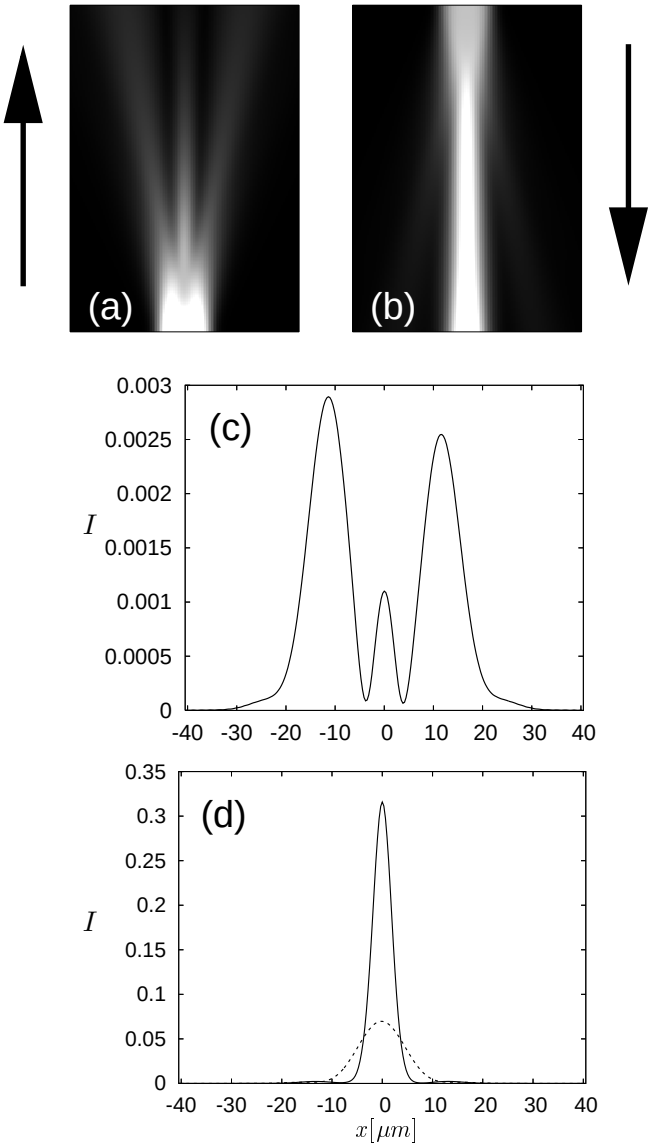


Figure 6.9: Counterpropagation of two beams in a $1mm$ long crystal. The crystal is assumed to be tilted by $\alpha = 10°$ with respect to the propagation direction. (a) shows the evolution of the forward beam (propagating from bottom to top), (b) shows the backward beam (propagating in the opposite direction). (c) shows the profile of the forward beam as it leaves the crystal. In (d) the dashed line shows the backward beam leaving the crystal after *linear* propagation, whereas the solid line shows it after nonlinear propagation. Note that at their respective input faces both beams have the same power.

shifted with respect to the modulation of the light intensity.

To see whether the combination of these features leads to a propagation behaviour that is a mixture of self-focusing and pattern-formation, we simulated the counterpropagation of two beams with initial profiles $F = B = 0.3\exp[-x^2/(2\sigma^2)]$ with $\sigma = 4\mu m$. We assumed an angle $\alpha = 10°$ and an external voltage of $E_0 = 3kV/cm$. We considered a $1mm$ thin slice of an SBN:75 crystal. The result of the simulation is presented in figure 6.9. Figure 6.9(a) and (b) show how the profiles of the beams change as they propagate. (a) shows the forward beam and (b) the backward beam, with their direction of propagation being indicated by arrows on the side of the plots. (c) shows the profile of the forward beam as it leaves the crystal. It has split into three beams, reminiscent of the breaking of a uniform beam into stripes in experiments on pattern-formation in counterpropagating beams. Finally, the solid line in figure 6.9(d) shows the backward beam as it leaves the crystal. For comparison, the dashed line shows what the beam would look like were the nonlinearity absent. One can see that on the one hand the backward beam gets amplified while propagating through the crystal, on the other hand the self-focusing effect of the nonlinearity is also clearly visible. For this simulation we set $T = 300K$. The effect of the self-bending is weak due to the short propagation distance. However, it is clearly visible in the asymmetry of the beam profile in figure 6.9(c).

Concluding, one can state that working with photorefractive media in a counterpropagating geometry, one has to be extremely careful about a possible tilting of the crystal. However, the combination of mutual focusing and energy exchange between the counterpropagating beams might lead to interesting new ideas in the attempt to use photorefractive crystals in optical data processing.

# Chapter 7

# Future perspectives: Stability analysis of gap solitons

Throughout this work, only solitons in bulk homogeneous media were considered. The main reason for this restriction is that the mechanisms that stabilise or destabilise a soliton are most easily unveiled in the most simple possible case, i.e. in a homogeneous medium. However, as the interest in photonic crystals is constantly growing, this chapter includes a few remarks on the stability of gap solitons in photonic crystals [48, 69].

The term 'photonic crystal' or, more general, 'photonic structure' is used to describe media with a periodically modulated refractive index. In this chapter we will consider a medium with a refractive index that depends on $x$ and $y$ like $\delta n_p^2(x,y) = 1.2(\sin^2(2\pi x/D) + \sin^2(2\pi y/D))$, whereas it does not depend on the propagation direction $z$. The refractive index modulation is shown in figure 7.1. In the linear regime, the propagation of light through this medium is described by the equation

$$i\partial_z A(\mathbf{r}) = (\nabla_\perp^2 + \delta n_p^2(x,y))A(\mathbf{r})\,. \tag{7.1}$$

The above equation is well known from solid state physics, where is is used to calculate the eigenenergies and eigenfunctions of electrons in crystals. In that case, the periodic term does not come from a periodic index modulation, but represents the attracting forces of the atoms' nuclei on the electrons. The most striking consequence of the periodic term, in solid state physics as in the case of a photonic crystal, is that the eigenvalues of the above equation are subdivided into bands.

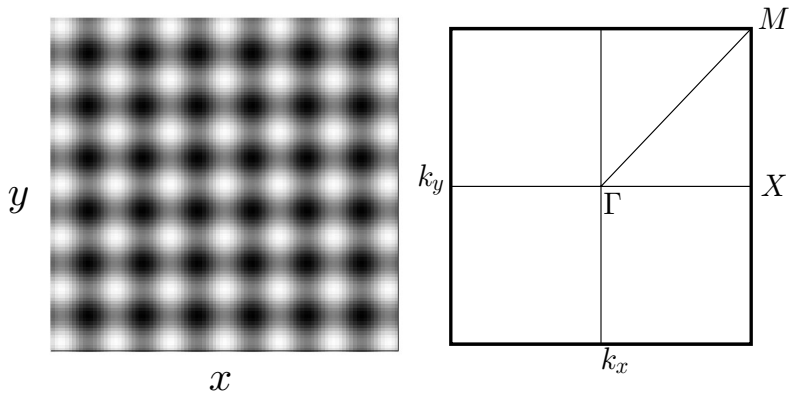


Figure 7.1: The left picture shows the periodic modulation of the refractive index. The geometry of the lattice leads to the quadratic Brillouin zone shown on the right.

According to the Bloch theorem all eigenfunctions of equation (7.1) are of the form $\phi(x,y) = u_{k_x,k_y}(x,y)\exp(i(k_x x + k_y y))\exp(i\mu_{k_x,k_y} z)$, where $u_{k_x,k_y}(x,y)$ is a function having the same periodicity as the lattice, i.e. $u_{k_x,k_y}(x+n_1 D, y+n_2 D) = u_{k_x,k_y}(x,y)$, with $n_1$ and $n_2$ being integer numbers. Inserting this into equation (7.1) we get

$$-\mu_{k_x,k_y} u_{k_x,k_y}(x,y) = ((i\nabla_\perp + k_x \mathbf{e}_x + k_y \mathbf{e}_y)^2 + \delta n_p^2(x,y)) u_{k_x,k_y}(x,y)\,, \quad (7.2)$$

which has to be solved for all values $k_y$ and $k_y$ lying within the first Brillouin zone shown in figure 7.1.

Equation (7.2) can easily be solved using standard linear algebra. The resulting dispersion relation is shown in figure 7.2. As can be seen, there are bands of permitted values for $\mu_{k_x,k_y}$ and band gaps between them. Note that in the absence of the periodic index modulation (i.e. $\delta n_p^2(x,y) = 0$) $\mu_{k_x,k_y}$ would be allowed to take any value smaller than zero and would depend on $k_y$ and $k_y$ like $\mu_{k_x,k_y} = -k_x^2 - k_y^2$. This can be easily seen when considering that in the case of an unmodulated medium the eigenfunctions of equation (7.2) are plane waves. Hence the $\nabla_\perp$ term vanishes and one recovers the simple quadratic dependence of $\mu_{k_x,k_y}$ on $k_x$ and $k_y$.

The curvature of the dispersion relation is essential for the propagation of localised light fields. As any localised light field can be described as a superposition of Bloch waves $A(x,y) = \sum_{k_x,k_y} C_{k_x,k_y} u_{k_x,k_y}(x,y)\exp(i(k_x x + k_y y))$, its evolution under propagation depends on the values of $\mu_{k_x,k_y}$. If all Bloch waves that the light field is composed of have the same value for $\mu_{k_x,k_y}$,

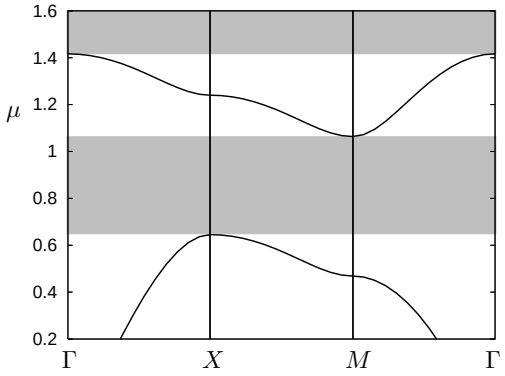


Figure 7.2: The dispersion relation of light inside the photonic structure. The top grey area indicates the semi-infinite gap, the bottom one the first band gap.

i.e. when the dispersion relation is a horizontal line $\mu_{k_x,k_y} = const.$, then the light field will not change under propagation. If, however, the dispersion relation is curved, then the light field will diffract. The basic idea of spatial solitons is to compensate this curvature by a nonlinear medium response. It is hence easy to understand that the propagation constants of solitons cannot lie within one of the bands.

Throughout this work we were considering homogeneous media and hence the only band gap that was available for the generation of solitons was the semi-infinite band gap. In the case of a homogeneous medium the semi-infinite gap extents from $\mu = 0$ to infinity. In figure 7.2 the semi-infinite gap extents from $\mu \approx 1.4$ to infinity. This shifting is physically irrelevant, because one could rescale $\mu$ by an additional constant, thus making the semi-infinite gap in the case of a homogenous medium coincide with the semi-infinite gap in a photonic structure.

In contrast to homogeneous media, photonic structures offer the possibility to generate solitons in the gap between the first and the second band. In particular, we will focus on solitons lying close to the lower edge of the first band. Note that there the curvature of the dispersion relation is positive, whereas it is negative at the top edge of the band. This has a remarkable consequence for the kind of nonlinearity needed to create a soliton. To create a soliton at the bottom edge of the band, one does not need a self-focusing, but a self-*de*focusing nonlinearity. We will consider a self-defocusing Kerr-

nonlinearity and hence work with the equation

$$-i\partial_z A(\mathbf{r}) = (\nabla_\perp^2 + \delta n_p^2(x,y) - I)A(\mathbf{r})\,. \tag{7.3}$$

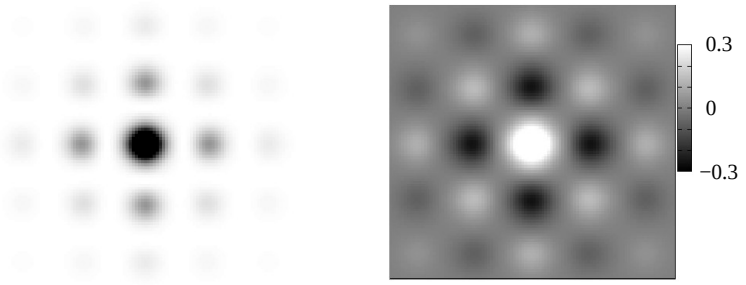


Figure 7.3: The total intensity (left) and the real part of the electric field component of a soliton with propagation constant $\beta = 1.03$.

An example for such a gap soliton is shown in figure 7.3. Figure 7.3(a) shows the total intensity and (b) the real part of the electric component associated with the light field. The imaginary part can be chosen to be zero. As can be seen, the light field has maxima in the regions with maximum refractive index, and the phase correlation between two of these lattice sites is $\pi$. The fact that the light field is $\pi$ out of phase for two neighbouring lattice sites reveals that Bragg reflections play a key role in the formation of gap solitons. It also clearly distinguishes gap solitons from all other solitons considered so far in this work.

To further motivate the investigation of such gap solitons, one has to mention that equation (7.3) can also be used to describe a Bose-Einstein condensate in an optically induced lattice. Hence, all the results obtained for gap solitons in nonlinear photonic structures can be applied immediately to the highly active field of research on BEC [70].

Before starting any attempt to generate solitons like the one shown in figure 7.3 experimentally, one will have to address the question of its stability. The simplest possible way to answer that question is to numerically propagate the soliton under the influence of noise and to observe its evolution. This is done in figure 7.4. As can be seen, the soliton is unstable. Repeating this procedure for solitons with a somewhat smaller propagation constant, however, one observes stable propagation, as is shown in figure 7.5. As the

power of the solitons increases with decreasing propagation constant, one can state that only gap solitons of sufficiently high power are stable. This was already observed by Ostrovskaya and Kivshar in 2003 [71].

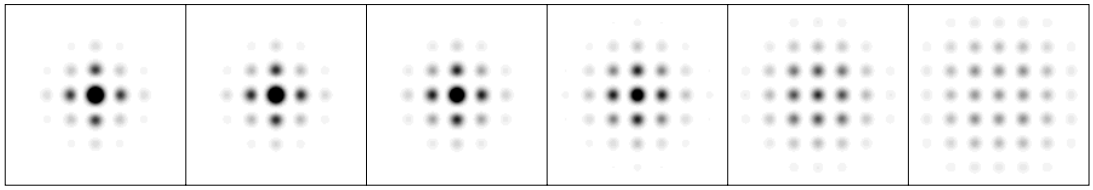

Figure 7.4: The numerical propagation of the soliton shown in figure 7.3. The snapshots are taken after different propagation distances $z$, with $z$ increasing from left to right, showing the decay of the soliton.

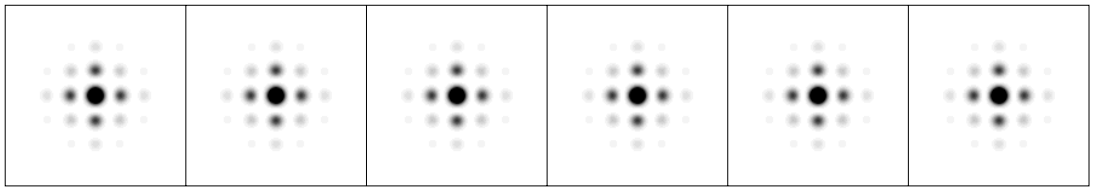

Figure 7.5: The numerical propagation of the soliton with propagation constant $\beta = 1.01$. The power of the soliton is roughly 10% above the power of the soliton shown in figure 7.4. The snapshots are taken after different propagation distances $z$, with $z$ increasing from left to right. There is no sign of any instability.

Having observed such a transition from stable to unstable propagation, one immediately has to ask whether the Vakhitov-Kolokolov-criterion given by equation (3.5) can be applied to explain this instability. Calculating the derivative $\partial P/\partial\beta$ for different gap solitons, one finds that it is always negative, for stable as well as for unstable solitons. Hence, the Vakhitov-Kolokolov-criterion fails in this situation. This is not surprising, as one of the assumptions made in deriving the criterion was that the soliton's intensity must not be zero anywhere. However, when the system can be approximated to be a discrete system, the Vakhitov-Kolokolov-criterion could be shown to predict the onset of instability correctly [72, 73].

Alternatively, one can try to use standard linear algebra to determine the unstable eigenmodes and eigenvalues of gap solitons. The problem one faces when doing this is that even when using a very low spatial resolution of the

soliton of only $512 \times 512$ grid points, the matrix whose eigenvectors have to be found has almost 69 billion elements and is non-symmetric.

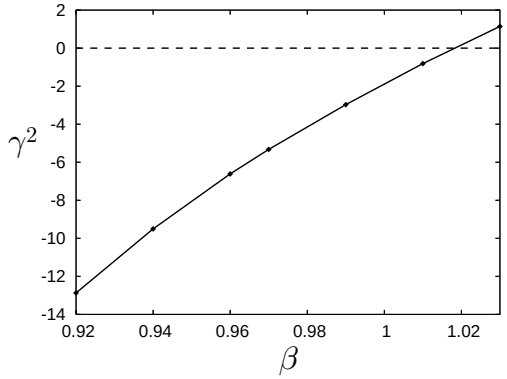


Figure 7.6: The value of $\gamma^2$ for solitons with different propagation constants $\beta$. If $\gamma^2 < 0$, then the eigenvalue $\gamma$ of the eigenmode found is purely imaginary and is therefore an oscillatory mode of the soliton. If $\gamma^2 > 0$ one has found two real eigenvalues, one of which is positive and therefore is linearly unstable.

Hence, it is advisable to simplify the problem without changing its physics. One way to do this is to perform the calculation not in direct space, but in the space spawned by the Bloch waves solving the linear problem. That alone does not reduce the computational resources needed. However, from looking at figure 7.3 one can see that the soliton should be described rather accurately as a superposition of Bloch waves from the first few bands only. That impression is confirmed by a decomposition of the soliton into Bloch waves. Since the higher-order bands do not play a role for the soliton itself, it would seem very unlikely that they play a role for its unstable eigenmodes. Hence, for the calculation of the unstable eigenmodes it is sufficient to only consider the Bloch waves from the first two bands. As a first approach, this yields results that are qualitatively correct and allow for an insight into the physical mechanisms of the instability.

As in chapter 3 we use an ansatz of the form of equation (3.6) and get

$$\gamma v = -\hat{L} w \tag{7.4}$$

$$\gamma w = \hat{L} v - 2Iv\,, \tag{7.5}$$

with $\hat{L} = -\beta + \nabla_\perp^2 + \delta n_p^2 - I$. These two equations can be cast into one:

$$\gamma^2 v = -\hat{L}(\hat{L} - 2I)v\,. \tag{7.6}$$

This equation is easier to handle numerically than the system of equations (7.4) and (7.5).

Now, unless all eigenvalues of the operator $\hat{L}(\hat{L} - 2I)$ are real and $\leq 0$, the soliton is unstable. For numerical calculations, is it most convenient to use the space spawned by the Bloch waves, i.e.

$$v(x, y) = \sum_{k_x, k_y} C_{k_x, k_y} u_{k_x, k_y}(x, y) \exp(i(k_x x + k_y y)) \,, \tag{7.7}$$

because in the case $I \equiv 0$ one would get a diagonal matrix. As mentioned previously, only Bloch waves from the first and second band are considered. This reduces the matrix whose eigenvalues have to be found to $800 \times 800$.

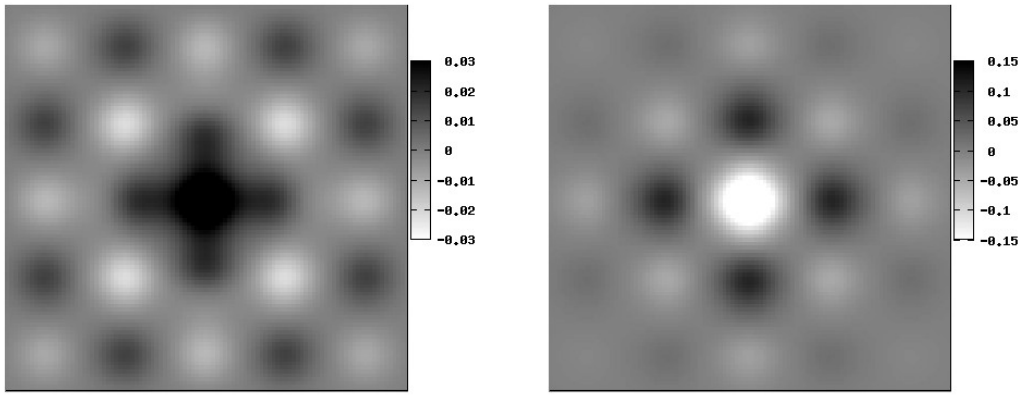


Figure 7.7: The real (left) and the imaginary (right) part of the unstable eigenmode of the soliton shown in figure 7.3.

Using the method described above, the eigenmodes of several solitons were calculated. Figure 7.6 shows the value of the biggest nontrivial eigenvalue $\gamma^2$ of equation (7.6) as a function of the soliton's propagation constant $\beta$. (The trivial eigenvalue $\gamma^2 = 0$ of the neutral mode is ignored.) As can be seen, somewhere around $\beta \approx 1.02$ the eigenvalue $\gamma^2$ gets bigger than zero, indicating the transition from stable to unstable solitons. This differs considerably from the stability threshold found using numerical propagation, which yields a stability threshold somewhere around $\beta \approx 0.98$. However, considering the approximations made, it is still reasonably close.

In order to understand the physical mechanisms that control the instability, one has to take a look at the unstable eigenmode. Figure 7.7 shows the real and the imaginary part of the eigenmode. The imaginary part is much stronger than the real part. Considering equations (7.4) and (7.5), this shows that at the stability threshold $v \equiv 0$ and $w = \varphi_{cr}$, where $\varphi_{cr}$ is the profile of the gap soliton at the threshold being neutrally stable. This is also confirmed by the similarity of the imaginary part of the eigenmode in figure 7.7 and the soliton profile in figure 7.3(b).

The real part of the unstable eigenmode transfers light intensity from the central lattice site to the neighbouring sites. This is in agreement with the dynamics of the decay of the soliton shown in figure 7.4.

Having identified the unstable eigenmode, one can also decompose it into Bloch waves. Doing so for the imaginary part does not yield any surprises, as the imaginary part is largely identical to the solitary beam profile itself and hence dominated by the same Bloch waves centred around the point $M$ in the Brillouin zone. However, it is interesting to note that for the real part of the eigenmode all Bloch waves lying along the line between $X$ and $M$ are rather important. A further analysis of the unstable eigenmode and its relation to the dispersion relation might lead to an improved understanding and might eventually enable researchers to design photonic structures in which low power solitons are stable as well.

Concluding, it could be shown that the analytical and numerical tools used to investigate the stability of solitons in bulk homogeneous media can also be used for gap solitons in photonic crystals. An in-depth investigation of these, however, is left for the future.

# Chapter 8

# Conclusions and outlook

Despite the intensive research on spatial solitons in the last decades, their stability is an open question that only relatively few publications deal with systematically. This is most probably not due to the relevance of the subject, but rather to the demanding techniques required to treat the problem of stability. Analytical approaches can only account for the most simple cases and numerical calculations of the unstable eigenmodes are far more difficult than the simple numerical simulation of light propagation in a nonlinear medium. However, the stability of solitons will be of eminent importance if spatial solitons can make the step out of research laboratories and into technological applications. This work has investigated several aspects of soliton instabilities in saturable nonlinear media.

First, two different kinds of instabilities are compared. On the one hand the symmetry-conserving instabilities that are rather well understood and that can be predicted using the Vakhitov-Kolokolov-criterion. On the other hand, examples of symmetry-breaking instabilities are presented that demand a careful numerical treatment. It is shown that the Vakhitov-Kolokolov-criterion cannot account for these. The symmetry-breaking unstable eigenmodes have a more complex structure than the symmetry-conserving ones. In some cases a soliton can have many different symmetry-breaking unstable eigenmodes. This can lead to rather complex dynamics during the decay of the soliton. In these cases a numerical stability analysis is the only method to distinguish between the effects of the linearly unstable mode and subsequent higher-order effects.

Then, there is the problem of the influence of the degree of coherence of the light on the stability of the soliton. Numerical simulations of modula-

tional and transverse instabilities of incoherent light in isotropic and local media are repeated and extended to the case of the anisotropic and nonlocal nonlinearity of a photorefractive crystal. A comparison with experimental results shows good agreement. Furthermore, a snake instability of an incoherent light stripe is presented – a type of instability that usually does not occur in self-focusing media.

The stabilising merits of incoherent light are then applied to bright vortex rings. The stabilising effect of the incoherent light can be shown. To examine incoherent vortex solitons in more detail, their spatial coherence function and its evolution under propagation are calculated, revealing that the vorticity of the beam is conserved, even though its visible manifestations might be more subtle than in the coherent case.

In chapter 5.3 a very simple model is proposed that can successfully explain most of the features of incoherent vortex solitons. The model not only allows for easier and quicker numerical calculations, but also for a more intuitive approach to understand incoherent vortex solitons.

In addition to the time-independent instabilities in the first part of the work, chapter 6 investigates temporal instabilities of counterpropagating solitons in nonlinear media. It is shown that although the solitary solutions are identical to the copropagating case, the temporal evolution of the light beams can no longer be ignored in counterpropagating geometry. The length of the medium is identified as the decisive factor that determines whether the solitary solution is stable or unstable in time. In the most simple case, an instability leads to a steady-state after a certain time. However, some situations are presented where the instability leads to dynamic periodic states of the system. Hence, irradiating a nonlinear medium with constant light beams at either side can lead to a dynamic behaviour that never settles into a steady state.

To allow for a comparison between numerical results and experiments, a model is developed for the nonlinearity of a photorefractive crystal that is irradiated by two counterpropagating beams. The existence of an interference pattern along the propagation direction is shown to have remarkable consequences. In particular, tilting the crystal by only a tiny amount can lead to important changes. The model developed is mathematically simple and easy to implement numerically.

Based upon the results gained so far about the instabilities of solitons in bulk homogeneous media, it will soon be possible to better understand the properties of novel kinds of solitons that might become important in the

future. Solitons in photonic crystals are of particular interest, as photonic structures are already used in wide-spread technological devices and adding nonlinear features to these might bring research a bit closer to the dream of all-optical data processing. A very first step into the stability analysis of solitons in photonic crystals is presented in the chapter 7. The results suggest that it will be necessary to investigate photonic structures of many different geometries to optimise them for the stable propagation of solitons. An ongoing effort in this direction is needed, also because the results gained for solitons in photonic crystals can be useful for the research on solitons in Bose-Einstein condensates as well.

# Chapter 9

# Zusammenfassung und Ausblick (in german)

Trotz der intensiven Forschungstätigkeit der letzten Jahrzehnte auf dem Gebiet der räumlichen Solitonen ist deren Stabilität nach wie vor ein Feld mit vielen offenen Fragen. Vergleichsweise wenige Publikationen nehmen sich dieses Themas an, was wohl weniger an dessen Relevanz, sondern vielmehr an den analytischen und numerischen Schwierigkeiten liegen dürfte, die zu überwinden sind. Die Stabilität von räumlichen Solitonen wird aber spätestens dann zu einem unbedingt zu behandelnden Problem werden, wenn es gelingen sollte, Solitonen nicht nur in Forschungslabors, sondern auch in technischen Anwendungen zu etablieren. Die vorliegende Arbeit behandelt verschiedene Aspekte der Instabilitäten von räumlichen Solitonen in sättigbaren nichtlinearen Medien.

Zunächst werden zwei grundsätzlich verschiedene Arten der Instabilität verglichen. Auf der einen Seite gibt es die symmetrieerhaltenden Instabilitäten, die heute gut verstanden sind und sich mit Hilfe des Vakhitov-Kolokolov Kriteriums einfach vorhersagen lassen. Auf der anderen Seite werden in dieser Arbeit Beispiele von symmetriebrechenden Instabilitäten gezeigt, die zu berechnen eines recht hohen numerischen Aufwands bedarf. Es wird gezeigt, dass das Vakhitov-Kolokolov Kriterium bei diesen Instabilitäten versagt. Die symmetriebrechenden instabilen Eigenmoden haben eine mitunter deutlich komplexere Struktur als die symmetrieerhaltenden. Zusätzlich kann ein Soliton mehrere symmetriebrechende instabile Eigenmoden gleichzeitig haben, was zu einer komplexen Dynamik des Zerfalls führt. In diesen Fällen ist eine genaue Kenntnis der Eigenmoden notwendig,

um zwischen der durch die lineare Instabilität bedingten Dynamik und Effekten höherer Ordnung zu unterscheiden.

Eines der aktuellen Themen in der Forschung über räumliche Solitonen ist der Gebrauch inkohärenten Lichts. In dieser Arbeit werden frühere Berechnungen zu Modulations- und transverser Instabilität von inkohärenten Lichtfeldern in isotropen lokalen Medien wiederholt und verallgemeinert auf den Fall der anisotropen und nichtlokalen Nichtlinearität der photorefraktiven Kristalle. Die dabei erzielten Ergebnisse stimmen gut mit experimentellen Daten überein. Weiterhin wird ein Beispiel einer 'Snake' Instabilität gezeigt – eine Instabilität, die gemeinhin nur in defokussierenden Medien auftritt.

Im Folgenden werden dann die stabilisierenden Eigenschaften inkohärenten Lichts auf Vortex-Ringe übertragen. Es kann gezeigt werden, dass es tatsächlich möglich ist, die Vortices zu stabilisieren. Um die inkohärenten Vortices genauer zu untersuchen, wird deren räumliche Kohärenzfunktion berechnet und ihre Entwicklung während der Propagation untersucht. Es kann gezeigt werden, dass die topologische Ladung der Vortices während der Propagation erhalten bleibt, obwohl sie sich in der Intensitätsverteilung deutlich weniger stark manifestiert als im Falle kohärenten Lichts.

Es wird ein einfaches Modell inkohärenter Vortex-Solitonen eingeführt, das – zumindest qualitativ – deren Eigenschaften erklären kann. Dieses Modell reduziert nicht nur den numerischen Aufwand, der betrieben werden muss, auf einen Bruchteil, sondern ermöglicht auch ein 'intuitives' Verständnis inkohärenter Vortex-Solitonen.

Die im ersten Teil der Arbeit vorgestellen zeitunabhängigen Instabilitäten werden ergänzt durch die zeitabhängigen Instabilitäten kontrapropagierender Solitonen. Obwohl die solitären Lösungen identisch sind mit denen im Falle der Kopropagation, kann gezeigt werden, dass im kontrapropagierenden Fall die zeitliche Dynamik nicht mehr vernachlässigt werden kann. Als entscheidender Faktor, der darüber entscheidet, ob eine solitäre Lösung stabil oder instabil ist, wird die Länge des Mediums identifiziert. Im einfachsten Fall führt die Instabilität nach einer gewissen Zeit zu einem neuen stationären Zustand. Allerdings können in dieser Arbeit Simulationen präsentiert werden, die zeigen, dass auch periodische dynamische Lösungen existieren. Das bedeutet, dass aus einem nichtlinearen Medium, in das zeitlich konstante Lichtfelder eingestrahlt werden, ein dynamisches System werden kann.

Um Vergleiche zwischen theoretischen Aussagen und experimentellen Ergebnissen zu ermöglichen, wird ein Gleichungssystem abgeleitet, das die nichtlineare Antwort eines photorefraktiven Kristalls auf kontrapropagierende

Lichtfelder beschreibt. Die Existenz von Interferenzmustern entlang der Propagationsrichtung kann dabei erstaunliche Konsequenzen haben. Insbesondere kann schon ein geringes Verkippen des Kristalls deutlichen Einfluss auf die Propagation der Lichtstrahlen haben. Trotzdem ist die mathematische Struktur der abgeleiteten Gleichungen denkbar einfach und numerisch ohne großen Aufwand zu implementieren.

Aufbauend auf den Erkenntnissen zur Stabilität von Solitonen in homogenen nichtlinearen Medien wird es bald möglich sein, die Eigenschaften neuer Arten von Solitonen zu verstehen, die in Zukunft eine wichtige Rolle spielen könnten. Dabei sind insbesondere Solitonen in photonischen Strukturen von Interesse, da bereits heute photonische Kristalle in technischen Anwendungen eingesetzt werden, und das Hinzufügen einer Nichtlinearität die Forschung dem Traum von der optischen Datenverarbeitung ein Stück näherbringen könnte. Ein erster Schritt in Richtung der Stabilitätsanalyse von Solitonen in photonischen Kristallen wird in Kapitel 7 gezeigt. Aus den Ergebnissen lässt sich schließen, dass es notwendig sein wird, photonische Strukturen zu entwickeln, die darauf optimiert sind, dass in ihnen auch Solitonen geringer Intensität stabil propagieren können. Erkenntnisse auf diesem Gebiet sind auch deshalb von großem Interesse, weil sie sich leicht auf das derzeit sehr aktive Feld der Solitonen in Bose-Einstein Kondensaten übertragen lassen.

# Bibliography


[1] M. Remoissenet, *Waves called solitons, 2nd ed.* (Springer, Berlin, 1996).

[2] M. Segev, *Optical spatial solitons*, Opt. Quant. Electron. **30**, 503 (1998).

[3] N. J. Zabusky and M. D. Kruskal, *Interaction of solitons in a collisionless plasma and recurrence of initial states*, Phys. Rev. Lett. **15**, 240 (1965).

[4] N. G. Vakhitov and A. A. Kolokolov, Radiophys. Quantum Electron. **16**, 783 (1973).

[5] N. G. Vakhitov and A. A. Kolokolov, Radiophys. Quantum Electron. **17**, 1016 (1974).

[6] A. A. Zozulya and D. Z. Anderson, *Propagation of an optical beam in a photorefractive medium in the presence of a photogalvanic nonlinearity or an externally applied electric-field*, Phys. Rev. A **51**, 1520 (1995).

[7] N. V. Kukhtarev, V. B. Markov, S. G. Odulov, M. S. Soskin, and V. L. Vinetskii, *Holographic storage in electrooptic crystals .1. Steady-state*, Ferroelectrics **22**, 949 (1979).

[8] J. Petter, C. Denz, A. Stepken, and F. Kaiser, *Anisotropic waveguides induced by photorefractive (2+1)D solitons*, J. Opt. Soc. Am. B **19**, 1145 (2002).

[9] M. Ahles, K. Motzek, A. Stepken, F. Kaiser, C. Weilnau, and C. Denz, *Stabilization and breakup of coupled dipole-mode beams in an anisotropic nonlinear medium*, J. Opt. Soc. Am. B **19**, 557 (2002).

[10] D. N. Christodoulides and M. I. Carvalho, *Bright, dark, and gray spatial soliton states in photorefractive media*, J. Opt. Soc. Am. B **12**, 1628 (1995).

[11] M. Mitchell, M. Segev, T. H. Coskun, and D. N. Christodoulides, *Theory of self-trapped spatially incoherent light beams*, Phys. Rev. Lett. **79**, 4990 (1997).

[12] J. J. García-Ripoll, V. M. Pérez-García, E. A. Ostrovskaya, and Y. S. Kivshar, *Dipole-mode vector solitons*, Phys. Rev. Lett. **85**, 82 (2000).

[13] T. Carmon, C. Anastassiou, S. Lan, D. Kip, Z. H. Musslimani, M. Segev, and D. Christodoulides, *Observation of two-dimensional multimode solitons*, Opt. Lett. **25**, 1113 (2000).

[14] W. Królikowski, G. McCarthy, Y. S. Kivshar, C. Weilnau, C. Denz, J. J. García-Ripoll, and V. M. Pérez-García, *Scattering of dipole-mode vector solitons: Theory and experiment*, Phys. Rev. E **68**, 016612 (2003).

[15] K. Motzek, A. Stepken, F. Kaiser, M. R. Belić, M. Ahles, C. Weilnau, and C. Denz, *Dipole-mode vector solitons in anisotropic photorefractive media*, Opt. Comm. **197**, 161 (2001).

[16] M. Belić, Z. Ljuboje, M. Sauer, and F. Kaiser, *Computational chaos in nonlinear optics*, Appl. Phys. B **55**, 109 (1992).

[17] V. I. Petviashvili, Fiz. Plasmy **2**, 469 (1976).

[18] A. A. Zozulya, D. Z. Anderson, A. V. Mamaev, and M. Saffman, *Solitary attractors and low-order filamentation in anisotropic self-focusing media*, Phys. Rev. A **57**, 522 (1998).

[19] K. Motzek, *Vektorsolitonen in anisotropen photorefraktiven Medien* (Diplomarbeit, Technische Universität Darmstadt, Darmstadt, 2002).

[20] J. J. Rasmussen and K. Rypdal, *Blow-up in nonlinear Schrödinger equations - I. A general review*, Phys. Scr. **33**, 481 (1986).

[21] D. E. Pelinovsky, V. V. Afanasjev, and Y. S. Kivshar, *Nonlinear theory of oscillating, decaying, and collapsing solitons in the generalized nonlinear Schrödinger equation*, Phys. Rev. E **53**, 1940 (1996).

[22] D. E. Pelinovsky and Y. S. Kivshar, *Stability criterion for multicomponent solitary waves*, Phys. Rev. E **62**, 8668 (2000).

[23] E. A. Ostrovskaya, Y. S. Kivshar, D. V. Skryabin, and W. J. Firth, *Stability of multihump optical solitons*, Phys. Rev. Lett. **83**, 296 (1999).

[24] J. K. Yang and D. E. Pelinovsky, *Stable vortex and dipole vector solitons in a saturable nonlinear medium*, Phys. Rev. E **67**, 016608 (2003).

[25] T. Carmon, R. Uzdin, C. Pigier, Z. H. Musslimani, M. Segev, and A. Nepomnyashchy, *Rotating propeller solitons*, Phys. Rev. Lett. **8714**, 143901 (2001).

[26] A. S. Desyatnikov, Y. S. Kivshar, K. Motzek, F. Kaiser, C. Weilnau, and C. Denz, *Multicomponent dipole-mode spatial solitons*, Opt. Lett. **27**, 634 (2002).

[27] K. Motzek, F. Kaiser, C. Weilnau, C. Denz, G. McCarthy, W. Królikowski, A. Desyatnikov, and Y. S. Kivshar, *Multi-component vector solitons in photorefractive crystals*, Opt. Comm. **209**, 501 (2002).

[28] Y. S. Kivshar and D. E. Pelinovsky, *Self-focusing and transverse instabilities of solitary waves*, Phys. Rep. **331**, 118 (2000).

[29] D. Kip, M. Soljačić, M. Segev, S. M. Sears, and D. N. Christodoulides, *(1+1)-Dimensional modulation instability of spatially incoherent light*, J. Opt. Soc. Am. B **19**, 502 (2002).

[30] D. Kip, M. Soljačić, M. Segev, E. Eugenieva, and D. N. Christodoulides, *Modulation instability and pattern formation in spatially incoherent light beams*, Science **290**, 495 (2000).

[31] D. N. Christodoulides, T. H. Coskun, M. Mitchell, and M. Segev, *Theory of incoherent self-focusing in biased photorefractive media*, Phys. Rev. Lett. **78**, 646 (1997).

[32] V. V. Shkunov and D. Z. Anderson, *Radiation transfer model of self-trapping spatially incoherent radiation by nonlinear media*, Phys. Rev. Lett. **81**, 2683 (1998).

[33] D. N. Christodoulides, E. D. Eugenieva, T. H. Coskun, M. Segev, and M. Mitchell, *Equivalence of three approaches describing partially incoherent wave propagation in inertial nonlinear media*, Phys. Rev. E **6303**, 035601 (2001).

[34] Z. Chen, S. M. Sears, H. Martin, D. N. Christodoulides, and M. Segev, *Clustering of solitons in weakly correlated wavefronts*, Proc. Nat. Acad. Sci. **99**, 5223 (2002).

[35] B. Gütlich, T. König, C. Denz, K. Motzek, and F. Kaiser, *Secondary modulation instability in partially coherent beams*, Opt. Comm. **255**, 57 (2005).

[36] C. Anastassiou, M. Soljačić, M. Segev, E. D. Eugenieva, D. N. Christodoulides, D. Kip, Z. H. Musslimani, and J. P. Torres, *Eliminating the transverse instabilities of Kerr solitons*, Phys. Rev. Lett. **85**, 4888 (2000).

[37] S. P. Gorza, N. Roig, P. Emplit, and M. Haelterman, *Snake instability of a spatiotemporal bright soliton stripe*, Phys. Rev. Lett. **92**, 084101 (2004).

[38] V. Tikhonenko, J. Christou, B. LutherDavies, and Y. S. Kivshar, *Observation of vortex solitons created by the instability of dark soliton stripes*, Opt. Lett. **21**, 1129 (1996).

[39] G. Theocharis, D. J. Frantzeskakis, P. G. Kevrekidis, B. A. Malomed, and Y. S. Kivshar, *Ring dark solitons and vortex necklaces in Bose-Einstein condensates*, Phys. Rev. Lett. **90**, 120403 (2003).

[40] K. Motzek, F. Kaiser, W. H. Chu, M. F. Shih, and Y. S. Kivshar, *Soliton transverse instabilities in anisotropic nonlocal self-focusing media*, Opt. Lett. **29**, 280 (2004).

[41] Y. S. Kivshar and B. Luther-Davies, *Dark optical solitons: physics and applications*, Phys. Reports-Rev. Section Phys. Lett. **298**, 81 (1998).

[42] V. I. Kruglov and R. A. Vlasov, *Spiral self-trapping propagation of optical beams in media with cubic nonlinearity*, Phys. Lett. A **111**, 401 (1985).

[43] W. J. Firth and D. V. Skryabin, *Optical solitons carrying orbital angular momentum*, Phys. Rev. Lett. **79**, 2450 (1997).

[44] G. V. Bogatyryova, C. V. Fel'de, P. V. Polyanskii, S. A. Ponomarenko, M. S. Soskin, and E. Wolf, *Partially coherent vortex beams with a separable phase*, Opt. Lett. **28**, 878 (2003).

[45] C. C. Jeng, M. F. Shih, K. Motzek, and Y. Kivshar, *Partially incoherent optical vortices in self-focusing nonlinear media*, Phys. Rev. Lett. **92**, 043904 (2004).

[46] D. Briedis, D. E. Petersen, D. Edmundson, W. Królikowski, and O. Bang, *Ring vortex solitons in nonlocal nonlinear media*, Opt. Exp. **13**, 435 (2005).

[47] D. M. Palacios, I. D. Maleev, A. S. Marathay, and G. A. Swartzlander, *Spatial correlation singularity of a vortex field*, Phys. Rev. Lett. **92**, 143905 (2004).

[48] Y. S. Kivshar and G. P. Agrawal, *Optical solitons: from fibers to photonic crystals* (Academic Press, San Diego, 2003).

[49] K. Motzek, F. Kaiser, J. R. Salgueiro, Y. Kivshar, and C. Denz, *Incoherent vector vortex-mode solitons in self-focusing nonlinear media*, Opt. Lett. **29**, 2285 (2004).

[50] M. Haelterman, A. P. Sheppard, and A. W. Snyder, *Bimodal counterpropagating spatial solitary-waves*, Opt. Comm. **103**, 145 (1993).

[51] O. Cohen, R. Uzdin, T. Carmon, J. W. Fleischer, M. Segev, and S. Odoulov, *Collisions between optical spatial solitons propagating in opposite directions*, Phys. Rev. Lett. **89**, 229901 (2002).

[52] O. Cohen, S. Lan, T. Carmon, J. A. Giordmaine, and M. Segev, *Spatial vector solitons consisting of counterpropagating fields*, Opt. Lett. **27**, 2013 (2002).

[53] O. Sandfuchs, *Self-organization, amplitude-equations and Fourier control in a nonlinear optical feedback system* (Dissertation, Shaker Verlag, Aachen, 2002).

[54] T. Richter, *Dynamik gegenläufiger Solitonen* (Diplomarbeit, Technische Universität Darmstadt, Darmstadt, 2004).

[55] M. R. Belić, A. Stepken, and F. Kaiser, *Spatial screening solitons as particles*, Phys. Rev. Lett. **84**, 83 (2000).

[56] W. Królikowski, E. A. Ostrovskaya, C. Weilnau, M. Geisser, G. McCarthy, Y. S. Kivshar, C. Denz, and B. Luther-Davies, *Observation of dipole-mode vector solitons*, Phys. Rev. Lett. **85**, 1424 (2000).

[57] M. Belić, P. Jander, K. Motzek, A. Desyatnikov, D. Jović, A. Strinić, M. Petrović, C. Denz, and F. Kaiser, *Counterpropagating self-trapped beams in photorefractive crystals*, J. Opt. B: Quantum Semiclass. Opt. **6**, S190 (2004).

[58] M. Belić, M. Petrović, D. Jović, A. Strinić, D. Arsenović, K. Motzek, F. Kaiser, P. Jander, C. Denz, M. Tlidi, and P. Mandel, *Transverse modulational instabilities of counterpropagating solitons in photorefractive crystals*, Opt. Exp. **12**, 708 (2004).

[59] D. Jović, D. Arsenović, A. Strinić, M. Belić, and M. Petrović, *Counterpropagating optical vortices in photorefractive crystals*, Opt. Exp. **13**, 4379 (2005).

[60] M. Petrović, D. Jović, M. Belić, J. Schröder, P. Jander, and C. Denz, *Two dimensional counterpropagating spatial solitons in photorefractive crystals*, Phys. Rev. Lett. **95**, 053901 (2005).

[61] J. Schröder, P. Jander, C. Denz, T. Richter, K. Motzek, and F. Kaiser, *Counterpropagating dipole-mode vector soliton*, Opt. Lett. **30**, 1042 (2005).

[62] Y. Silberberg and I. B. Joseph, *Instabilities, self-oscillation, and chaos in a simple non-linear optical interaction*, Phys. Rev. Lett. **48**, 1541 (1982).

[63] A. L. Gaeta, R. W. Boyd, J. R. Ackerhalt, and P. W. Milonni, *Instabilities and chaos in the polarizations of counterpropagating light fields*, Phys. Rev. Lett. **58**, 2432 (1987).

[64] M. Belić, P. Jander, A. Strinić, A. Desyatnikov, and C. Denz, *Self-trapped bidirectional waveguides in a saturable photorefractive medium*, Phys. Rev. E **68**, 025601 (2003).

[65] E. DelRe, A. Ciattoni, B. Crosignani, and P. Di Porto, *Nonlinear optical propagation phenomena in near-transition centrosymmetric photorefractive crystals*, J. Nonlinear Opt. Phys. & Mater. **8**, 1 (1999).

[66] K. Motzek, M. R. Belić, T. Richter, C. Denz, A. Desyatnikov, J. P., and F. Kaiser, *Counterpropagating beams in biased photorefractive crystals: Anisotropic theory*, Phys. Rev. E **71**, 016610 (2005).

[67] C. Rotschild, O. Cohen, O. Manela, T. Carmon, and M. Segev, *Interactions between spatial screening solitons propagating in opposite directions*, J. Opt. Soc. Am. B **21**, 1354 (2004).

[68] P. Yeh, *Introduction to photorefractive nonlinear optics* (John Wiley & Sons, New York, 1993).

[69] K. Motzek, A. A. Sukhorukov, F. Kaiser, and Y. S. Kivshar, *Incoherent multi-gap optical solitons in nonlinear photonic lattices*, Opt. Exp. **13**, 2916 (2005).

[70] B. Eiermann, T. Anker, M. Albiez, M. Taglieber, P. Treutlein, K. P. Marzlin, and M. K. Oberthaler, *Bright Bose-Einstein gap solitons of atoms with repulsive interaction*, Phys. Rev. Lett. **92**, 230401 (2004).

[71] E. A. Ostrovskaya and Y. S. Kivshar, *Matter-wave gap solitons in atomic band-gap structures*, Phys. Rev. Lett. **90**, 160407 (2003).

[72] S. F. Mingaleev and Y. S. Kivshar, *Self-trapping and stable localized modes in nonlinear photonic crystals*, Phys. Rev. Lett. **86**, 5474 (2001).

[73] E. W. Laedke, K. H. Spatschek, S. K. Turitsyn, and V. K. Mezentsev, *Analytic criterion for soliton instability in a nonlinear fiber array*, Phys. Rev. E **52**, 5549 (1995).

# Danksagung

Auf die unterschiedlichste Art und Weise haben mir viele Personen dabei geholfen, meine Promotion zu einem glücklichen Abschluss zu bringen. Insbesondere bei den folgenden will ich mich für die Unterstützung bedanken:

Ich danke *Friedemann Kaiser* dafür, dass er es mir ermöglicht hat in seiner Arbeitsgruppe stets den aktuellen Entwicklungen des Arbeitsgebietes und meinen persönlichen Forschungsinteressen nachzugehen. Von seinen umfassenden Erfahrungen auf dem Gebiet der nichtlinearen Dynamik habe ich sehr profitiert. Auch bei den gewesenen und aktuellen Mitgliedern der Arbeitsgruppe 'Nichtlineare Dynamik' *Hauke Busch, Andreas Bohn, Tobias Richter, Erik Glatt, Martin Gassel* und *Ivona Jakovljević* bedanke ich mich für die kollegiale Zusammenarbeit.

I would like to thank *Yuri Kivshar* for the opportunity to visit his group at the Australian National University on several occasions and for a never ending stream of interesting ideas.

*Cornelia Denz* und ihrer Arbeitsgruppe an der Westfälischen Wilhelms-Universität Münster (insbesondere *Björn Gütlich, Philip Jander* und *Jochen Schröder*) danke ich für die hervorragende Zusammenarbeit bei dem Versuch, eine Brücke zwischen experimentellem und theoretischem Arbeiten zu schlagen.

Der Arbeitsgruppe Halbleiteroptik am IAP danke ich dafür, dass sie mich als 'Mitglied ehrenhalber' adoptiert haben.

Den Herren *Tobias Gensty, Michael Peil* und *Mark Aurel Gregor* gilt mein besonderer Dank für die häufig geleistete Erste Hilfe bei der Bewältigung von Motivationsminima und außerdem für die Einblicke in Gebiete der Forschung abseits der Solitonen.

Je remercie *Claire, Edythe* et *Rían Muller*! Vous m'avez appris bien plus que l'on peut apprendre à l'université.

Den größten Dank schulde ich meinen Eltern und meiner Schwester. Für einfach Alles!!!

# Curriculum Vitae

**Persönliche Daten**

| | |
|---|---|
| Name | Christian Motzek |
| Geburtsdatum | 14.4.1976 |
| Geburtsort | Idar-Oberstein |
| Nationalität | deutsch |
| Adresse | Schaffnitstr. 11, 64285 Darmstadt |

**Ausbildung**

| | |
|---|---|
| 1995 | Abitur am Adolf-Reichwein-Gymnasium in Heusenstamm |
| 1995 - 2002 | Physikstudium an der Technischen Universität Darmstadt |
| 1997 | Vordiplom in Physik |
| 1998 - 1999 | EU-SOCRATES Austauschjahr an der École Nationale Supérieure de Physique de Grenoble |
| 2001 - 2002 | Diplomarbeit am Institut für Angewandte Physik, TU Darmstadt<br>Titel: *Vektorsolitonen in anisotropen photorefraktiven Medien*<br>Betreuer: Prof. F. Kaiser und Dr. A. Stepken |
| 2002 | Abschluss des Physikstudiums |

| | |
|---|---|
| November - Dezember 2001 | Aufenthalt in der 'Nonlinear Physics Group' an der Australian National University |
| 2002 - 2006 | Promotion am Institut für Angewandte Physik, TU Darmstadt, Betreuer: Prof. F. Kaiser |
| Oktober - November 2003 | Aufenthalt in der 'Nonlinear Physics Group' an der Australian National University |
| September 2004 | Aufenthalt in der 'Nonlinear Physics Group' an der Australian National University |

**Sonstiges**

| | |
|---|---|
| 1999 - 2001 | Tutor in den Übungen zu den Vorlesungen in theoretischer Physik *Quantenmechanik, Statistische Physik* und *Komplexe dynamische Systeme* |
| 2004 - 2005 | Übungsassistent für die Vorlesungen in theoretischer Physik *Quantenmechanik, Statistische Physik* |
| 2002 & 2004 | Betreuer von Diplomarbeiten |

Hiermit erkläre ich an Eides statt, dass ich die vorliegende Dissertation selbstständig verfasst habe und nur die angegebenen Hilfsmittel verwendet habe. Ich habe bisher keinen Versuch unternommen, an einer anderen Hochschule das Promotionsverfahren einzuleiten.

Darmstadt, im Oktober 2005